Title
Live Imaging of Spontaneous and Drug-induced Recovery After Stroke

Author
Bechay, Kirollos Raouf

Publication Date
2021

Peer reviewed|Thesis/dissertation

UNIVERSITY OF CALIFORNIA

Los Angeles

Live Imaging of Spontaneous and Drug-induced Recovery After Stroke

A dissertation submitted in partial satisfaction of the

requirements for the degree Doctor of Philosophy

in Neuroscience

by

Kirollos Raouf Bechay

2021

ABSTRACT OF THE DISSERTATION

Live Imaging of Spontaneous and

Drug-induced Recovery After Stroke

by

Kirollos Bechay

Doctor of Philosophy in Neuroscience

University of California, Los Angeles 2021

Professor Stanley Thomas Carmichael, Chair

ABSTRACT

Stroke is a leading cause of disability and there is a need for therapies which enhance the spontaneous amount of brain recovery that occurs naturally. PDE2a is a promising molecular target which may limit recovery. Here, two-photon calcium imaging is employed to study the primary motor cortex (M1) and the premotor cortex (M2) of mice before and after inducing a PT stroke to M1. Mice received daily PDE2a-inhibitor as a recovery agent after stroke, and were imaged weekly for 5 weeks. Head-fixed behavior was concurrently assessed during spontaneous and forced-use contexts. Calcium recordings were processed and analyzed, and functional connectivity (FC) was assessed based on the correlations of the neurons in the recording. Stroke was found to have significant negative effects on FC, especially in M1. Stroke had differential effects in M2 during Spontaneous behavior vs forced use behavior. Finally, PDE2a-inhibition shows a strong trend for improving head-fixed recovery after stroke and it is a significantly positive enhancer of FC in M1 and M2. The results suggest that calcium imaging can act as a biomarker for stroke and that PDE2a-inhibition is an ideal molecular target.

The dissertation of Kirollos Bechay is approved.

Peyman Golshani

Michael Levine

Alcino Silva

Stanley Thomas Carmichael, Committee Chair

University of California, Los Angeles

2021

Dedication

To my parents,
who sacrificed all that they knew
to give my brother and I, a chance at a better life.

To my wife,
for her endless support from the first days of
graduate school till the last.

Table of Contents

List of Figures

List of Data Tables (Statistics)

Chapter 5

My time as a graduate student in the Carmichael lab has been one of great professional development, and even more so for personal development. I learned to think critically and explore the vast literature of scientific fields which I knew nothing about. I learned to collaborate and listen to the expert advise of others, while applying it to an independent project. Live imaging of the brain is a marvelous achievement for modern science and will continue to amaze me for the rest of my life. Most of all, I gained insight about my own skills and limitations and the confidence to create and apply tools to address research questions.

Tom has been a model scientist and mentor from my first interactions with him. He has been patient and generous with his time when I needed it. Our consistent scientific discussions have always left me with a deeper understanding of my work or with interesting questions to begin to address. On a personal level, Tom has always treated me and others in the lab with respect and kindness. The other lab members, the post-docs, graduate students and other researchers, have made the lab a lively and a joy to work in. They have also been a valuable resource anytime I had a question or an issue in the lab. There have been too many individuals and too many encounters to list, but I am eternally grateful. The advice and mentorship I have received in this lab will continue with me throughout my medical training and career.

My thesis committee has been a great inspiration for me through my graduate training. I remember being initially intimidated by the caliber of scientific work of Dr. Silva when I rotated in his lab in 2014. I was met instead with a sympathetic and excited mentor who took me to lunch, and has offered great advice to me since then. Dr. Golshani has been an immense help, allowing me to visit and learn the in-vivo imaging methods in his own lab. He has offered his technical expertise when I needed it, and has thoroughly discussed my project with me. Similarly, Dr. Levine has spoken to me at lengths about my project, and pushed me to address certain aspects of the analysis. I hope to one day pass on the mentorship which I received to future students.

I met my wife, Tina, very early in graduate school and our relationship grew throughout my training. My parents, my brother and my wife have all been pillars of support for me throughout this time and anything I achieve during my career would not have been possible without them. Graduate school has been often challenging, but ultimately highly fulfilling from a personal and a professional level. I am excited to apply what I have learned from my time here to my future clinical and academic career.

Kirollos Bechay

EDUCATION

MD-PhD Candidate Expected 2023

Medical Scientist Training Program

University of California, Los Angeles

B.S. Biological Sciences Spring 2014

Neurobiology Major, Honors *cum laude* University of California, Irvine

RESEARCH EXPERIENCE

PhD Thesis Lab

Dr. Thomas Carmichael, UCLA June 2016-Present

Imaging live brain circuits of rodents during natural stroke recovery vs drug-enhanced recovery

PhD Summer Rotations

Dr. Peter Tontonoz, Howard Hughes Medical Investigator, UCLA June2015-August 2015

Dr. Alcino Silva, UCLA July 2014-August 2014

Undergraduate Research

Dr. Marcelo Wood, UCI August 2011- July 2014

Dr. Susan Mango, Harvard University, Cambridge, MA July 2013-August 2013

Dr. Manolis Fanto, King's College, London July 2012-August 2012

Dr. Luis Mota-Bravo, UCI January 2011 – August 2011

PUBLICATIONS

"HDAC inhibition via RGFP966 releases the brakes on sensory cortical plasticity and the specificity of memory formation"; The Journal of Neuroscience; Kasia Biezczcad, Kirollos Bechay, James Rusche, Vincent Jacques, Shashi Kudugunti, Wenyan Miao, Norman Weinberger, James McGaugh, Marcelo Wood; University of California, Irvine; August, 2015.

AWARDS AND GRANTS

AHA Summer 2018 Predoctoral Fellowship June 2018

Scored in the 99th percentile for American Heart Association 2-year predoctoral grant

Howard Schneiderman Prize for Excellence in Research June 2014

Awarded to 4 UCI students per year for outstanding undergraduate research

Phi Beta Kappa Academic Honors Society May 2014

CCDD Annual Outreach Conference at Harvard Public Health May 2014

Fully funded conference

1st Place AAAS Student Poster Competition February 2014

Winner in "Brain and Behavior"; mentioned in Science *magazine*

Neuroscience Scholars Program September 2013-September 2015

3 year career-development fellowship from the Society for Neuroscience; includes membership to the society, personal career enrichment funds, and all expenses paid to annual conference.

NuRhoSci Neuroscience Honors Society November 2012-June 2014

Outstanding Poster Presentation and Interdisciplinary November 2012 **Integration at ABRCMS conference**

Travel Award by Society for Developmental Biology November 2012

Illinois Summer Neuroscience Program (ISNI) May 2012

Minority Access to Research Careers (MARC) September 2012- June 2014 **Dean's Honor List** Fall, Winter, Spring 2010-2013

LEADERSHIP EXPERIENCE

M202 Neuroanatomy Graduate Course Assistant Winter 2020

-TA for Neuroanatomy for NSIDP Graduate Students

UCLA/USC Minority Health Conference (MHC) 2015

Organizational Committee

SIGN (Student Interest Group in Neurology) Student Coordinator 2015-2016

UCLA David Geffen School of Medicine

Class of 2018 Social Chair 2014-2015

UCLA David Geffen School of Medicine

Recruitment Ambassador 2014-2015

UCLA David Geffen School of Medicine

Chapter I: Introduction

Stroke is a common cerebrovascular condition, associated with aging and metabolic syndrome, which occurs when the brain is deprived of oxygenated blood. Ischemic strokes, due to dislodged blood clots, are more likely than hemorrhagic sources, representing 87% and 10% of all strokes, respectively. Currently approved therapy is based on reperfusion of the tissue; this is effective but ineligible in the majority of patients due to its time sensitivity. Modern medicine has not yet found effective therapy to attenuate the chronic symptoms of stroke, and this is an ultimate goal of stroke research programs.

Section 1.1 Stroke is a major public health concern

Stroke is a pervasive disease of modern society, consistently in the top five leading causes of death worldwide[1]. 7.6 million Americans self-reporting having had a stroke in 2018[2] and an estimated 795,000 new and recurrent attacks per year in the United States[1]. It is estimated that an additional 3.4 million Americans will have a stroke in the next ten years, a 20% increase in prevalence. The lifetime risk of stroke was calculated at 24.9% in 2016, a 9% increase from 1990[2]. Even yet, the American Heart Association (AHA) believes stroke is still underdiagnosed in the United States.

Between 10-20 percent of strokes are fatal, leaving the remaining victims to live with the debilitations following the neural insult. From the ages of 45 and up, stroke is the largest contributor of years lost due to disability worldwide[3]. Currently, the approved treatment for stroke in the US is based on reperfusion and clot dissolution therapies. Intravenous tissue plasminogen activator (IV tPA) is the gold standard for acute ischemic stroke patients, but the patient must be treated within 3-4.5 hours of their last known normal, including a head computed tomography

(CT) scan rule out any intracranial hemorrhage. The AHA recommends that medical centers obtain a CT within 20 minutes of patient arrival and door-to-needle time of under 60 minutes for tPA administration; while these standards are difficult to meet, studies have shown that the risks outweigh the benefits tPA administered after this window[4]. In large vessel strokes, mechanical thrombectomy may be indicated after a CT angiogram or MR angiogram. Recent studies have shown that the time window for eligible thrombectomies may be pushed out to 24 hours. Nevertheless, most stroke victims are ineligible for clot-busting therapies and are only administered aspirin to decrease the risk of another stroke.

With most patients surviving stroke but not receiving therapy, up to 50% of survivors are estimated to be left with a chronic disability. An estimated 25.7 million stroke survivors globally designate stroke as a leading cause of adult disability. There is a degree of spontaneous recovery that will occur without intervention, but this is highly variable between patients. One large study described this highly variable nature of stroke recovery and found that the amount of initial deficit was inversely correlated with recovery; the milder the deficit of an initial stroke, as measured by the Fugl-Meyer motor upper extremity scale, the greater the expected amount of recovery[5]. Rehabilitation after stroke is also known to enhance spontaneous recovery, but the ideal course of training after stroke has not been determined. Studies have shown that the time, intensity, and use of the unaffected limb are all variables that can affect recovery. In addition, there is evidence that rehabilitation may be combined with another therapy, such as a drug or brain stimulation, to produce further recovery. Finally, technological advancements now allow noninvasive tracking of brain activity, and these tools hold promise for tracking recovery on an individual basis.

Section 1.2 Symptoms after Stroke and Modeling the Disease

Stroke symptoms result from the ischemic cascade: the molecular events that follow after blood loss to tissue. These symptoms will thus correlate to the location and size of the ischemic block. The location of the clot in the brain determines the potential behavioral deficits that ensue, as they correspond to that tissue's natural functions. These diverse symptoms can be categorized under five possible neurological domains: motor, sensory, visual, language, or cognitive.

The Behavioral Sequela After Stroke

The majority of patients who suffer a stroke will have some level of disability. A significant predictor of severity of the disability is the initial assessment of neurological impairment, which is routinely measured by a 15-item NIHSS scale. Another important predictor of the severity of the disability is the size of the infarct on MRI or CT scan and its location[6]. Occlusions in large vessels, such as the carotid, basilar, or large intracranial arteries, have the worst outcomes[7], while infarcts along the boundaries of arterial territories typically show good outcomes. Recovery occurs spontaneously but not entirely in most patients. The most significant recovery occurs in the 3-6 months[8], with more significant disabilities requiring more time. Accumulating evidence suggests that the corticospinal tract is necessary for recovery[9], and the amount of damage to this tract is proportional to future recovery[10].

Similarly, there is evidence that this behavioral recovery after stroke is mediated by plasticity within corticospinal tracts[11]. Some of the common neurological deficits experienced after stroke include hemiplegia, aphasia, dysphagia, sensory loss, and visuospatial neglect. Six months after stroke, one study found that 50% of patients had hemiparesis and cognitive deficits, while 20% had hemianopia and sensory deficits[12].

Rodent Models of Stroke and Rehabilitation

Studying stroke in human patients is challenging as it typically only allows retrospective studies. Rodent stroke models allow behavioral studies before and after experimentally induced lesions due to lesion sizes and location heterogeneity. Several stroke models exist, with different properties, to model human strokes[13], such as MCAo (middle cerebral artery occlusion), photothrombotic and vasoconstrictive approaches. There are also various behavioral assays for measuring behavior at baseline versus post-injury[14]. These include the rotarod test, a rotating cylinder that rodents try to remain on top of, and "latency to fall" has been commonly used to measure motor function after stroke[14,15]. The cylinder task is a forelimb asymmetry assay in which the touching of a glass cylinder by a rodent inside is compared between the two forelimbs. After a cortical motor stroke, there is a significant asymmetric preference to the non-affected limb[16]. Another simple test of forelimb deficit is the foot fault test: a mouse is placed on an elevated grid, and mistakes while gripping the grid are counted in each forelimb. The number of foot faults increases in the affected limb after stroke[17,18], and this deficit decreases with recovery and treatment[16]. There is a 2% foot fault rate in a naive mouse at baseline, but this increases to roughly 8% within seven days of cortical stroke. A gradual improvement was observed for the next six weeks until a plateau phase of 4% was reached by week 7. Genetic manipulations were able to enhance or deteriorate this spontaneous behavioral recovery.

A contested question in the field is the effect of forced or non-use of the paretic or non-paretic limbs following a forelimb stroke. In one study, rats were induced with strokes to the forelimb cortex and fitted with casts to immobilize the paretic or unimpaired limb for 15 days[19]. Immobilization of the "good" limb caused a dramatic exaggeration of the injury due to overuse of the paretic limb. At the same time, immobilization of the paretic limb causes a decrease in

recovery[19]. Motor skill training of the non-paretic limb was also associated with a significant reduction in recovery and neuronal activation[20]. Electron microscopy demonstrated that this training was associated with a paradoxical increase in axodendritic synaptic density increased in the peri-infarct, negatively correlated with functional performance. More studies on rehabilitation will be highlighted in Section 2.3 and the other factors that affect spontaneous recovery.

Another study forced rats to use their impaired forelimb after intracranial hemorrhage. In contrast to the Kozlowski study, these rats demonstrated improved recovery and expanded the forelimb representation on the ipsilesional side[21]. Additionally, this group used the loss of function experiments to show that the cortico-rubral pathway was causally linked to this recovery. Several studies agree that the success of rehabilitation is based on timing and on overcoming inhibitory forces in the peri-infarct[11]. For example, growth-promoting neurotherapy (anti-Nogo) was able to boost recovery only when combined with forced training following the treatment[22]. Furthermore, novel corticospinal tract rewiring was demonstrated in this group of animals correlating to the level of recovery. These selected studies demonstrate the complex nature of stroke, signifying the for novel studies to better understand these mechanisms.

Section 1.3 References

1. Xu, J., Murphy, S. L., Kockanek, K. D. & Arias, E. Mortality in the United States, 2018. *NCHS Data Brief* 1–8 (2020).
2. Virani, S. S. *et al. Heart Disease and Stroke Statistics-2021 Update: A Report From the American Heart Association*. *Circulation* vol. 143 (2021).
3. Grefkes, C. & Fink, G. R. Recovery from stroke: current concepts and future perspectives. *Neurol. Res. Pract.* **2**, (2020).
4. Lees, K. R. *et al.* Time to treatment with intravenous alteplase and outcome in stroke: an updated pooled analysis of ECASS, ATLANTIS, NINDS, and EPITHET trials. *Lancet* **375**, 1695–1703 (2010).
5. van der Vliet, R. *et al.* Predicting Upper Limb Motor Impairment Recovery after Stroke: A Mixture Model. *Ann. Neurol.* **87**, 383–393 (2020).
6. Schiemanck, S. K., Kwakkel, G., Post, M. W. M., Kappelle, L. J. & Prevo, A. J. H. Predicting long-term independency in activities of daily living after middle cerebral artery stroke: Does information from MRI have added predictive value compared with clinical information? *Stroke* **37**, 1050–1054 (2006).
7. Smith, W. S. *et al.* Prognostic significance of angiographically confirmed large vessel intracranial occlusion in patients presenting with acute brain ischemia. *Neurocrit. Care* **4**, 14–17 (2006).
8. Jorgensen, H. S., Nakayama, H., Raaschou, H. O. & Olsen, T. S. Stroke: Neurologic and functional recovery the Copenhagen Stroke Study. *Physical Medicine and Rehabilitation Clinics of North America* vol. 10 887–906 (1999).
9. DeVetten, G. *et al.* Acute Corticospinal Tract Wallerian Degeneration Is Associated With

Stroke Outcome. (2010) doi:10.1161/STROKEAHA.109.573287.

10. Byblow, W. D., Stinear, C. M., Barber, P. A., Petoe, M. A. & Ackerley, S. J. Proportional recovery after stroke depends on corticomotor integrity. *Ann. Neurol.* **78**, 848–859 (2015).

11. Wahl, A. S. *et al.* Asynchronous therapy restores motor control by rewiring of the rat corticospinal tract after stroke. *Science (80-.).* **344**, 1250–1255 (2014).

12. Kelly-Hayes, M. *et al.* The influence of gender and age on disability following ischemic stroke: The Framingham study. *J. Stroke Cerebrovasc. Dis.* **12**, 119–126 (2003).

13. Carmichael, S. T. Rodent models of focal stroke: Size, mechanism, and purpose. *NeuroRx* **2**, 396–409 (2005).

14. Balkaya, M., Kröber, J. M., Rex, A. & Endres, M. Assessing post-stroke behavior in mouse models of focal ischemia. *J. Cereb. Blood Flow Metab.* **33**, 330–338 (2013).

15. Brooks, S. P. & Dunnett, S. B. Tests to assess motor phenotype in mice: A user's guide. *Nat. Rev. Neurosci.* **10**, 519–529 (2009).

16. Li, S. *et al.* GDF10 is a signal for axonal sprouting and functional recovery after stroke. *Nat. Neurosci.* **18**, 1737–1745 (2015).

17. Chen, J. *et al.* Atorvastatin induction of VEGF and BDNF promotes brain plasticity after stroke in mice. *J Cereb Blood Flow Metab* **25**, 281–290 (2005).

18. Gibson, C. L., Bath, P. M. & Murphy, S. P. G-CSF reduces infarct volume and improves functional outcome after transient focal cerebral ischemia in mice. *J. Cereb. Blood Flow Metab.* **25**, 431–439 (2005).

19. Kozlowski, D. A., James, D. C. & Schallert, T. Use-dependent exaggeration of neuronal injury after unilateral sensorimotor cortex lesions. *J. Neurosci.* **16**, 4776–4786 (1996).

20. Kim, S. Y. *et al.* Experience with the "good" limb induces aberrant synaptic plasticity in

the perilesion cortex after stroke. *J. Neurosci.* **35**, 8604–8610 (2015).

21. Ishida, A. *et al.* Causal link between the cortico-rubral pathway and functional recovery through forced impaired limb use in rats with stroke. *J. Neurosci.* **36**, 455–467 (2016).

22. Li, S. *et al.* Blockade of Nogo-66, myelin-associated glycoprotein, and oligodendrocyte myelin glycoprotein by soluble Nogo-66 receptor promotes axonal sprouting and recovery after spinal injury. *J. Neurosci.* **24**, 10511–10520 (2004).

Chapter II: Reviews of Selected Literature

Ischemia induces intracellular cascades of injury and extracellular cascades that involve surviving neural and inflammatory cells. There is considerable evidence that the initial pathological cascades of ischemia become positive regulators of recovery in the later phases of stroke[1]. The excitability of neurons in the peri-infarct has been linked to spontaneous recovery after stroke, and enhancing neuronal excitability has been linked to enhanced recovery. Converging evidence demonstrates that enhancing brain excitation has the potential of enhancing behavioral recovery after stroke, and that the molecular mechanisms underlying recovery overlap with those for neurodevelopment and memory formation. Understanding these excitatory mechanisms and developing tools to non-invasively modulate them is a promising route to stroke therapies.

Section 2.1 The Pathological Cascades of Ischemia

The ischemic cascade, which occurs in response to stroke, is a series of cellular responses to hypoxia. Neurons are especially vulnerable to hypoxia and die within 5 minutes of interrupted blood flow, whereas it takes 20-40 minutes to kill cardiac or kidney cells[2]. In a large-vessel human stroke, it is estimated that 1.9 million neurons, along with 14 billion synapses, die per minute of hypo-perfusion[3]. At the margins of stroke, away from the core, is the ischemic penumbra- the brain region that has not yet undergone irreversible damage. In-vivo rodent imaging has revealed marked swelling ('blebbing') and loss of dendritic spines within minutes in this region, but restoration of blood flow is associated with a return to standard structure [4]. Current reperfusion therapies, such as tissue plasminogen activator (tPA), aim to protect this tissue by restoring blood flow and limiting the ischemic cascade.

One of the first neuronal responses to hypoxia is potassium efflux which leads to hyperpolarization of the neuron. Hyperpolarization is followed by ATP deprivation and an inability to maintain the resting membrane potential. It is thought that this results in a spreading anoxic depolarization which moves out radially from the stroke site[5]. A positive feedback cycle involving glutamate results in a massive release of this excitatory neurotransmitter- a series of sequela termed neuronal excitotoxicity. Glutamate acts on NMDA and AMPA receptors, resulting in calcium and sodium influx, respectively. Additional calcium influx may flow through pathologically open voltage-gated calcium channels, increasing levels of intracellular calcium. Mitochondria swell up as they uptake and buffer calcium until they can no longer maintain their membrane potential. Mitochondrial breakdown is a stimulus for apoptosis and is seen as an early hallmark of irreversible cell injury.

Calcium is a central actor in cellular communication across the body, acting as an amplification signal molecule with diverse functions based on the cell type, including facilitating all synaptic transmission in the nervous system. Due to these critical roles, calcium concentrations are tightly regulated in the sub-compartments of the cell. In the hypoxic environment, the ATP-consuming regulatory mechanisms are disrupted due to a lack of ATP. Increases in cytoplasmic calcium concentration mediate proteolysis, lipolysis, and DNA degradation involved in necrotic cell death. Calcium-activated proteins also generate free radicals, which can degrade the plasma membrane and cellular machinery. In the lab dish, calcium is just as toxic. Increasing intracellular calcium by exposure to NMDA for 3-5 minutes triggers widespread death in cultured cortical neurons, while NMDAR antagonists were neuroprotective in these cells when exposed to hypoxia[6]. Due to anaerobic respiration in hypoxic neurons, lactic acid accumulation has also been implicated in the pathological cascade following ischemia[2].

These unique features after an ischemic event result in waves of excitability and depression in the cortex[1]. AMPA and NMDA (and potentially Kainate) receptors respond to the increases in glutamate dumping by hypoxic neurons, resulting in the excitotoxicity described. In the acute phase of hypoxia, tonic and phasic GABA signaling is neuroprotective but may chronically hamper recovery.

The unique environment of the peri-infarct cortex

While the penumbra region is fated to die without reperfusion, the peri-infarct area refers to the surviving brain cells along the stroke's perimeter. Blood flow to this region diminishes immediately after stroke but recovers gradually, depending on the stroke center's distance[7]. After a stroke, this region is in a hypoxic and pro-inflammatory environment demonstrated to have unique and substantial structural and functional remodeling.

The neurons in the peri-infarct have unique transcriptional profiles and undergo morphological changes to their axons and dendrites. In a pivotal study by Carmichael et al., quantitative RT-PCR demonstrates transcriptional changes in the 500 uM of cortex adjacent to the stroke in a time and distance-dependent manner. These changes include enhancing several growth-promoting genes and a class of inhibitory genes known as chondroitin sulfate proteoglycans (CSPGs)[8]. This study also demonstrated the existence of "sprouting neurons," extending their axons as closely as 300 uM to the center of the insult after stroke. Seven days after a focal cortical stroke in rodents, these sprouting neurons have distinct transcriptional profiles, including cell surface receptors, growth factors, cytoskeletal proteins, and several transcription factors[9]. As the rodents age, the transcriptional profile of sprouting neurons changes, including increases to ephrin and myelin, which may explain the inferior recovery in older rodents and humans.

Additionally, it was shown that regulating GDF10 expression in the peri-infarct can enhance axonal sprouting and behavioral recovery[10]. Epigenetic forces are also at play in the peri-infarct neuron, as HDAC4 is shuttled into neuronal nuclei and decreases the expression of various dendritic, axonal, and myelin-related proteins11 limit the rate of recovery. These studies and others link the peri-infarct to significant neuroplasticity after stroke and also with behavioral recovery. Neuroplasticity mechanisms at play in the peri-infarct will facilitate or hamper behavioral recovery, depending on the context. Thus, modulating these factors and the plasticity in the peri-infarct is a highly promising route to effective therapies for stroke.

Immune involvement post-infarct

The ischemic environment is a potent stimulant of the immune system. Marked increases of RNA expression of several pro-inflammatory genes, including interleukin 1(IL1), interleukin 6 (IL6), and TNFa, are observed within 2-6 hours after forebrain ischemia in the rat[11,12]. There is conflicting data on the benefit or harm due to cytokines and growth factors in the post-ischemic brain. IL6 has been shown to promote neuronal survival against NMDA toxicity in striatal neurons[13], while others have linked it to neurodegeneration[14]. Several growth factors have been shown to attenuate ischemic and excitotoxic damage, including transforming growth factor B and fibroblast growth factor[15]. These same growth factors have been associated with aberrant scar formation, which hinders brain recovery[16]. IL1 has been consistently linked with microglial activation, acute-phase protein expression (adhesion molecules, Beta-APP, and complement proteins), and neurotoxicity[17]. However, IL1 has also exhibited neuroprotective features in specific environments[18]. The immune response is involved in both the acute phase of ischemic damage and the chronic phase of recovery. More modern studies are currently needed to understand the nuances of each of the many aspects concerning immune interactions in the stroke core and penumbra.

While neurons have received the majority of attention in the peri-infarct, other brain cells play critical roles in mediating damage and recovery. Within a week of stroke, there is significantly enhanced neurogenesis from the migrating cells of the supraventricular zone (SVZ) to the infarct core[19,20]. Erythropoietin has been implicated in this aspect of recovery[21] and decreased neurogenesis in the SVZ after stroke significantly. GFAP expressing progenitor cells have also been implicated as a source of these newly born neurons, and they were linked with angiogenesis in the peri-infarct[22]. Furthermore, GFAP knockout mice demonstrated reduced axonal sprouting, worse behavioral outcomes, and increased CSPGs. These findings have established the "neurovascular niche," a neuro- and angiogenic cellular environment in the peri-infarct, allowing behavioral recovery. Surviving and proliferating astrocytes are also highly involved in stroke recovery, modulating water (edema), and blood flow. As expected, astrocytes' well-established role of glutamate buffering is an important neuroprotective agent[23], and the receptor regulating this is down-regulated during ischemia[24]. Some astrocytic functions may also be toxic, such as the release of S-100B and the generation of nitrogen oxide[25]. Additionally, Ephrin A5 expression is increased in reactive astrocytes after stroke and is associated with decreased axonal sprouting and worse behavioral outcomes after a cortical stroke to the mouse's motor cortex[26]. Blocking this expression enhances sprouting in new motor and premotor circuits and presents another possible route to a pharmaceutical therapeutic.

Another essential cell type in the brain's response to injury is microglia, the brain's resident immune cell. In healthy conditions, these cells play a significant role in the phagocytosis of debris. After a stroke, a subset of microglia become "activated," display different morphology, and release pro-inflammatory cytokines, referred to by some as the M1 phenotype. In contrast, the M2 phenotype reflects an anti-inflammatory, alternative expression pattern which involves

phagocytosis of debris[27]. These additional cell types are substantially complex in their own right, and any translational stroke study must consider their role in the damage and recovery of the brain.

Section 2.2 Neuronal Excitability in Learning and Memory

Neuroplasticity refers to the modern understanding that the brain possesses a remarkable ability to adapt based on its combination of sensory input. In 1951, Donald Hebb postulated that one neuron's excitation of its post-synaptic partner enhances the efficiency of that particular connection. This theory has been restated as "neurons wire together if they fire together" and remains the leading model for how the brain organizes and reorganizes itself. A potential molecular mechanism to explain 'Hebbian Plasticity' was discovered in 1966 and coined long-term potentiation (LTP)[28]. After brief trains of electrical stimulation, hippocampal circuits in the live rabbit demonstrate increased efficiency, or potentiation, of synaptic signaling. This potentiation of a single synapse could last for several hours and remains an integral part of the modern theory of memory formation.

An essential purpose of the nervous system is to alter the behavior of an organism based on its prior experiences. Memories serve this purpose by encoding, storing, and later retrieving information about an experience. Memories are thus inextricably linked to the change of behavior and an archetypal example of neuroplasticity. In 1969, the first evidence linking LTP to behavioral adaptation was demonstrated in the gill-withdrawal reflex of the sea slug, *Aplysia*[29]. Countless studies have substantiated and built upon these results and have led to the branch of neuroscience known as learning and memory. Advancements in molecular biology and genetics have allowed for increasingly detailed studies to further our understanding of neuroplasticity and memory formation.

Molecular biology of plasticity and memory

Interrogation of the *Aplysia* gill-withdrawal reflex revealed that the potentiation in LTP was causally linked to the synaptic release of serotonin[30] and its increase of cyclic AMP (cAMP) in the post-synaptic neuron. Simultaneously, the cyclic nucleotides cAMP and cGMP were recently discovered as ubiquitous "2nd messengers" that relayed and amplified cellular signals. cAMP was first identified from human liver extracts in 1958, and Earl Sutherland was awarded the Nobel Prize for this discovery in 1971. cGMP was discovered in rat urine a few years later[31]. G-protein coupled receptors (GPCRs) hormonal stimulation leads to membrane-bound adenylyl cyclase, an enzyme that produces cAMP. Cytosolic guanylyl cyclase is stimulated by nitrous oxide (NO)[32] and synthesizes cGMP but remains less well-understood.

cAMP is a ubiquitous regulator of various cell functions, such as lipolysis in adipocytes, gluconeogenesis in hepatocytes, and aquaporin integration in principal kidney cells. A family of cAMP-dependent kinases- Protein Kinase A (PKA)- was described in 1968 as an effector of cAMP and its many effects on a cell[33]. PKA is made of four subunits: two regulatory subunits which inhibit the catalytic subunits. As cAMP concentration rises, it binds the regulatory subunits and actively releases the catalytic subunits to phosphorylate PKA targets. Direct injection of the catalytic subunits of PKA was found to enhance neurotransmitter release in *Aplysia*, similar to the administration of high-frequency stimulation when inducing LTP[34]. Thus, this was some of the earliest evidence of cAMP and PKA participating in LTP and memory formation.

It was later discovered that repeated stimulation of LTP gives rise to long-lasting behavioral changes, or long-term memories, while a single session only lasted a few minutes. In cultured neurons, repeated applications of serotonin versus a single application mimicked these results[35]. Prolonged LTP, or long-term facilitation (LTF), versus brief LTP induction, or short-

term facilitation (STF), was analogous to long-term memory and short-term memory formation. The addition of protein synthesis inhibitors37 disrupted the conversion of STF to LTF and, by extension, short-term memory to long-term memory. Further studies have provided converging evidence that induction of long-term memory requires gene transcription and translation.

Within the genome, a conserved sequence was found in the promoter elements of cAMP-responsive genes, and it was coined 'cAMP response element' (CRE). These elements may be bound by specific transcription factors and increase RNA polymerase activity at the respective gene[36]. CRE-Binding Protein (CREB) was first discovered in 1987 as a transcription factor with a high affinity for these elements and a potential link to long-term memory formation. Upon Ser133 phosphorylation by PKA, MAPK, or CaMK, CREB dimerizes, moves to the nucleus, and enhances transcription of CRE-responsive genes. Injection of CRE oligonucleotides, functioning to block CREB binding to genetic CRE, inhibited long-term facilitation without altering short-term facilitation[37]. Gene targets of CREB have been termed *immediate early genes* (IEGs) due to their transcription and translation shortly after LTF. Well-studied target genes include the transcription factor *cFos*, the growth factor *BDNF,* and the cytoskeletal protein *Arc*[38]. There is some contentious evidence that, in some contexts, mRNA for these genes is already localized to the synapse, and CREB-mediated transcription may not be required for these instances of LTF.

Homeostasis of these pathways requires inhibitory mechanisms in place to balance the excitatory mechanisms described above. Memory suppressor genes, such as CREB2 inhibit LTF and memory formation[39]. These genes can be considered the inhibitory counterpart to CREB activity, which enhances IEG transcription. Similarly, phosphatases counteract the excitatory effects of protein kinases by dephosphorylating proteins. For example, Protein Phosphatase (PP) and calcineurin-1 can both dephosphorylate PKA targets. Phosphodiesterases (PDEs) are a

widespread class of enzyme which balance the effects of cyclases. These molecules are a crucial inhibitory drive on neuronal excitability and will be discussed in greater detail in Section 2.5.

The cAMP-PKA-CREB pathway described above is one of many molecular mechanisms of neuroplasticity, which may collectively explain the changes which a particular neuron undergoes during LTF and participating in long-term memory formation. However, an apparent paradox is that phosphorylated CREB (pCREB) acts in the nucleus to induce protein synthesis across the entire cells, yet only particular synapses would experience LTF. Studies have since confirmed the process of synaptic tagging: while pCREB synthesizes IEG gene products throughout the cell, only synapses that had recently been activated will incorporate these proteins into their synapses[40] and maintain LTP.

Memory engrams and neuronal allocation

Neurons form thousands of inhibitory or excitatory synapses with other neurons, forming functional circuits which compute outputs and control behavior. Studies interrogating the roles of circuits, not only individual neurons, were required to further our understanding of memory formation. CREB has been identified as an essential molecule in the recruitment of circuits for memory formation. The level of CREB in a lateral amygdala neuron, while the animal is learning contextual fear conditioning, is correlated to the likelihood that this neuron is incorporated into the circuit for that memory[41]. This view argues for competition between neurons, based on their amount of CREB, for incorporation into a memory circuit. A follow-up study demonstrated that CREB is *necessary* to form fear memory, as the ablation of amygdala neurons with high CREB during encoding blocked expression of that memory[42]. Similar findings in *Drosophila* demonstrate that particular memories may be blocked and then recovered by manipulating CREB [43]. These studies provide converging evidence that CREB is a controller of memory allocation in neurons.

Molecular studies have demonstrated that CREB enhances neuronal excitability, increasing the likelihood of that neuron to be recruited for a particular memory. Neurogenesis from the subventricular zone (SVZ) to the dentate gyrus is a well-known phenomenon; these newly born neurons have enhanced excitability. Computational models of hippocampal circuitry predict newly born neurons have a role in encoding time, as their hyper-excitability lasts a particular amount of time since their birth and provides a time-locked event for connecting memories[44]. 'Clustered-plasticity' models predict that LTP at a specific synapse will increase the probability for LTP at neighboring synapses, within 10um, by lowering the threshold for LTP induction[45], and this has also been substantiated[40]. The theory that synaptic excitability, coupled with pCREB activity, increases the likelihood of incorporation into a memory trace coined the 'neuronal allocation' hypothesis and is the leading theory for memory formation. Neuronal allocation has also been demonstrated in cortical studies, such as during barrel cortex plasticity[46].

Cortical studies of neuronal allocation led to the reinvigoration of the search for the engram, an ensemble of neurons which show 1) a persistent change after an event occurs, 2) is activated with retrieval cues for that event, 3) may make predictions about the outcome after activation of the ensemble and 4) can exist in a dormant, inactive state[47]. During encoding of memory, excitable neurons are preferentially recruited into an engram which consolidates into a dormant phase; when retrieval is initiated, the engram is reactivated and can compute a behavioral output. Recent evidence has demonstrated memory recall also transiently increases engram excitability, mediated by Kir2.1channel-internalization, and this is associated with enhanced context recognition[48]. It is possible to visualize an engram by analyzing IEG expression *ex-vivo*. Still, genetic labeling strategies, such as the TetTag approach[49], now allow permanent fluorescent labeling of active neurons at a particular time. Studies have used these techniques to demonstrate

that ensembles of neurons active in the hippocampus or cortex during an event are the same neurons reactivated during retrieval of that event.

Advanced tools continue to allow researchers to probe the engram with greater detail. The tag-and-erase strategy uses the labeling strategies outlined above and combines an inhibitory signal to attenuate the neuronal activity of the tagged neurons [47]. Inhibiting the labeled neurons disrupts the retrieval of the engram and disrupts normal behavior in response to the memory. Allocation of an engram refers to the artificial stimulation of subsets of neurons to induce them into a memory trace. Overexpression of CREB in a subset of amygdala neurons was able to recruit these neurons to the engram for a contextual fear memory[50]. Allocate-and-erase strategies combine an inhibitory signal, such as inhibitory DREADDs or opsins, to selectively encode memory and then erase it at a later time point. Ablating engram neurons in the amygdala could selectively silence a fear memory, effectively causing amnesia for a particular event[42]. Optogenetic silencing of hippocampal engram neurons similarly prevented memory retrieval using this strategy[51]. Remarkably, optogenetic stimulation was also able to allocate a fear-memory to hippocampal neurons; later, optogenetic stimulation, without the fear context, induced the freezing behavior[52]. A recent study has furthered our understanding of how memories may be linked by the proportion of overlapping neurons in an engram[53]. Furthermore, this phenomenon was decreased in aged mice; increasing excitability of neurons within these mice rescues this deficit. Aging is one context that presents with neural and behavioral dysfunction, as are the many forms of neural injury.

Cortical plasticity underlying motor learning

The engram and the neuronal allocation hypothesis help explain how neurons are recruited and allocated to a memory trace from a molecular and cellular perspective. Other studies, especially those rooted in clinical science, approach the problem from a behavioral perspective.

Behavioral experiences are a potent driver of cortical plasticity, including excitatory and inhibitory synaptic remodeling[54]. After learning, there is an increasing number of synaptic 'spines' in excitatory neurons, some of which stabilize and do not persist. These morphological changes are also observed during development and in environmental enrichment. The plasticity of these spines has been linked to increases in CREB and IEG products, such as Arc, Homer1, and BDNF. New spines which grow during motor learning are stabilized with each subsequent training session[55]. The stabilization of new synapses is thus associated with the learning and consolidation of a behavioral memory.

Skilled learning and dexterous control of behavior are activated and stimulated by the cortical motor areas. The primary motor cortex, M1, is the cortical area in the frontal lobe most directly associated with motor control, forming the lateral corticospinal tract after the pyramidal decussation at the medulla. The organization of M1 in the mouse may be mapped by using intracortical microstimulations (ICMS) and characterizing forelimb movement representations[56]. A motor homunculus corresponds to the neural map of which muscles are under control by M1. In young mice, learning of a skilled reaching task led to rapid changes in M1 representations, as proximal movements increased in size at the expense of distal movements[57]. In aged mice, however, these changes did not occur and were linked to behavioral deficits. Optogenetic inhibition of the contralateral motor cortex can transiently suppress a mouse's ability to reach and grab a food pellet, causing freezing behavior instead[58]. Another study demonstrated that M1 is necessary to acquire skilled motor movements but not for its retrieval[59]. In this model, M1 circuits tutor subcortical circuits after motor learning such that M1 is no longer required for activation of the motor command. Cortical layers of M1 also have delineated function: while some layer 2/3 neurons were highly predictive of a self-initiated lever pull task, their overall predictive accuracy

does not increase throughout training[51]. Layer 5 neurons, in contrast, demonstrate increasing predictive accuracy throughout the training sessions.

The primary motor cortex is not the only area that controls motor signals in the brain. The anterior premotor cortex and the supplementary motor have also been called the secondary motor areas, or M2. Bordering anteriorly and medial to M1, these areas also control movement but indirectly compared to M1. One recent study has demonstrated that motor learning, like engrams in the hippocampus, recruits specific neuronal ensembles which require M2[60]. Arc expression was used to track these ensembles and predict the recruitment of a neuron into the M2 ensemble. *In vivo* two-photon imaging provided further evidence that layer 5 neurons in M2 demonstrate preparatory activity, predicting complex movements[61]. Dramatic remapping of M2 has also been shown in human tetraplegics. In these patients, the "hand knob" area of the premotor cortex becomes tuned to the entire body[62]. Studies of the primary and secondary motor areas provide robust evidence for plasticity related to motor learning, as demonstrated with dramatic ICMS differences pre-training versus post-training[63]. Skilled reaching expands the caudal and rostral forelimb representations, while unskilled lever presses increased the elbow and shoulder muscles.

The studies outlined here represent decades of brain research on the molecular and circuit mechanisms governing neuroplasticity. CREB was presented as a critical regulator of neuronal allocation into an engram. Cyclic nucleotides (cAMP, cGMP), protein kinases, and IEGs were also highlighted as molecular modulators of neuronal excitability. Cortical plasticity in response to motor learning exhibits similar properties to other forms of neuroplasticity. The primary and secondary motor areas control skilled motor movements and demonstrate an ability to remap these movements in response to learning. The following section will continue this discussion of

neuroplasticity but in the context of stroke. Spontaneous mechanisms of recovery will be reviewed, followed by a review of studies attempting to enhance aspects of that recovery.

Section 2.3 Spontaneous and Augmented Recovery after Stroke

The mammalian brain possesses a remarkable ability to adapt, whether it is to developmental cues, behavioral experience, or neural injury. Stroke may be described in two phases: the initial cascades of damage to neural cells and circuits and the compensatory reactions of the brain to recover some of the lost function. Some of the pathological cascades which ensue after an infarct have been described in Section 2.1. This section will be dedicated to reviewing the mechanisms for recovery. While there are significant overlaps between injury and recovery, this section will elaborate on the later phases of stroke recovery in animal models and patients. The section will end by briefly discussing the noninvasive techniques being tested to enhance recovery in humans.

Animal models of stroke allow scientists to probe the typical cascades during stroke recovery and manipulate these cascades to alter the behavioral outcome. Chemical and electrical signals radiating from an ischemic event create radial zones with distinct features[64]. Glutamate and NMDAR-mediated neurotoxicity cause positive feedback cycles, leading to calcium-mediated proteolysis and necrotic cell death in the infarct core. The peri-infarct is the area surrounding the core that survives and contributes significantly to recovery. The transition between the core and the peri-infarct is the *penumbra*, an electrically silent region that may be saved by therapeutic intervention. These radiating zones from the infarct also exhibit morphological changes, namely axonal sprouting and dendritic remodeling. The circuits that these affected neurons are a part of are also necessarily disturbed, and studies of these recovery circuits are another emerging field of

stroke biology. Several studies of mechanisms of spontaneous recovery in animal models are outlined below, followed by studies that have improved the rate of recovery with therapeutic intervention. The analogous findings in human patients are compared to these studies, including behavioral rehabilitation and noninvasive stimulations for enhanced recovery.

Molecular and circuitry changes during spontaneous recovery

Neurons in the peri-infarct send axons to the stroke core, a phenomenon coined axonal sprouting and highly correlated with stroke recovery[65–67]. Selective isolation of sprouting neurons and whole-genome expression identified a 'sprouting transcriptome' of genes upregulated in these neurons[9]. This expression profile included genes for axonal guidance, cytoskeletal modifications, and growth factors, such as GDF 10. Growth and differentiation factor 10 (GDF10) is expressed in peri-infarct neurons and promotes axonal sprouting *in vitro* and *vivo*[10]. Inhibiting expression of GDF10 blocked sprouting and reduced behavioral recovery, indicating its *necessity* for axonal sprouting and spontaneous recovery. In contrast, there are also inhibitory signals which are expressed in the peri-infarct. These molecules include NOGO (Kartje Cheatwood 2008), chondroitin sulfate proteoglycans (CSPs)[68], and Ephrin-A5[26]. The promotion of growth-promoting factors and the attenuation of growth-inhibitory factors are two potential approaches for stroke intervention.

After cortical damage to the forelimb area of the motor cortex, layer 5 pyramidal neurons subsequently increasing dendritic arborization until approximately three weeks after stroke, after which there is a pruning of branches[69]. These dendritic spine changes are correlated to the degree of ischemia and may be rapidly reversed with quick reperfusion[70]. *In vivo* two-photon imaging confirmed these findings, demonstrating 5-8 fold spine turnover in the peri-infarct region one to two weeks post-stroke[71] and still evident six weeks out. The premotor cortex of the primate brain

has also been implicated in behavioral recovery. In adult squirrel monkeys, ischemic infarcts were induced, which destroyed at least 50% of hand representations in M1 and expanded representation for hand areas in secondary motor areas[72]. This also presented evidence for reduced somatosensory input to the injured M1 and a proportional increase in intracortical sprouting, potentially replacing the lost inputs. Another study has confirmed that the medial premotor cortex (AGm) mediates recovery of skilled reach in mice after focal cortical stroke, with a corresponding decrease in inhibitory markers in the region[73]. These studies highlight some of the molecular events which occur during recovery. One of the ultimate goals of stroke biology is to differentiate beneficial versus detrimental factors at specific time points after the ischemic attack. The role of excitatory versus inhibitory currents is a clear example of the delicate balance of forces at different time points in the recovering brain.

Neurogenesis also has a role in recovery following stroke. Focal ischemia has been shown to increase subventricular zone (SVZ) neurogenesis and migration towards the infarct[22]. The 'neurovascular niche' refers to newly born immature neurons closely associating with the remodeling vasculature after stroke and is dependent on vascular proteins such as stromal-derived factor 1 and angiopoietin. There is also evidence for increased proliferation of neural progenitors and glial cells[74]. Endothelial-derived factors such BDNF and BEGF promote neuronal differentiation and angiogenesis[65,75]. Importantly, BDNF is a well-known IEG under CREB control, and enhancement of BDNF enhances post-stroke recovery via CREB signaling[76]. Analysis of postmortem brain tissue also suggests this increased post-stroke neurogenesis is present in humans[77]. Genetic knockdowns of erythropoietin (EPO) or its receptor (EPOR) cause post-stroke neurogenesis defects and a decreased potential for recovery[21]. These studies highlight the role of

newly incorporated cells in the circuit for recovery and their necessary interactions with the endothelial cells of the vasculature.

Post-ischemic excitation and inhibition

Excitatory and inhibitory currents in the peri-infarct are in an inconsistent balance between neuroprotection and allowing recovery[1]. AMPA and NMDA signaling are known effectors of excitotoxicity in the peri-infarct[78], while tonic and phasic GABA signaling are neuroprotective in the acute phase of stroke. Chronically, however, AMPA and NMDA stimulation enhance recovery, while GABA currents restrain the recovery. Genetically or pharmaceutically decreasing tonic GABA, thus increasing the excitability of the peri-infarct, was shown to improve recovery in rodent models[79]. There is often also electrical dysfunction remote from the ischemic site, sometimes termed diaschisis, which results in network disconnections. Remote disconnections can cause delayed cell death in the downstream neurons, such as in the thalamus or substantia nigra.

Focal injury of the forelimb representations of the squirrel monkey, without any rehabilitative training or therapeutic intervention, shrinks the area's representation and is replaced by other arm representations[80]. In these animals, rehabilitation preserves or slightly expands the forelimb representation in the cortex, and this behaviorally-modulated recovery will be discussed further later in this section. In the peri-infarct of primate brains, NMDA receptors are upregulated, and GABA receptors are down-regulated[81], confirming the role of excitation in recovery. Modulating excitation and inhibition throughout recovery is a promising mechanism for enhancing post-stroke recovery. Still, these studies highlight the importance of timing of these therapies, as a beneficial therapy may be detrimental at the wrong timepoint. Furthermore, the timing of these mechanisms in human patients versus animal models must be determined. Personalized

biofeedback via noninvasive brain imaging is one of the most promising areas of stroke research and will be discussed at the end of the current section.

CRE and CREB mediated effects post-stroke

Excitation and inhibition have complex roles for protection and plasticity in the neuron, but there may still be a molecular target that can benefit multiple phases of the ischemic cascade. CREB and the associated pathways discussed in the plasticity of memory are ideal candidates for this purpose. Phosphorylated CREB (pCREB) has been shown to increase in the hippocampus after ischemia[82] beginning 30 minutes after stroke and lasting at least three days. The total levels of CREB were not increased, indicating that pCREB is activated by ischemia directly and necessarily an IEG itself. The cyclic nucleotides, cAMP and cGMP, and their kinases are an initial molecular signal of ischemia, and pCREB is. The neuroprotective effects of CREB, both *in vitro* and *in vivo* have also been well documented. For example, environmental enrichment in rodents has been linked to increases in pCREB and a neuroprotective effect against excitotoxicity[83]. Hypoxemia of hippocampal slices *in vitro* has also demonstrated increased levels of pCREB without increasing total CREB[84]. These studies suggest that the cAMP-PKA-CREB pathway has a protective role in the early phases of post-stroke recovery. Another modern study has demonstrated intra-axonal translation of CREB from its mRNA transcripts has an essential part in neuronal survival[85]. Overall, these data suggest CREB as a neuroprotective agent in the early phases of ischemia, contrasting with AMPA-R and NMDA-R mediated neurotoxicity of that time.

Another study confirmed a persistent increase of CRE-mediated gene expression in the peri-infarct[86], a role with which CREB is causally associated. In a comprehensive study, CREB was directly demonstrated to enhance recovery after stroke in a non-neuroprotective manner[87]. Viral overexpression of CREB in ~15% of cortical motor neurons was enhanced axonal sprouting

and cortical stroke recovery. Combining CREB overexpression with an inhibitory DREADD demonstrated enhanced recovery. Adding the ligand activates the DREADD receptor and inhibits infected neurons' functions, blocking the prior recovery. Washout of the DREADD ligand reinstates the recovery, thus providing evidence that these experiments captured the engram for recovery. This study is analogous to an 'allocate and manipulate' experiment, where the memory in question is the recovered behavioral functions. Mapping of the somatosensory and motor circuits in the animals of these experiments demonstrates that CREB enhances the remapping of injured circuits and induces formations of new connections. CREB overexpression was not associated with decreased infarct size throughout recovery in these studies, indicating that CREB enhanced neuroplasticity without necessarily reducing the ischemic damage. One crucial distinction between these studies and the studies of CREB's neuroprotective effects is that the mice were injected with CREB at the time of stroke; therefore, the infected neurons were not exposed to CREB at the time of the ischemic event. These findings do not argue against the neuroprotective role of CREB, but rather that CREB has distinct neuroprotective and neuroplastic functions, both of which are beneficial against ischemia. These studies present this molecular pathway as a point for potential intervention with more forgiving timing than modulators of excitation or inhibition. Phosphodiesterases will be later presented for as prime candidates for pharmacological control of CREB.

Behavioral modulation of recovery

Rehabilitation in the adult rat after a cortical injury significantly enhances the recovery of lost skilled motor tasks[88]. Intensive rehabilitation also enhances spine turnover and dendritic architecture in these animals in a cholinergic-dependent manner. Meta-analysis studies on human rehabilitation after stroke suggest that rehabilitation after stroke improves behavioral outcomes[89].

An inverse correlation between days of initiating therapy and the functional recovery at discharge was found[90], implying that patients start rehabilitation as soon as possible. Behavioral studies in rodents demonstrate that hyper-reliance on the non-paretic limb likely places a restraint on recovery[91]. Electron microscopy analysis also determined that that training of the non-paretic limb increases peri-infarct synaptic density, but these changes were distinct from the synaptic turnover cited in a normal recovery. Constraint-induced movement therapy (CIMT) was developed relying on the principle of restraining the non-paretic limb[92]. This approach operates on the theory of 'learned disuse' of the affected limb and counteracts it by forcing the patient to use it functionally. The EXCITE phase III clinical trial has demonstrated that CIMT therapy induces significant functional gains compared to typical rehabilitation[93]. In a comprehensive longitudinal study, CIMT was evaluated in squirrel monkeys without stroke induction[94]. While CIMT induced changes to ICMS maps, these changes were reversed with the removal of the CIMT cast, suggesting that CIMT is a safe form of rehabilitation.

The timing of rehabilitation is a critical factor to consider. In rodents, rehabilitation five days after stroke improves behavioral outcomes, but 30 days out does not (Biernaskie 184). Additionally, it was reported that CIMT initiation *too early* relative to the stroke could exacerbate the damage[95]. The duration, intensity, and frequency of treatment are also essential factors to consider. In the VECTORS study, human stroke patients were randomized to different intensity levels of CIMT[96]. Paradoxically, high-intensity CIMT was correlated with less functional improvement than lower-intensity therapy. These perplexing results demonstrate the complexity of neurorehabilitation and highlight the need for more well-powered studies on optimizing timing, dosing, and intensity. Broadly, the literature suggests initiating rehabilitation as early as three days after stroke and at a moderate intensity have the best functional results. In contrast to the current

stroke treatment, patients would benefit from increasing intensity and dosage of therapy in the first month and potentially combining it with noninvasive stimulation[97].

Noninvasive stimulation for stroke recovery

Stimulation of the brain has a long history of clinical application, but recent technological breakthroughs have made noninvasive and targeted stimulation feasible. Noninvasive cortical stimulation is still immature, with many unanswered questions that need to be experimentally tested. Two primary modalities currently exist for noninvasive stimulation, TCDS, and TMS, and both have been associated with recovery in stroke.

Transcranial direct stimulation (TCDS) is a noninvasive method of providing weak electrical currents for anodal stimulation of the cortex or cathodal inhibition. The applied current of 1-2 mA falls well beneath currents that cause brain damage (25mA) but were sufficient to stimulate cortical excitability and regional blood flow[98]. NMDA antagonists have been shown to eliminate TCDS effects, suggesting the involvement of NMDA receptors[99]. The feasibility of TCDS stimulation was tested in primates. After months of spontaneous recovery on a motor task, rehabilitation and TCDS independently positively affected recovery and the remapping of cortical motor maps[72]. TCDS stimulation of the peri-infarct of the motor lesion significantly enhances motor task performance and excitability of the lesional hemisphere in chronic stroke patients[100]. Cathodal inhibition of the contralesional cortex using TCDS has also been reported to strengthen stroke recovery[98] and may have advantages over perilesional stimulation. However, a number of studies report no significant enhancement over controls, leaving open the question of how best to implement this technique to the general population.

Transcranial Magnetic Stimulation (TMS) is another stimulation technique based on electromagnetic induction and delivers a similar set of advantages and disadvantages as TCDS.

Studies have demonstrated that stimulation of the perilesional cortex in chronic stroke patients enhanced performance on motor tasks. Still, there are contradictory results on whether these performance benefits are long-lasting[99,101]. In a more recent study, 5Hz repetitive TMS enhanced motor learning in individuals with unilateral chronic stroke[102]). As with TCDS, some studies have reported negative results using TMS. A small study of 41 stroke patients received excitatory theta-burst stimulation, a form of repetitive transcranial magnetic stimulation (TMS) with rehabilitation[103] but found no enhancement of upper-limb function over rehabilitation alone.

While there is growing evidence that noninvasive stimulation has a beneficial effect on recovery after brain injury, the data is inconsistent, and there are conflicting studies on their efficacy. Further complications which need to be considered include the timing of this therapy, integration with rehabilitation, and which area to stimulate or inhibit. One study attempted to predict response to stimulation after cortex and found that magnetic resonance imaging (MRI) could predict the patient's response in a clinical trial examining TCDS[104,105]. The physiologic integrity of the motor system, measured by MRI measures of the gray and white matter and by motor evoked responses, was highly correlated with responsiveness to stimulation. These studies are highly promising and are a significant headway for personalized medicine and truly optimize a patient's recovery route after stroke.

Section 2.4 Imaging in Stroke: From Rodent to Human

In the early twentieth century, Ramon y Cajal began cataloging histology slides and drawings of the microanatomy of the nervous system. Since then, researchers have innovated and modernized visualization techniques to probe the nervous system in increasing detail. Several vital advancements in optical imaging have been crucial for this purpose, including electron, confocal

and two-photon microscopy. Advancing genetics tools, such as DREADD and optogenetic receptors, give researchers a toolbox to excite, inhibit and modulate the nervous system. In combination with *in vivo* imaging, researchers can now optically visualize and interrogate specific neural circuits[106] without invasive experiments' limiting factors. X-ray-based imaging and Magnetic Resonance Imaging (MRI) have similarly revolutionized clinical visualization of the nervous system. This section will discuss these innovative technologies, animal studies employing them in stroke, and human imaging studies that promise noninvasive tracking of recovery following stroke.

The innovation of two-photon microscopy

In animal neuroscience research, two-photon microscopy has been uniquely poised for *in vivo* imaging and evaluation of function and structure. Fluorescent microscopy uses a light source, typically in the visible spectrum (400-500nm), to excite a molecule and then captures the emitted light, pictured as the emission spectrum of the molecule. The innovation of multi-photon microscopy was to excite fluorescent molecules using multiple photons, typically two, with lower energy light in the infrared spectrum (700-1000nm). Higher wavelength light is less energetic and minimizes phototoxicity, as well as possessing deeper penetration in tissue. Furthermore, single scattered photons cannot excite tissue outside a small volume around the laser beam, leading to decreased background fluorescence and a higher resolution. A pulsed laser focuses through an objective that scans and excites a particular field of view, while a CCD camera captures the emitted photons. If the bone of the skull is thinned or replaced with a cover glass, two-photon microscopy can safely image the cortex of a living rodent.

Fluorescent dyes, such as Fura2AM, Fluo4AM, and Indo-1AM, were initially used *in vitro* and *in vivo* two-photon imaging, such as in layer 2/3 neurons somatosensory cortex[107]. Genetically

encoded molecules, however, have replaced these dyes because of their increasing levels of sensitivity and the ability to target these reporters to specific subpopulations of cells. Static fluorescent molecules, such as GFP and YFP, can fill neurons and report structural changes such as spine turnover[108]. Genetically encoded pH sensors, glutamate sensors, and voltage indicators have all had several generations of development, with increasing sensitivity. For tracking neuronal activity, voltage indicators are exciting as they are a direct reporter of potential changes across the neurons. Although they are a less direct reporter of neuronal activity, genetically encoded calcium indicators (GECIs) have gained widespread use in neuroscience research. The development of GECI indicators has been very successful, and the recently described GCaMP6s produce a maximum fluorescent change over 50x that of Twitch-2B, a commonly used voltage indicator. The same neurons can be tracked in large-scale calcium datasets in behaving mice over multiple days[109]. Researchers can easily customize a cover glass to image hundreds of thousands of neurons112 simultaneously. One study used GCaMP to closely monitor motor learning during a forelimb lever-press in live rodents: inhibitory neurons were found to have stable activity, while excitatory neurons initially had a highly variable activity refined later[110]. As demonstrated here, two-photon microscopy is a versatile technique for tracking neuronal activity before and after an acute event, such as ischemia. The precise application of GCaMP in the current experiments will be described in greater detail in Section 3.2, while correlations between neurons as a biological readout are discussed in Section 3.3.

In Vivo imaging after stroke in animal models

A handful of studies have employed two-photon imaging to stroke in mouse models and have already contributed novel data on the morphology and activity of the peri-infarct. Of course, each study has its own sets of limitations based on the technicalities of the experiments: the

fluorescent reporter used, the field of view which is recorded, and the methods used for analyzing the signal.

Two-photon studies of cell morphology have already demonstrated significant effects in the peri-infarct after stroke, although they do not measure the activity of the cells. One study used GFP-expressing transgenic mice to image spine dynamics and blood flow after a somatosensory stroke[7]. This study tracked the dendritic spines of neurons over three months and found a significant decrease in spine density in peri-infarct neurons than the sham controls. This study concluded that the degree of ischemia predicts the dendritic spine changes in excitatory neurons. Interestingly, angiogenesis was not noted in the peri-infarct after stroke, contradicting prior studies. An earlier study used two-photon imaging to demonstrate that the vascular system redistributes blood flow after small and large strokes[111]. *In vivo* imaging of the spinal cord has provided evidence for Wallerian degeneration, axonal outgrowth, and vascular coupling after an induced injury[112]. These studies highlight the ability of *in vivo* imaging to capture morphological changes after an acute event, such as stroke. Of course, not all changes will involve significant morphological changes; for functional changes after stroke, a functional reporter, such as a GECI or GEVI, is required.

In vivo calcium imaging was used to track the activity of single somatosensory neurons after stroke[113]. GCaMP was used to track the same neurons over 2-8 weeks after a somatosensory stroke in anesthetized mice, and their response to limb stimulation was measured. Neurons that were initially specific to one limb became active to multiple limbs; these changes to limb selectivity peaked one month after stroke and returned to their single-limb selectivity by two months out. This study suggests a period of plasticity that expands peri-infarct neurons' excitability, followed by a later retraction to their regular activity. This study indicates that

neuronal excitability and functional connectivity (FC) are linked, but this hypothesis requires further scrutiny. Section 3.3 will explore the theory and modeling of FC, and its use in human noninvasive imaging will be evaluated, setting up the use of FC as a primary analytical method of assessing calcium imaging in the present experiments.

Lower-magnification objectives can capture a wide field of view in exchange for decreased resolution. This adjustment is effective for mesoscale and macroscale studies of the cortex. Transgenic GCaMP-expressing mice were imaged with widefield calcium imaging of the entire cortex. Photothrombotic stroke was applied to the motor cortex and demonstrated increased autofluorescence ipsilesionally. This increased autofluorescence decreased back to normal by Day 56 after stroke and is likely a marker of stroke toxicity[114]. This whole-brain GCaMP data from the mouse is analogous to the noninvasive functional imaging studies in humans, thus lending itself to FC analysis. The group also identified FC changes across ten networks and found that the ipsilesional cortex had decreased FC across these networks after stroke, but this FC normalized by Day 56. The contralesional cortex, in contrast, had significantly higher FC consistently from Day 1-28. It is important to note that these studies are in anesthetized mice, not while participating in a motor task, and the authors state this as a potential inhibitory force on the measured FC.

A recent study in the Carmichael lab further investigated the usefulness of FC in live brain imaging of mouse circuits[115]. This study used a high-resolution objective to image the same population of excitatory and inhibitory neurons over a few months. Mice were randomly given a stroke or sham, and imaging continued and freely moved during their head-fixed imaging. This study found decreases in FC in both the motor and premotor cortex after stroke. Still, there were subtle changes between the motion and non-motion behavioral states and differences between

excitatory and inhibitory neurons. The methods in this study are further evaluated in Section 3.3, as it is similar to the FC analysis in the present studies of this thesis.

Section 2.5 Phosphodiesterases in Physiology and Disease

Phosphodiesterases (PDEs) are a super-family of enzymes that hydrolyze phosphodiester bonds in cyclic nucleotides, namely cyclic adenosine monophosphate (cAMP) and cyclic guanosine monophosphate (cGMP). As introduced in Section 2.2, the intracellular concentrations of these cyclic molecules relay critical messages in practically every animal cell. These studies have identified PDEs as the enzymes that inactivate cAMP/cGMP, and caffeine was the first proposed partial PDE inhibitor. By producing cAMP and cGMP, cyclases function as an excitatory counterpart to the inhibitory PDEs.

The far-reaching effects of cAMP and cGMP include transcriptional and post-translational changes. Protein Kinase A (PKA) is a family of proteins activated by intracellular cAMP, releasing its catalytic subunit to phosphorylate nearby targets. Furthermore, the cAMP-response-element (CRE) was noted as a nucleotide sequence that acts as an enhancer for specific genes when cAMP was present. CREB (CRE-Binding protein) was discovered as the link between cAMP, PKA, and transcriptional regulation, as it binds CRE sites and acts as a transcription factor when phosphorylated by PKA. Likewise, the family of cGMP-dependent kinases, Protein Kinase G (PKG), are activated by intracellular cGMP and phosphorylate their own series of targets.

PDE Enzymes: The brakes of the cAMP/cGMP systems

Regulation of intracellular cAMP and cGMP levels is critical to optimize the cell's resources regarding these diverse functions, and thus PDEs must also be tightly controlled. In the context of disease, PDE inhibitors offer investigators an opportunity to modulate this critical system. By

decreasing the breakdown of cAMP and cGMP, the effector molecules described above are essentially enhanced. While these findings indicate that PDE inhibitors are an up-and-coming class of drugs, they equally suggest caution and subtlety when manipulating such critical components of cell biology. PDE inhibitors certainly warrant further investigation by researchers, especially selective inhibition based on subfamily localization in tissue. For example, drugs developed for stroke recovery would be well-served by decreasing any effects outside the central nervous system.

Three sub-families of PDE enzymes were initially proposed: cAMP-specific, cGMP-specific, and calmodulin-sensitive PDEs[116]. With advancements to sequencing and molecular expression assays, PDE enzymes were divided into 11 families with several identified isoforms within each family. A catalytic domain is shared between all PDEs and is located in the carboxy-terminal portion. Family-specific domains determine cAMP and cGMP affinity, while yet other domains bind a modulator, such as calmodulin, and change their activity when it is attached. For example, PDE4 and PDE8 are cAMP selective, while PDE5 has a higher affinity for cGMP hydrolysis.

Furthermore, cAMP can act as a modulator to PDE11, while cGMP inhibits PDE3 but activates PDE2. As highlighted here, the peptide domains observed in the PDE enzymes allow for various isoenzymes expressed for a particular purpose. The diversity of these enzymes helps to explain the diverse expression of PDE isoenzymes in different tissue. Several comprehensive reviews have gathered tissue expression data for each family and the phenotypes of specific genetic knockouts of a particular PDE family[117–119]. An individual PDE gene expression may be broad, localized to a particular type of cell, or even compartmentalized within a cell, such as the plasma membrane, mitochondria, or the Golgi[116].

Biological research on cyclic nucleotides and PDEs has already had a tremendous impact on human health through PDE inhibitors. Although many PDE-family selective inhibitors have been

synthesized, only a select number of second-generation compounds have been approved for clinical use, while dozens of others are either in development or trial for approval. Highlighted below are brief historical discussions of three PDE families and approved the clinical use of their inhibitors: PDE3, PDE4, and PDE5.

PDE Inhibition in medicine

PDE3: The PDE3 family has four identified variants, is activated by cGMP and has a catalytic affinity for cAMP. PDE3 genes were expressed broadly but significantly more so in cardiac and vascular myocytes[117]. PDE3 inhibition has been shown to relax vascular myocytes, inhibit platelet aggregation and produce a robust inotropic response in cardiac myocyteshis[120]. Milrinone, a PDE3 inhibitor known as Primacor, was developed for congestive heart failure, but chronic use was associated with increased mortality[121]. This finding was likely due to increased arrhythmias and cardiac arrest. Acute use of milrinone is still approved for decompensated heart failure or patients awaiting transplant. Cilostazol, another PDE3 inhibitor known as Pletal, was developed for intermittent claudication, a painful vascular disease caused by ischemia to the lower extremities. Cilostazol was shown to decrease pain symptoms and increase walking distance in patients on the drug[122].

PDE4: PDE4 is the most prominent family of PDE molecules and includes multiple variants under four subfamilies: PDE4A-D. These enzymes are broadly expressed in the body but significantly so in inflammatory cells[123]. PDE 4 inhibition was also noted to regulate immune functions, relax airway myocytes[124], and successfully rescues acute inflammation in animal models of asthma[125].

Rolipram, a potent PDE4 inhibitor, was designed in the 1970s as a potential therapeutic for inflammatory lung diseases, such as asthma, COPD, and pulmonary fibrosis. These diseases are

characterized by airway inflammation, and obstruction of breathing and rolipram decreased this progression. Likely due to PDE4 expression in the gastrointestinal system; however, rolipram exhibited significant side effects of nausea, emesis, and diarrhea, which halted its clinical development[126]. The high promise of PDE4 as a target has encouraged two orally active PDE4 selective inhibitors: cilomilast and roflumilast[127]. These second-generation PDE4 inhibitors have both shown promising anti-inflammatory and bronchodilatory effects, but the only roflumilast has gained FDA approval for COPD exacerbations.

Rolipram was also noted to increase cAMP levels in the brain and have positive cognitive and mood effects. Rolipram has been investigated as a treatment for depression, but its side-effect profile hampered its positive impact. Further discussion of PDE inhibition in the CNS will be covered in Section 3.2, as it more directly relates to PDE inhibition as a stroke treatment.

PDE5: Three variants of the PDE5 family have been identified, all of which are cGMP activated catalyze its breakdown, thus acting as a negative feedback loop for cGMP. PDE5 was first identified in rat platelets, and an early PDE5 inhibitor (Zaprinast) was initially designed as a bronchodilator for allergic reactions. While Zaprimast did have mild bronchodilatory effects, it was quickly determined to induce vascular smooth muscle relaxation[128] and was considered a candidate for cardiovascular disease. Shortly after, Pfizer designed sildenafil, a PDE5 inhibitor that was approximately 240 times more potent than Zaprinast[128]. In 1991, studies commenced trying sildenafil as a treatment for angina[129], but it did not significantly improve nitrate therapy. In a serendipitously profitable accident for Pfizer, penile erection was a commonly reported side effect.

The discovery of nitrogen oxide (NO) as an essential negative regulator of vascular tone was awarded the Nobel Prize in 1998. NO was shown to activate guanylyl cyclase, increasing cGMP

and hyperpolarizing the cell. In smooth muscle, cGMP activates phosphatases which dephosphorylate myosin light chains and allows these cells to relax. In males, penile erection requires NO-induced vasodilation and is thus dependent on cGMP concentration. PDE5 enzymes were are highly expressed in the corpus cavernosum of the penis and were suspected of exacerbating erectile dysfunction by catalyzing cGMP. Capitalizing on this biology, Pfizer began clinical trials examining sildenafil as a treatment for erectile dysfunction in 1993, and sildenafil was FDA-approved for the ailment. Vardenafil, Tadalafil, and Avanafil are second-generation PDE5 inhibitors that have been developed and approved for erectile dysfunction, with slightly different half-lives and side-effect profiles. Furthermore, additional doses of sildenafil, tadalafil, and vardenafil are marketed and approved for treating pulmonary hypertension due to their vasodilatory effects on the smooth muscle of the lungs[130].

Section 2.6 Figures

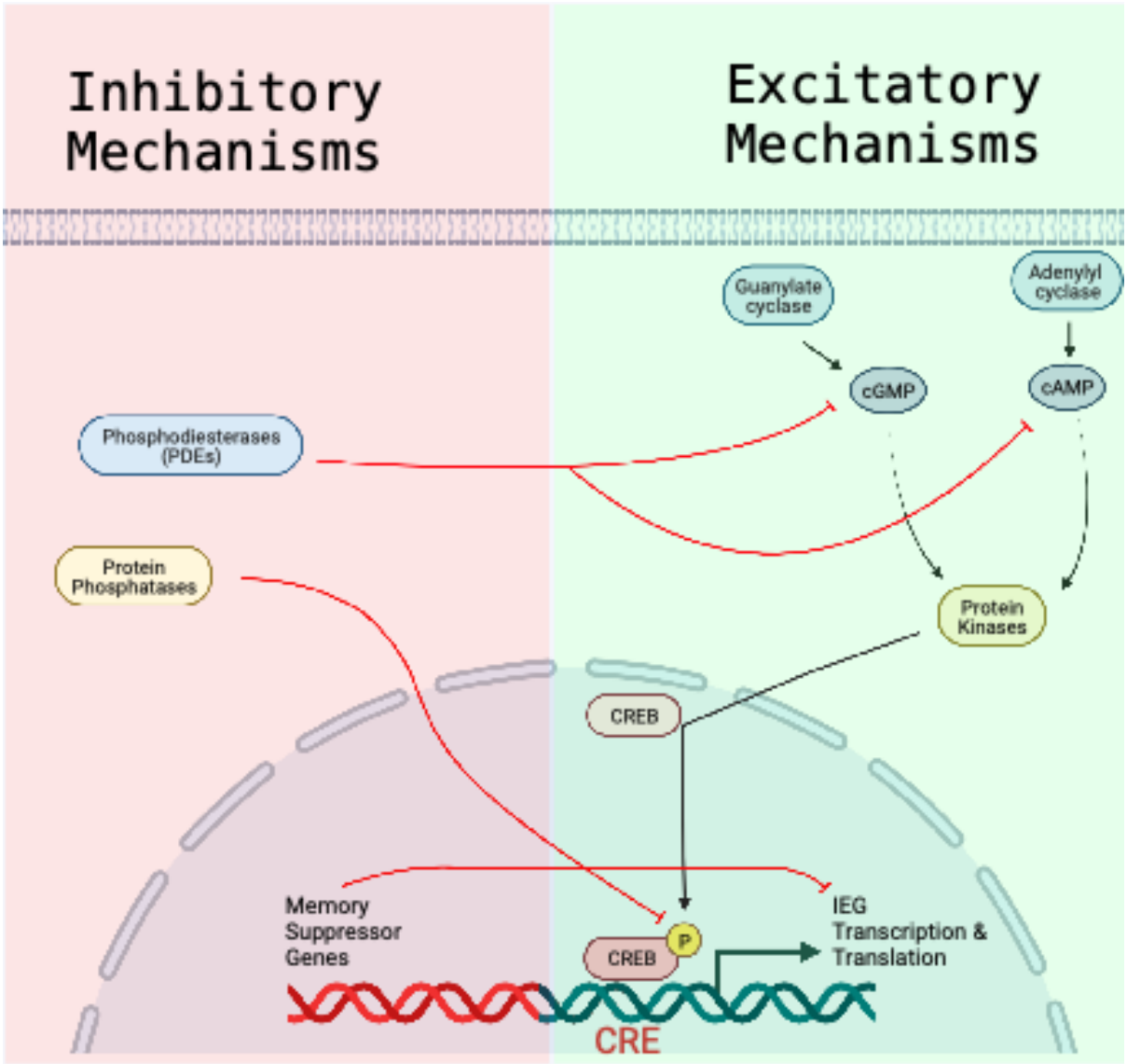

Figure 2.1 Excitatory and inhibitory mechanisms in neurons are in a dynamic homeostasis during learning and recovery. PDEs catalyze cAMP and cGMP, suppressing their excitatory effects. PDE inhibitors increase cAMP/cGMP levels and has a stimulatory effect on excitability.

Section 2.7 References

1. Carmichael, S. T. Brain excitability in stroke: The yin and yang of stroke progression. *Arch. Neurol.* **69**, 161–167 (2012).
2. Lee, J. M., Grabb, M. C., Zipfel, G. J. & Choi, D. W. Brain tissue responses to ischemia. *J. Clin. Invest.* **106**, 723–731 (2000).
3. Saver, J. L. Time is brain - Quantified. *Stroke* **37**, 263–266 (2006).
4. Sigler, A. & Murphy, T. H. In vivo 2-photon imaging of fine structure in the rodent brain: Before, during, and after stroke. *Stroke* **41**, S117–S123 (2010).
5. Thomas Carmichael, S. Emergent properties of neural repair: Elemental biology to therapeutic concepts. *Ann. Neurol.* **79**, 895–906 (2016).
6. Choi, D. W. Calcium-mediated neurotoxicity: relationship to specific channel types and role in ischemic damage. *Trends Neurosci.* **11**, 465–469 (1988).
7. Mostany, R. *et al.* Local hemodynamics dictate long-term dendritic plasticity in peri-infarct cortex. *J. Neurosci.* **30**, 14116–14126 (2010).
8. Carmichael, S. T. *et al.* Growth-associated gene expression after stroke: Evidence for a growth-promoting region in peri-infarct cortex. *Exp. Neurol.* **193**, 291–311 (2005).
9. Li, S. *et al.* An age-related sprouting transcriptome provides molecular control of axonal sprouting after stroke. *Nat. Neurosci.* **13**, 1496–1506 (2010).
10. Li, S. *et al.* GDF10 is a signal for axonal sprouting and functional recovery after stroke. *Nat. Neurosci.* **18**, 1737–1745 (2015).
11. Minami, M., Kuraishi, Y., Yabuuchi, K., Yamazaki, A. & Satoh, M. Induction of Interleukin-1β mRNA in Rat Brain After Transient Forebrain Ischemia. *J. Neurochem.* **58**, 390–392 (1992).

12. Taupin, V., Toulmond, S., Serrano, A., Benavides, J. & Zavala, F. Increase in IL-6, IL-1 and TNF levels in rat brain following traumatic lesion. Influence of pre- and post-traumatic treatment with Ro5 4864, a peripheral-type (p site) benzodiazepine ligand. *J. Neuroimmunol.* **42**, 177–185 (1993).

13. Toulmond, S., Vige, X., Fage, D. & Benavides, J. Local infusion of interleukin-6 attenuates the neurotoxic effects of NMDA on rat striatal cholinergic neurons. *Neurosci. Lett.* **144**, 49–52 (1992).

14. Campbell, I. L. *et al.* Neurologic disease induced in transgenic mice by cerebral overexpression of interleukin 6. *Proc. Natl. Acad. Sci. U. S. A.* **90**, 10061–10065 (1993).

15. Rothwell, N. J. & Hopkins, S. J. Cytokines and the nervous system II: actions and mechanisms of action. *Trends Neurosci.* **18**, 130–136 (1995).

16. Logan, A. & Berry, M. Transforming growth factor-ß1 and basic fibroblast growth factor in the injured CNS. *Trends Pharmacol. Sci.* **14**, 337–343 (1993).

17. Rothwell, N., Allan, S. & Toulmond, S. Perspectives Series: Cytokines and The Brain The Role of Interleukin 1 in Acute Neurodegeneration and Stroke: Pathophysiological and Therapeutic Implications. *J. Clin. Invest* **100**, 2648–2652 (1997).

18. Pringle, A. K., Niyadurupola, N., Johns, P., Anthony, D. C. & Iannotti, F. Interleukin-1β exacerbates hypoxia-induced neuronal damage, but attenuates toxicity produced by simulated ischaemia and excitotoxicity in rat organotypic hippocampal slice cultures. *Neurosci. Lett.* **305**, 29–32 (2001).

19. Arvidsson, A., Collin, T., Kirik, D., Kokaia, Z. & Lindvall, O. Neuronal replacement from endogenous precursors in the adult brain after stroke. *Nat. Med.* **8**, 963–970 (2002).

20. Parent, J. M., Vexler, Z. S., Gong, C., Derugin, N. & Ferriero, D. M. Rat forebrain

neurogenesis and striatal neuron replacement after focal stroke. *Ann. Neurol.* **52**, 802–813 (2002).

21. Tsai, P. T. *et al.* A critical role of erythropoietin receptor in neurogenesis and post-stroke recovery. *J. Neurosci.* **26**, 1269–1274 (2006).
22. Ohab, J. J., Fleming, S., Blesch, A. & Carmichael, S. T. A neurovascular niche for neurogenesis after stroke. *J. Neurosci.* **26**, 13007–13016 (2006).
23. Rothstein, J. D., Van Kammen, M., Levey, A. I., Martin, L. J. & Kuncl, R. W. Selective loss of glial glutamate transporter GLT-1 in amyotrophic lateral sclerosis. *Ann. Neurol.* **38**, 73–84 (1995).
24. Dallas, M. *et al.* Hypoxia suppresses glutamate transport in astrocytes. *J. Neurosci.* **27**, 3946–3955 (2007).
25. Zhao, Y. & Rempe, D. A. Targeting Astrocytes for Stroke Therapy. *Neurotherapeutics* **7**, 439–451 (2010).
26. Overman, J. J. *et al.* A role for ephrin-A5 in axonal sprouting, recovery, and activity-dependent plasticity after stroke. *Proc. Natl. Acad. Sci. U. S. A.* **109**, E2230-9 (2012).
27. Taylor, R. A. & Sansing, L. H. Microglial responses after ischemic stroke and intracerebral hemorrhage. *Clin. Dev. Immunol.* **2013**, (2013).
28. Lømo, T. The discovery of long-term potentiation. doi:10.1098/rstb.2002.1226.
29. Mayford, M. *et al.* Control of memory formation through regulated expression of a CaMKII transgene. *Science (80-.).* **274**, 1678–1683 (1996).
30. Brunelli, M., Castellucci, V. & Kandel, E. R. Synaptic facilitation and behavioral sensitization in Aplysia: Possible role of serotonin and cyclic AMP. *Science (80-.).* **194**, 1178–1181 (1976).

31. Ashman, D. F., Lipton, R., Melicow, M. M. & Price, T. D. Isolation of adenosine 3′,5′-monophosphate and guanosine 3′,5′-monophosphate from rat urine. *Biochem. Biophys. Res. Commun.* **11**, 330–334 (1963).

32. Ghalayini, I. F. Nitric oxide-cyclic GMP pathway with some emphasis on cavernosal contractility. *International Journal of Impotence Research* vol. 16 459–469 (2004).

33. Corbin, J. D. & Krebs, E. G. A cyclic AMP - stimulated protein kinase in adipose tissue. *Biochem. Biophys. Res. Commun.* **36**, 328–336 (1969).

34. Hilfiker, S., Czernik, A. J., Greengard, P. & Augustine, G. J. Tonically active protein kinase A regulates neurotransmitter release at the squid giant synapse. *J. Physiol.* **531**, 141–146 (2001).

35. Montarolo, P. G. *et al.* A critical period for macromolecular synthesis in long-term heterosynaptic facilitation in Aplysia. *Science (80-.).* **234**, 1249–1254 (1986).

36. Felinski, E. A., Kim, J., Lu, J. & Quinn, P. G. Recruitment of an RNA Polymerase II Complex Is Mediated by the Constitutive Activation Domain in CREB, Independently of CREB Phosphorylation. *Mol. Cell. Biol.* **21**, 1001–1010 (2001).

37. Dash, P. K., Hochner, B. & Kandel, E. R. Injection of the cAMP-responsive element into the nucleus of Aplysia sensory neurons blocks long-term facilitation. *Nature* **345**, 718–721 (1990).

38. Zukin, R. S., Jover, T., Yokota, H., Simionescu, M. & Geofflau, C. Molecular and Cellular Mechanisms of Ischemia-Induced Neuronal Death. doi:10.1016/B0-443-06600-0/50049-3.

39. Abel, T., Martin, K. C., Bartsch, D. & Kandel, E. R. Memory suppressor genes: Inhibitory constraints on the storage of long- term memory. *Science (80-.).* **279**, 338–341 (1998).

40. Silva, A. J., Zhou, Y., Rogerson, T., Shobe, J. & Balaji, J. Molecular and cellular approaches to memory allocation in neural circuits. *Science (80-.).* **326**, 391–395 (2009).

41. Han, J. H. *et al.* Neuronal competition and selection during memory formation. *Science (80-.).* **316**, 457–460 (2007).

42. Han, J.-H. H. *et al.* Selective Erasure of a Fear Memory. *Science (80-.).* **323**, 1492–1496 (2009).

43. Zhou, Y. *et al.* CREB regulates excitability and the allocation of memory to subsets of neurons in the amygdala. *Nat. Neurosci.* **12**, 1438–1443 (2009).

44. Aimone, J. B., Wiles, J. & Gage, F. H. Potential role for adult neurogenesis in the encoding of time in new memories. *Nat. Neurosci.* **9**, 723–727 (2006).

45. Harvey, C. D. & Svoboda, K. Locally dynamic synaptic learning rules in pyramidal neuron dendrites. *Nature* **450**, 1195–1200 (2007).

46. Gdalyahu, A. *et al.* Associative fear learning enhances sparse network coding in primary sensory cortex. *Neuron* **75**, 121–132 (2012).

47. Josselyn, S. A., Köhler, S. & Frankland, P. W. Finding the engram. *Nat. Rev. Neurosci.* **16**, 521–534 (2015).

48. Pignatelli, M. *et al.* Engram Cell Excitability State Determines the Efficacy of Memory Retrieval. *Neuron* **101**, 274-284.e5 (2019).

49. Reijmers, L. G., Perkins, B. L., Matsuo, N. & Mayford, M. Localization of a stable neural correlate of associative memory. *Science (80-.).* **317**, 1230–1233 (2007).

50. Josselyn, S. A. *et al.* Long-term memory is facilitated by cAMP response element-binding protein overexpression in the amygdala. *J. Neurosci.* **21**, 2404–2412 (2001).

51. Masamizu, Y. *et al.* Two distinct layer-specific dynamics of cortical ensembles during

learning of a motor task. *Nat. Neurosci.* **17**, 987–994 (2014).

52. Liu, X. *et al.* Optogenetic stimulation of a hippocampal engram activates fear memory recall. *Nature* **484**, 381–385 (2012).

53. Cai, D. J. *et al.* A shared neural ensemble links distinct contextual memories encoded close in time. *Nature* **534**, 115–118 (2016).

54. Caroni, P., Donato, F. & Muller, D. Structural plasticity upon learning: Regulation and functions. *Nat. Rev. Neurosci.* **13**, 478–490 (2012).

55. Xu, T. *et al.* Rapid formation and selective stabilization of synapses for enduring motor memories. *Nature* **462**, 915–919 (2009).

56. Tennant, K. A. *et al.* The organization of the forelimb representation of the C57BL/6 mouse motor cortex as defined by intracortical microstimulation and cytoarchitecture. *Cereb. Cortex* **21**, 865–876 (2011).

57. Tennant, K. A. *et al.* Skill learning induced plasticity of motor cortical representations is time and age-dependent. *Neurobiol. Learn. Mem.* **98**, 291–302 (2012).

58. Guo, J. Z. *et al.* Cortex commands the performance of skilled movement. *Elife* **4**, 1–18 (2015).

59. Kawai, R. *et al.* Motor Cortex Is Required for Learning but Not for Executing a Motor Skill. *Neuron* **86**, 800–812 (2015).

60. Cao, V. Y. *et al.* Motor Learning Consolidates Arc-Expressing Neuronal Ensembles in Secondary Motor Cortex. *Neuron* **86**, 1385–1392 (2015).

61. Li, N., Chen, T. W., Guo, Z. V., Gerfen, C. R. & Svoboda, K. A motor cortex circuit for motor planning and movement. *Nature* **519**, 51–56 (2015).

62. Willett, F. R. *et al.* Hand Knob Area of Premotor Cortex Represents the Whole Body in a

Compositional Way. *Cell* **181**, 396-409.e26 (2020).

63. Nudo, R. J. Recovery after brain injury: Mechanisms and principles. *Front. Hum. Neurosci.* **7**, 887 (2013).

64. Carmichael, S. T. The 3 Rs of Stroke Biology: Radial, Relayed, and Regenerative. *Neurotherapeutics* **13**, 348–359 (2016).

65. Benowitz, L. I. & Thomas Carmichael, S. Promoting Axonal rewiring to improve outcome after stroke. *Neurobiol. Dis.* (2010).

66. Overman, J. J. & Carmichael, S. T. Plasticity in the injured brain: More than molecules matter. *Neuroscientist* **20**, 15–28 (2014).

67. Dancause, N. *et al.* Extensive cortical rewiring after brain injury. *J. Neurosci.* **25**, 10167–10179 (2005).

68. Hobohm, C. *et al.* Decomposition and long-lasting downregulation of extracellular matrix in perineuronal nets induced by focal cerebral ischemia in rats. *J. Neurosci. Res.* **80**, 539–548 (2005).

69. Jones, T. A. & Schallert, T. Overgrowth and pruning of dendrites in adult rats recovering from neocortical damage. *Brain Res.* **581**, 156–160 (1992).

70. Zhang, S., Boyd, J., Delaney, K. & Murphy, T. H. Rapid reversible changes in dendritic spine structure in vivo gated by the degree of ischemia. *J. Neurosci.* **25**, 5333–5338 (2005).

71. Brown, C. E., Li, P., Boyd, J. D., Delaney, K. R. & Murphy, T. H. Extensive turnover of dendritic spines and vascular remodeling in cortical tissues recovering from stroke. *J. Neurosci.* **27**, 4101–4109 (2007).

72. Plautz, E. J. *et al.* Post-infarct cortical plasticity and behavioral recovery using concurrent

cortical stimulation and rehabilitative training: A feasibility study in primates. *Neurol. Res.* **25**, 801–810 (2003).

73. Zeiler, S. R. *et al.* Medial premotor cortex shows a reduction in inhibitory markers and mediates recovery in a mouse model of focal stroke. *Stroke* **44**, 483–489 (2013).

74. Zhang, R. L., Zhang, Z. G. & Chopp, M. Ischemic stroke and neurogenesis in the subventricular zone. *Neuropharmacology* **55**, 345–352 (2008).

75. Chen, Z. Y. *et al.* Variant Brain-Derived Neurotrophic Factor (BDNF) (Met66) Alters the Intracellular Trafficking and Activity-Dependent Secretion of Wild-Type BDNF in Neurosecretory Cells and Cortical Neurons. *J. Neurosci.* **24**, 4401–4411 (2004).

76. Clarkson, A. N., Parker, K., Nilsson, M., Walker, F. R. & Gowing, E. K. Combined ampakine and BDNF treatments enhance poststroke functional recovery in aged mice via AKT-CREB signaling. *J. Cereb. Blood Flow Metab.* **35**, 1272–1279 (2015).

77. Macas, J., Nern, C., Plate, K. H. & Momma, S. Increased generation of neuronal progenitors after ischemic injury in the aged adult human forebrain. *J. Neurosci.* **26**, 13114–13119 (2006).

78. Murphy, T. H., Li, P., Betts, K. & Liu, R. Two-photon imaging of stroke onset in vivo reveals that NMDA-receptor independent ischemic depolarization is the major cause of rapid reversible damage to dendrites and spines. *J. Neurosci.* **28**, 1756–1772 (2008).

79. Clarkson, A. N., Huang, B. S., MacIsaac, S. E., Mody, I. & Carmichael, S. T. Reducing excessive GABA-mediated tonic inhibition promotes functional recovery after stroke. *Nature* **468**, 305–309 (2010).

80. Nudo, R. J. & Milliken, G. W. Reorganization of movement representations in primary motor cortex following focal ischemic infarcts in adult squirrel monkeys. *J. Neurophysiol.*

75, 2144–2149 (1996).

81. Redecker, C., Wang, W., Fritschy, J. M. & Witte, O. W. Widespread and long-lasting alterations in GABAA-receptor subtypes after focal cortical infarcts in rats: Mediation by NMDA-dependent processes. *J. Cereb. Blood Flow Metab.* **22**, 1463–1475 (2002).

82. Hu, B. R., Fux, C. M., Martone, M. E., Zivin, J. A. & Ellisman, M. H. Persistent phosphorylation of cyclic amp responsive element-binding protein and activating transcription factor-2 transcription factors following transient cerebral ischemia in rat brain. *Neuroscience* **89**, 437–452 (1999).

83. Young, D., Lawlor, P. A., Leone, P., Dragunow, M. & During, M. J. Environmental enrichment inhibits spontaneous apoptosis, prevents seizures and is neuroprotective. *Nat. Med.* **5**, 448–453 (1999).

84. Walton, M. R. & Dragunow, M. Is CREB a key to neuronal survival? *Trends Neurosci.* **23**, 48–53 (2000).

85. Cox, L. J., Hengst, U., Gurskaya, N. G., Lukyanov, K. A. & Jaffrey, S. R. Intra-axonal translation and retrograde trafficking of CREB promotes neuronal survival. *Nat. Cell Biol.* **10**, 149–159 (2008).

86. Sugiura, S. *et al.* CRE-Mediated Gene Transcription in the Peri-Infarct Area after Focal Cerebral Ischemia in Mice. *J. Neurosci. Res.* **75**, 401–407 (2004).

87. Caracciolo, L. *et al.* CREB controls cortical circuit plasticity and functional recovery after stroke. *Nat. Commun.* **9**, (2018).

88. Okabe, N. *et al.* Rehabilitative skilled forelimb training enhances axonal remodeling in the corticospinal pathway but not the brainstem-spinal pathways after photothrombotic stroke in the primary motor cortex. (2017) doi:10.1371/journal.pone.0187413.

89. Ottenbacher, K. J. & Jannell, S. The results of clinical trials in stroke rehabilitation research. *Arch. Neurol.* **50**, 37–44 (1993).

90. Maulden, S. A., Gassaway, J., Horn, S. D., Smout, R. J. & DeJong, G. Timing of initiation of rehabilitation after stroke. *Arch. Phys. Med. Rehabil.* **86**, 34–40 (2005).

91. Kim, S. Y. *et al.* Experience with the "good" limb induces aberrant synaptic plasticity in the perilesion cortex after stroke. *J. Neurosci.* **35**, 8604–8610 (2015).

92. Taub, E., Crago, J. E. & Uswatte, G. Constraint-induced movement therapy: A new approach to treatment in physical rehabilitation. *Rehabil. Psychol.* **43**, 152–170 (1998).

93. Wolf, S. L., Winstein, C. J., Miller, J. P. & Morris, D. Effect of Constraint-Induced Movement. *Jama* **296**, 2095–2104 (2006).

94. Milliken, G. W., Plautz, E. J. & Nudo, R. J. Distal forelimb representations in primary motor cortex are redistributed after forelimb restriction: A longitudinal study in adult squirrel monkeys. *J. Neurophysiol.* **109**, 1268–1282 (2013).

95. Kozlowski, D. A., James, D. C. & Schallert, T. Use-dependent exaggeration of neuronal injury after unilateral sensorimotor cortex lesions. *J. Neurosci.* **16**, 4776–4786 (1996).

96. Dromerick, A. W. *et al.* Very early constraint-induced movement during stroke rehabilitation (VECTORS): A single-center RCT. *Neurology* **73**, 195–201 (2009).

97. Krakauer, J. W., Carmichael, S. T., Corbett, D. & Wittenberg, G. F. Getting neurorehabilitation right: What can be learned from animal models? *Neurorehabil. Neural Repair* **26**, 923–931 (2012).

98. Schlaug, G., Renga, V. & Nair, D. Transcranial direct current stimulation in stroke recovery. *Arch. Neurol.* **65**, 1571–1576 (2008).

99. Antal, A., Kincses, T. Z., Nitsche, M. A. & Paulus, W. Modulation of moving phosphene

thresholds by transcranial direct current stimulation of V1 in human. *Neuropsychologia* **41**, 1802–1807 (2003).

100. Hummel, F. & Cohen, L. G. Improvement of motor function with noninvasive cortical stimulation in a patient with chronic stroke. *Neurorehabil. Neural Repair* **19**, 14–19 (2005).

101. Khedr, E. M., Ahmed, M. A., Fathy, N. & Rothwell, J. C. Therapeutic trial of repetitive transcranial magnetic stimulation after acute ischemic stroke. *Neurology* **65**, 466–468 (2005).

102. Brodie, S. M., Meehan, S., Borich, M. R. & Boyd, L. A. 5 Hz repetitive transcranial magnetic stimulation over the ipsilesional sensory cortex enhances motor learning after stroke. *Front. Hum. Neurosci.* **8**, 143 (2014).

103. Talelli, P. E. *et al.* Theta burst stimulation in the rehabilitation of the upper limb: A semirandomized, placebo-controlled trial in chronic stroke patients. *Neurorehabil. Neural Repair* **26**, 976–987 (2012).

104. Nouri, S. & Cramer, S. C. Anatomy and physiology predict response to motor cortex stimulation after stroke. *Neurology* **77**, 1076–1083 (2011).

105. Harvey, R. L. & Winstein, C. J. Design for the Everest Randomized Trial of Cortical Stimulation and Rehabilitation for Arm Function Following Stroke. (2008) doi:10.1177/1545968308317532.

106. Emiliani, V., Cohen, A. E., Deisseroth, K. & Häusser, M. All-optical interrogation of neural circuits. *J. Neurosci.* **35**, 13917–13926 (2015).

107. Stosiek, C., Garaschuk, O., Holthoff, K. & Konnerth, A. In vivo two-photon calcium imaging of neuronal networks. *Proc. Natl. Acad. Sci. U. S. A.* **100**, 7319–7324 (2003).

108. Lin, M. Z. & Schnitzer, M. J. Genetically encoded indicators of neuronal activity. *Nat. Neurosci.* **19**, 1142–1153 (2016).

109. Sheintuch, L. *et al.* Tracking the Same Neurons across Multiple Days in Ca2+ Imaging Data. *Cell Rep.* **21**, 1102–1115 (2017).

110. Peters, A. J., Chen, S. X. & Komiyama, T. Emergence of reproducible spatiotemporal activity during motor learning. *Nature* **510**, 263–267 (2014).

111. Schaffer, C. B. *et al.* Two-photon imaging of cortical surface microvessels reveals a robust redistribution in blood flow after vascular occlusion. *PLoS Biol.* **4**, 258–270 (2006).

112. Denecke, C. K., Aljović, A. & Bareyre, F. M. Combining molecular intervention with in vivo imaging to untangle mechanisms of axon pathology and outgrowth following spinal cord injury. *Experimental Neurology* vol. 318 1–11 (2019).

113. Winship, I. R. & Murphy, T. H. In vivo calcium imaging reveals functional rewiring of single somatosensory neurons after stroke. *J. Neurosci.* **28**, 6592–6606 (2008).

114. Cramer, J. V. *et al.* In vivo widefield calcium imaging of the mouse cortex for analysis of network connectivity in health and brain disease. *Neuroimage* **199**, 570–584 (2019).

115. Latifi, S. *et al.* Neuronal network topology indicates distinct recovery processes after stroke. *Cereb. Cortex* **30**, 6363–6375 (2020).

116. Maurice, D. H. *et al.* Advances in targeting cyclic nucleotide phosphodiesterases. *Nat. Rev. Drug Discov.* **13**, 290–314 (2014).

117. Conti, M. & Beavo, J. Biochemistry and physiology of cyclic nucleotide phosphodiesterases: Essential components in cyclic nucleotide signaling. *Annual Review of Biochemistry* (2007) doi:10.1146/annurev.biochem.76.060305.150444.

118. Francis, S. H., Blount, M. A. & Corbin, J. D. Mammalian cyclic nucleotide

phosphodiesterases: Molecular mechanisms and physiological functions. *Physiol. Rev.* (2011) doi:10.1152/physrev.00030.2010.

119. Keravis, T. & Lugnier, C. Cyclic nucleotide phosphodiesterase (PDE) isozymes as targets of the intracellular signalling network: Benefits of PDE inhibitors in various diseases and perspectives for future therapeutic developments. *British Journal of Pharmacology* (2012) doi:10.1111/j.1476-5381.2011.01729.x.

120. Schudt, C., Hatzelmann, A., Beume, R. & Tenor, H. *Phosphodiesterase inhibitors: History of pharmacology*. *Handbook of Experimental Pharmacology* vol. 204 (2011).

121. Packer, M. *et al.* Effect of Oral Milrinone on Mortality in Severe Chronic Heart Failure. *N. Engl. J. Med.* **325**, 1468–1475 (1991).

122. Kanlop, N., Chattipakorn, S. & Chattipakorn, N. Effects of cilostazol in the heart. *J. Cardiovasc. Med.* **12**, 88–95 (2011).

123. TORPHY, T. J. Phosphodiesterase Isozymes. *Am. J. Respir. Crit. Care Med.* **157**, 351–370 (1998).

124. Tralau-Stewart, C. J. *et al.* GSK256066, an exceptionally high-affinity and selective inhibitor of phosphodiesterase 4 suitable for administration by inhalation: In vitro, kinetic, and in vivo characterization. *J. Pharmacol. Exp. Ther.* **337**, 145–154 (2011).

125. Torphy, T. J. & Undem, B. J. Phosphodiesterase inhibitors: New opportunities for the treatment of asthma. *Thorax* **46**, 512–523 (1991).

126. Scott, A. I. F., Perini, A. F., Shering, P. A. & Whalley, L. J. In-patient major depression: is rolipram as effective as amitriptyline? *Eur. J. Clin. Pharmacol.* **40**, 127–129 (1991).

127. Lipworth, B. Phosphodiesterase-4 inhibitors for asthma and chronic obstructive pulmonary disease. *Lancet* 1–4 (2005).

128. Rabe, K. F. *et al.* Phosphodiesterase isozymes modulating inherent tone in human airways: Identification and characterization. *Am. J. Physiol. - Lung Cell. Mol. Physiol.* **264**, (1993).

129. Ghofrani, H. A., Osterloh, I. H. & Grimminger, F. Sildenafil: From angina to erectile dysfunction to pulmonary hypertension and beyond. *Nat. Rev. Drug Discov.* **5**, 689–702 (2006).

130. Kukreja, R. C. *et al.* Emerging new uses of phosphodiesterase-5 inhibitors in cardiovascular diseases. *Exp. Clin. Cardiol.* **16**, 30–35 (2011).

Chapter III: Theoretical Framework

The experiments in the present dissertation are based on the vast literature of post-stroke excitability and pilot experiments in our lab demonstrating positive effects of PDE-inhibition as a treatment after stroke. The PDE2a-subfamily of enzymes are relatively under-studied and specifically expressed in the cortex of the brain. In collaboration with a pharmaceutical company, Inhibitor X, an inhibitor of PDE2a, was investigated as potential therapy for stroke; pilot studies shared here have demonstrated this drug enhances behavioral recovery and axonal sprouting after stroke. The present studies measure the effects of brain networks, the primary and secondary motor areas, when this drug is injected daily in mouse subjects. Two-photon microscopy is the current gold standard for live, head-fixed imaging of the rodent brain and is used in the present experiments. Genetically encoded calcium indicators (GECIs) are used in this regard as a proxy for neuronal activity in the cortex. The fluorescent activity from cells that express these molecules creates a network of integrated nodes, which can be assessed to describe certain features of that network. Correlation of the cells over time can be described with Functional Connectivity (FC) and this has been used in human patients and in mouse models to track changes to brain networks after stroke.

Section 3.1 Strategically Targeting PDE Inhibition in the Brain

PDE inhibitors are a clinically successful family for manipulating cell function pharmacologically. As with any systemic drug manipulation, specificity of the target is critical to achieving the desired effect with as minor side-effects as possible. This section will be devoted to why PDE2 is an ideal target for stroke recovery, the proprietary PDE2 inhibitor used in the present experiments, and some preliminary data acquired before these experiments. The mechanisms of

PDE enzymes in the CNS and their inhibition will be summarized below. Next, the ongoing clinical trials for PDEi application to neural injury will be noted. Finally, the section will discuss a novel and promising PDE2 inhibitor, Inhibitor-X, and pilot data demonstrating that it enhances post-stroke recovery.

PDE Inhibition in the CNS

The cyclic nucleotides, cAMP and cGMP, are essential developmental messengers in neural cells and can promote differentiation of progenitor cells into functional neurons *in vitro*[1]. As discussed in Section 2.3, intracellular cAMP is highly correlated with neuronal excitability through the cAMP-PKA-CREB pathway. Molecular studies have shown that cAMP and cGMP are linked to increased neurogenesis, neuroprotection, myelination, and synaptic plasticity[2].

Other cAMP-mediated pathways include cyclic nucleotide-gated channels (CNGCs)[3] and *Epac* (exchange protein activated by cAMP). Epac has been shown to promote Akt, Rheb, and mTOR, a well-studied cell survival pathway[4]. Epac has since been shown to enhance neurite outgrowth and promote the differentiation of neurons *in vitro*[5]. PDE inhibition directly increases intracellular cAMP levels, thus amplifying all cAMP's effectors, those discovered and yet undiscovered.

Recent mRNA expression data from each PDE family has been analyzed and published, generating distribution patterns in the CNS and the periphery[6]. Within the CNS, the frontal lobe, temporal lobe, hippocampus, cerebellum, and spinal cord were dissected and analyzed individually. All families have a significant expression in the CNS, with the possible exceptions of PDE3 and PDE6 only in photoreceptors. Within the CNS, however, the expression for each family varies dramatically. As discussed in Section 3.1, the clinical history of first-generation PDE inhibitors has been hampered by their significant side-effect profiles (one of which proved

immensely profitable). Experimental data on PDE expression is critical for pharmaceutical companies when developing novel inhibitors as they are the key to understanding unwanted side effects.

There is strong evidence that cAMP and cGMP are essential molecules for mood and cognition, some of that evidence relating to CREB and the neuronal allocation hypothesis. Basal cGMP levels were found to be higher in the developing brain compared with the adult brain[7]. A PDE1 specific inhibitor, vinpocetine, was shown to facilitate LTP and enhanced cognitive abilities in adults[8]. PDE4 inhibition has also been linked to improved LTP in the CNS and enhanced performance on several learning tasks. These tasks include object recognition tasks[9] and contextual fear conditioning[10] in rodents and delayed response tasks in primates[11].

Similarly, PDE5 inhibition has also enhanced object recognition memory[12] in rodents and improved object retrieval in primates[9]. In humans, psychophysical tests[13] and verbal recognition memory[14] were also enriched in patients on sildenafil, a PDE5 inhibitor. Lesser-known PDE families have had far fewer studies on their inhibition in the CNS; nevertheless, at least one study has reported PDE9 inhibition improving memory consolidation[15], and another has indicated PDE10 inhibition as a potential target for schizophrenia[16]. PDE2 inhibition is also poorly studied, partly due to the lack of specific inhibitors available. These studies will be discussed further in this section and introduce a proprietary inhibitor used in the present experiments.

PDE Inhibition in neural injury

Many other studies reaffirm the generally positive correlation between PDE inhibition and learning performance[17], and there is growing evidence that it also enhances recovery after neural injury. TNFa and IL-1b are two hallmark cytokines associated with neuroinflammation, and both have been shown to decrease intracellular cAMP in microglia[18]. Furthermore, intracellular cAMP

levels are crucial in expressing the proinflammatory M1 phenotype versus the anti-inflammatory M2a phenotype of post-injury microglia[19]. PDE activity has also been linked to caspase-3 and cytochrome C[20]-- two proteins that are known to be necessary for glutamate-induced apoptosis following neurotrauma. Further studies collaborate these findings and provide a robust framework for PDE inhibition as an anti-inflammatory target following neural injury[2].

Several studies have also indicated positive morphological and functional effects of PDE inhibition on neuronal recovery following injury. Following spinal cord injury in rodents, PDE4 inhibition promoted axonal regeneration and active recovery with an attenuation of the glial scar[21]. This same PDE4 inhibitor was also shown to promote survival of hippocampal neurons after ischemia *in vivo* through CREB mediated mechanisms[22]. Other studies have linked higher levels of PDE activity to neurodegenerative disease, especially Alzheimer's Disease. Tissue expression of PDE enzymes in Alzheimer's brains was significantly increased relative to the non-diseased brain[23], and these increases are family-specific. For example, PDE4 and PDE7 activity were raised early, while PDE8 activity was observed in more severe stages[24]. The biological complexity of these protein families is immense, and further studies are needed further to understand the temporal and cell-specific expression for each subtype.

Nonetheless, as section 3.1 outlined, PDE inhibitors can be safe and beneficial in several clinical situations and are ideal candidates for stroke recovery. There are three trials using cilostazol, a PDE3 inhibitor, for lacunar stroke (NCT02481323) and platelet therapy for stroke prevention (NCT01995370). Additionally, earlier phase trials are exploring PDE5 inhibition after stroke (NCT02801032, NCT02628847). In the past, poor specificity of PDE inhibitors has hampered clinical use due to potential side effects.

PDE2a and its specific inhibitors

PDE2 is a promising but understudied PDE family. The PDE2a gene has four variants, cGMP stimulated and can hydrolyze cAMP and cGMP. cGMP binds to the GAF-B domain[25], which has been well documented to enhance the enzyme's catalytic activity. Thus, PDE2 is indicated in the negative feedback regulation of cGMP, but this role needs to be further elucidated. PDE2 is expressed in low levels broadly but has higher expression in the brain, heart, and liver[26]. Within the CNS, its reported expression was highest in the cortex, hippocampus, and striatum[27].

There are a handful of PDE2 inhibitors being used by researchers to uncover PDE2 biology, and they include EHNA[28], Bay 60-7550[7], and IC933[29]. Newer generations of PDE2 inhibitors, such as oxindole[30], are being synthesized to achieve further specificity and, by extension, a different side-effect profile. In any case, pro-excitatory effects on neural function have been reported by scientists using these inhibitors. One study applied Bay 60-7550 on cultured neurons and hippocampal slices and found increasing cGMP concentrations and enhanced LTP[7]. When given to rats, this inhibitor enhanced performance on novel object recognition and social learning tasks.

Pilot data for a specific PDE2aI: Inhibitor-X

Inhibitor-X is a PDE2A specific inhibitor that was synthesized and piloted by a partnered pharmaceutical company. Western blots from human tissue confirmed that PDE2A protein was in the highest levels in the CNS, especially the frontal lobe, hippocampus, striatum, and amygdala. In contrast, the cerebellum, thalamus, and medulla were significantly devoid of protein. Human mRNA expression further confirms the highest concentrations of the enzyme in the cortex.

The pharmacological profile of the Inhibitor-X was assessed. Inhibitor-X has an IC50 of <1nM and over 500-fold specificity for PDE2A inhibition over PDE1A inhibition. Rats had 31% bioavailability of the drug, while mice had 48%. The time of peak serum concentration was two

hours for the rat and approximately 40 minutes for the mouse. Different doses of Inhibitor-X were administered to rats, and cyclic nucleotide levels were measured two hours later. Inhibitor-X increased cGMP concentrations in a dose-dependent manner but did not affect cAMP levels in the rat brain. cGMP levels in the mouse demonstrated a similar dose-dependent trend with Inhibitor-X administration.

Inhibitor-X did not cause hyperlocomotion or prepulse inhibition in the rat, but several learning paradigms showed enhanced learning. These tasks included novel object recognition, contextual fear conditioning, the radial arm maze, and a serial reaction time task.

The Carmichael lab has collaborated with the pharmaceutical company to assess this inhibitor in the context of stroke. Young and aged mice were trained on the foot fault and cylinder tasks, and their baseline performance was evaluated. PT strokes were induced to the motor cortex, and mice were administered 3mg/kg Inhibitor-X daily, starting one day after stroke. As seen in Figure 3.1, both young and aged C57 mice had an enhanced recovery with the inhibitor.

Biotinylated dextran amine (BDA) is a neuroanatomical tracer used to label any new axonal sprouting since the time of injection. BDA was injected into the ipsilesional motor cortex in the mice described above, nine weeks after stroke. Mice treated with Inhibitor-X demonstrated significantly increased density of axonal labeling compared with vehicle-treated mice (Figure 3.2d). As PDE2 is highly expressed in the cortex, particularly the frontal lobe, this data supports that PDE2 inhibition may induce axonal sprouting after a cortical stroke to the frontal lobe. The known molecular actions of cyclic nucleotides, PKA, and CREB all support an excitatory mechanism of action for PDE2a inhibition in neurons. Inhibitor-X is a targeted and well-studied potential therapy to enhance cortical stroke recovery. The experimental data in Chapter 5 uses Inhibitor-X to understand further its effects on behavior and the firing of excitatory neurons after

stroke. Section 3.3 will explore the framework for visualizing neuronal activity through the incredible innovation known as GCaMP.

Section 3.2 Calcium as a Proxy for Neural Activity

Neuronal action potentials are a defining feature of the nervous system. Understanding how neuronal "firing" integrates into circuits of functional neurons and controls human behavior is the ultimate goal of brain research. The accurate measure of action potentials is membrane voltage over time, and, indeed, electrophysiological recordings are the most precise method of measuring neuronal firing. Further adaptations, such as whole-cell patch clamping and microelectrode arrays, have facilitated more accurate results and studied populations of neurons with electrophysiology.

While electrophysiology remains the gold standard for the most time-sensitive neuronal data, it does not visualize the cells which are being recorded. As described in Section 2.4, two-photon excitation microscopy revolutionized *in vivo* research by allowing the visualization of fluorescent molecules in the living brain. Like electrophysiological studies, a voltage-sensitive indicator is a highly desirable tool to employ with two-photon microscopy for visualizing the activity of populations of neurons; tools to visualize this electrical activity being actively developed. Voltage-sensitive dyes can be effective but cannot be genetically manipulated and are typically phototoxic[31]. One study reported the destruction of somatosensory maps after stroke and their replacement in the peri-infarct of mice, employing voltage-sensitive dye imaging[32]. Genetically encoded voltage indicators (GEVIs) were first described in 1997 but mostly were unused due to low expression in cortical neuronal membranes[33]. Newer generation GEVIs utilizing voltage-sensitive phosphatase domains, such as ArcLight and FlicR1, have been developed very recently and are promising tools for visualizing neuronal activity[34,35].

Unlike GEVIs, genetically-encoded calcium indicators (GECIs) have had wide adoption for neuroscience research. The remainder of this section will serve as a more detailed discussion of calcium as a proxy for neuronal activity and the details of the specific GECI used in the present studies: CaMKII-driven GCaMP6s.

Calcium is directly associated with neuronal activity

Calcium ions are a critical intracellular signaling mechanism in practically all human cells. Approximately 99% of the calcium in the body is stored in bone, and the concentrations of circulating calcium are highly regulated and localized. For example, calcium is stored in the sarcoplasmic reticulum of muscle cells and is the main stimulator of cell contraction. In neurons, calcium plays the critical role of controlling neurotransmitter-filled vesicular release via synaptotagmin-mediated exocytosis[36]. At the resting potential, neurons typically have a calcium concentration between 50-100nM but can transiently increase over 100-fold[37]. The highly compartmentalized regulation of calcium can is disrupted in ischemia, as outlined in Section 2.1, and leads to toxic feedback pathways that cause mitochondrial dysfunction and proteolysis. Voltage-gated calcium channels, ionotropic glutamate receptors, and nicotinic acetylcholine receptors contribute to calcium influx into neurons.

Calcium's role as a second messenger made it a top target for imaging in the live brain with two-photon microscopy. Early studies using calcium dyes in patch pipettes have indeed correlated with neuronal firing *in vivo*[38]. The timing of calcium transients is also favorable as they occur over a more extended period of 30-60ms than the 3-5ms typical of an action potential[33]. In the rat, a single action potential was estimated to increase intracellular calcium from 50nM in resting excitatory cortical neurons to 90nM[39]. Additional studies demonstrate that calcium can report the

firing rate of fast-firing inhibitory neurons, measure presynaptic activity, and correlate to neuromodulator release[40].

GCaMP: A bioengineering marvel

Genetically-encoded calcium indicators (GECIs) are one the most mature imaging tools for *in vivo* brain imaging. Two prominent families of GECIs have been developed: the FRET-based Twitch molecules, which report a ratio-based fluorescence of free calcium, and the GCaMP molecules, which have calcium-mediated GFP expression for single-fluorophore reporting. These approaches have their advantages, but the GCaMP family has seen the most significant improvements through many rounds of mutagenesis and mutations. GCaMP was initially developed in 2001 as a synthetic fusion protein between GFP, calmodulin, and a peptide sequence from the myosin light-chain kinase[41].

Iterative improvements from the Janelia Research Group have led to several families of GCaMP, including GCaMP3, GCaMP6, and R-CaMP, a version with a red fluorophore instead of green. GCaMP6 is a recent family of GCaMP which has outperformed prior reporters with higher peak fluorescence, longer half-lives and decreased background fluorescence[42]. Two variants of GCaMP6 are currently available: GCaMP6s, which has slightly slower kinetics but a brighter fluorescence profile, and GCaMP6f, with faster kinetics and less bright peak fluorescence. GCaMP has been validated in several animal models, including the fruit fly, the mouse, and the monkey. As discussed in Section 2.4, GCaMP has been used to track single neurons over longitudinal studies and in the context of stroke.

Adeno-associated virus (AAV) is the leading platform for gene delivery in animal models and promising future human studies. One of the main advantages of AAV vectors is the customization of the AAV serotype, capsid, and further genomic alterations[43]. The vector used in the studies of

Chapter 5 was a customized AAV9 vector that expressed GCaMP6s under the control of the CaMKII promoter (Figure). The Calcium/Calmodulin-dependent protein kinase II (CaMKII) is a serin/threonine kinase specific to excitatory neurons of the cortex and hippocampus[44]. Restricting imaging to only one cell type decreases the complexity of the dataset and does not require additional labeling of one of the cell types. Using promotor-specific GCaMP expression allows the researcher to select the population to be imaged genetically; in the present experiments, only excitatory neurons in the motor and premotor cortex will be transfected GCaMP.

Section 3.3 Functional Connectivity: A Biomarker of Neural Function

From a computational neuroscience perspective, the brain is a system of functional elements that interact. One branch of systems neuroscience computes positive and negative correlations of these elements to draw conclusions about their relationships. This computationally intense method may be applied to the microscale of neurons and synapses, the mesoscale of neuronal populations, and the macroscale of anatomically distinct regions[45]. The scale used for a particular study will depend on the subject and the imaging modality. In human imaging, the research's large brain size and noninvasive nature require functional MRI, which has a low spatial resolution relative to two-photon microscopy. In the mouse model, two-photon imaging coupled with GCaMP6s offers researchers high temporal and spatial resolution to interrogate microscale and mesoscale populations of neurons.

Functional imaging of stroke and the unique role of secondary motor areas

Functional magnetic resonance imaging (fMRI) is a technique that evaluates cerebral blood flow using blood-oxygenation-level-dependent (BOLD) contrast and interpreting neural activity within an overlayed MRI image. Positron emission tomography (PET) uses injected radiotracers

and a gamma-ray detector to form a 3D image of the tracer in the brain. Functional imaging of the brain, fMRI and PET, has demonstrated abnormal cortical activity in chronic stroke patients. For example, stroke patients with hand impairments show abnormal activity in the affected hand in both the ipsilesional and contralesional hemispheres[46]. Activity in the motor regions was also correlated with the performance of the affected hand. In patients with good motor recovery, fMRI shows enhanced neural activity in the motor areas after stroke and a slow return to normal levels[47]. Rehabilitation-induced improvements in chronic stroke patients are associated with increases in neural activity in the ipsilesional premotor cortex. Disruption of this network by TMS leads to deterioration of motor performance in stroke patients but not in healthy controls[48].

These studies provide converging evidence of the damaging effects of ischemia on circuits of M1 and the increasing activity of peri-infarct regions during recovery. Furthermore, this is further evidence for the unique role of secondary motor areas in motor recovery after M1 stroke. Tracing studies in non-human primates show that secondary motor areas, such as the supplementary motor area (SMA), make up at least 10% of the corticospinal tract axons[49]. These connections are distinctively situated to take over neuromuscular control of lost motor functions and explain the unique role of secondary motor areas in motor recovery. The extent of damage of the corticospinal tract has been linked to the potential for recovery[50,51], further verifying this theory.

Functional Connectivity (FC) and network analysis

Functional Connectivity (FC) refers to the temporal correlations between spatially separate elements, regardless of the resolution for those elements. Multivariate approaches, such as PCA and ICA, can decompose neuroimaging data into different functionally connected networks which are temporally correlated to one another[52]. FC models presume that aspects in a system compose a network if their time courses are consistently connected; molecular neuroscience and the

elements of Hebbian plasticity seem to support these models. Graph theory is a popular method to visualize FC. Graph theory represents neural elements as nodes and their correlation with each other as a weighted edge, and these graphs can formally describe neural networks[53]. The primary assumption for graph theory is that neural networks are optimized for the highest ratio of information transfer to energy cost; 'small world topology' features, such as local clustering of connections and a short path length between pairs of nodes, support this assumption[54,55]. Because these methods are statistically unbiased, they are instrumental in an unknown system in an exploratory fashion, such as in stroke. Studies of functional Connectivity will be considered an analytical method for post-stroke network disruption in human patients and mouse models of the disease.

Primate and human studies of FC post-stroke

Functional Connectivity (FC) has already led to exciting and corroborated findings after stroke. One study evaluated the FC of 47 cortical areas in macaque monkeys and found that lesions to particular well-connected 'hubs' produced more prominent disturbances than lesser connected regions[56]. Theoretical modeling of these systems has agreed with the experimental data that the location of the lesion is critical for its effects on the network and that the motor-related regions are the most likely to disrupt system-wide processes[57]. Several functional imaging studies have demonstrated converging evidence that stroke induces measurable differences in correlated activity between areas, and this activity is associated with behavioral recovery. Although the studies below will highlight, the association between FC and recovery is based on multiple variables and requires further studies to be implemented clinically in stroke.

Neuroimaging data recorded while the subject is not performing any task has been called the resting-state; the network topology from this data has also been called the default mode network

(DMN). One study evaluated the DMN of 20 control and 20 first-time stroke patients using resting-state fMRI[58]. PCA analysis found stroke-induced decreased FC in the medial temporal lobe, posterior cingulate, and medial prefrontal cortex. Furthermore, these deficits were correlated to the amount of performance deficit for a delayed recall learning test.

Resting-state fMRI in human stroke patients demonstrates that the ipsilesional FC of motor regions predicts behavioral deficits but not the FC of the contralesional hemisphere[59]. However, in visuospatial neglect, behavioral recovery was associated with FC recovery of the inter-hemispheric parietal cortex[60]. In aphasic stroke patients, preserved inter-hemispheric connection was also predictive of better performance in language tasks[61]. One study specifically investigated inter-hemispheric versus intra-hemispheric effects in the attention network and the somatomotor network and found that only interhemispheric FC correlated to performance on attention on motor tasks, respectively[59]. In patients with upper extremity paresis following stroke, three weeks of rehabilitation enhanced the activity of the perilesional premotor cortex over the contralesional premotor cortex[62]. Another recent study argued that homotopic regions in both hemispheres correlated most with recovery after upper-extremity dysfunction of stroke[63], rather than the ipsilesional or contralesional hemispheres per se. A recent review has outlined the roles of Connectivity in evaluating stroke dysfunctions and how several therapies may enhance FC to improve recovery[64].

Functional Connectivity using GCaMP in the mouse

Two-photon calcium imaging offers high temporal and spatial resolutions for individual neurons. A recent study by Latifi et al. employed two-photon GCaMP imaging to measure functional Connectivity in awake behaving mice[65]. In this study, mice were injected with viral GCaMP6s at the M1 and M2 cortices and habituated for head-fixed imaging on a Styrofoam ball,

allowing free movement for the mouse. After several baseline imaging sessions, a photothrombotic stroke was induced to M1, and the mice were imaged during their post-stroke recovery. The mice used were transgenic fluorescent reporters of GAD2, such that the researchers were able to determine which neurons were inhibitory through the red channel. GCaMP recordings were segmented into active neurons (ROIs). The fluorescent traces (ΔF/F) represent temporal correlations between each neuron, and FC can be applied to this data. Further details can be found in Chapter 4, as the methodology for acquiring FC was shared between this study and the experimental data presented in Chapter 5.

As predicted, stroke significantly alters the networks of the motor cortex and the premotor cortex, decreasing the average connectedness of both networks. This was mainly observed in both excitatory and inhibitory neurons in the motor cortex- close to the lesion. However, in the premotor cortex, excitatory neuronal FC was decreased by a minor degree, and inhibitory neurons were unaffected. This study also delineated the data from movement states and resting states. The tasks presented in Chapter 5 will use a similar paradigm to investigate the pharmaceutical enhancement of stroke with PDE-inhibition. An additional behavioral paradigm is added to capture the exact amount of motor deficit the mouse has at recording.

Section 3.4 Designing Functional Connectivity Studies of PDE2a-Inhibition

It is helpful at this point to summarize the chapters of this thesis thus far. Chapter one discusses the harmful and costly impact of stroke on society, the need for new therapies for chronic patients, and the animal models scientists employ to study the disease. Chapter two is a series of literature reviews for the molecular cascades of ischemic damage, the mechanisms of neuroplasticity in learning and recovery, the tools and insights from stroke imaging, and the introduction of PDE

inhibition as a potential drug target for stroke recovery. Finally, Chapter three has laid the theoretical framework for designing experiments based on these principles and ideas.

Two-photon calcium imaging has been proven to be a helpful tool for evaluating neural activity in live mice within the context of stroke. Functional Connectivity (FC) has also been a valuable method to analyze the correlations of populations and has been applied to an animal and human subjects of stroke. PDE inhibition has also been demonstrated to be a highly successful drug class, and PDDE2a is an understudied subfamily with high expression in the forebrain. Inhibitor-X was then presented as a unique target and some preliminary studies of its therapeutic effects on recovery.

Experiments were designed to image the primary motor (M1) and secondary motor (M2) using GCaMP two-photon microscopy. A commonly used task for assessing forelimb deficits in mice, the grid walk, was adapted for use in a head-fixed setting and allowed the scoring of behavioral deficits during each recording. Stroke was then induced to M1, and imaging was continued for six weeks after stroke. Groups of mice were randomized for receiving stroke or sham and for receiving Inhibitor-X treatment or vehicle. There were four groups in the experiments: 1) stroke + drug, 2) stroke + vehicle, 3) sham + drug, and 4) sham +vehicle. The specific protocols followed, and the cited studies they are based on will be given in Chapter 4. Based on the prior experiments in the lab, it was hypothesized that stroke would induce a reduction of FC with a more dramatic decrease in M1 compared to M2. The excitatory nature of PDE inhibition and its correlation with CREB, a potent neuroprotective agent and an enhancer of neuroplasticity, is expected to enhance FC in the drug groups.

Section 3.5 Figures

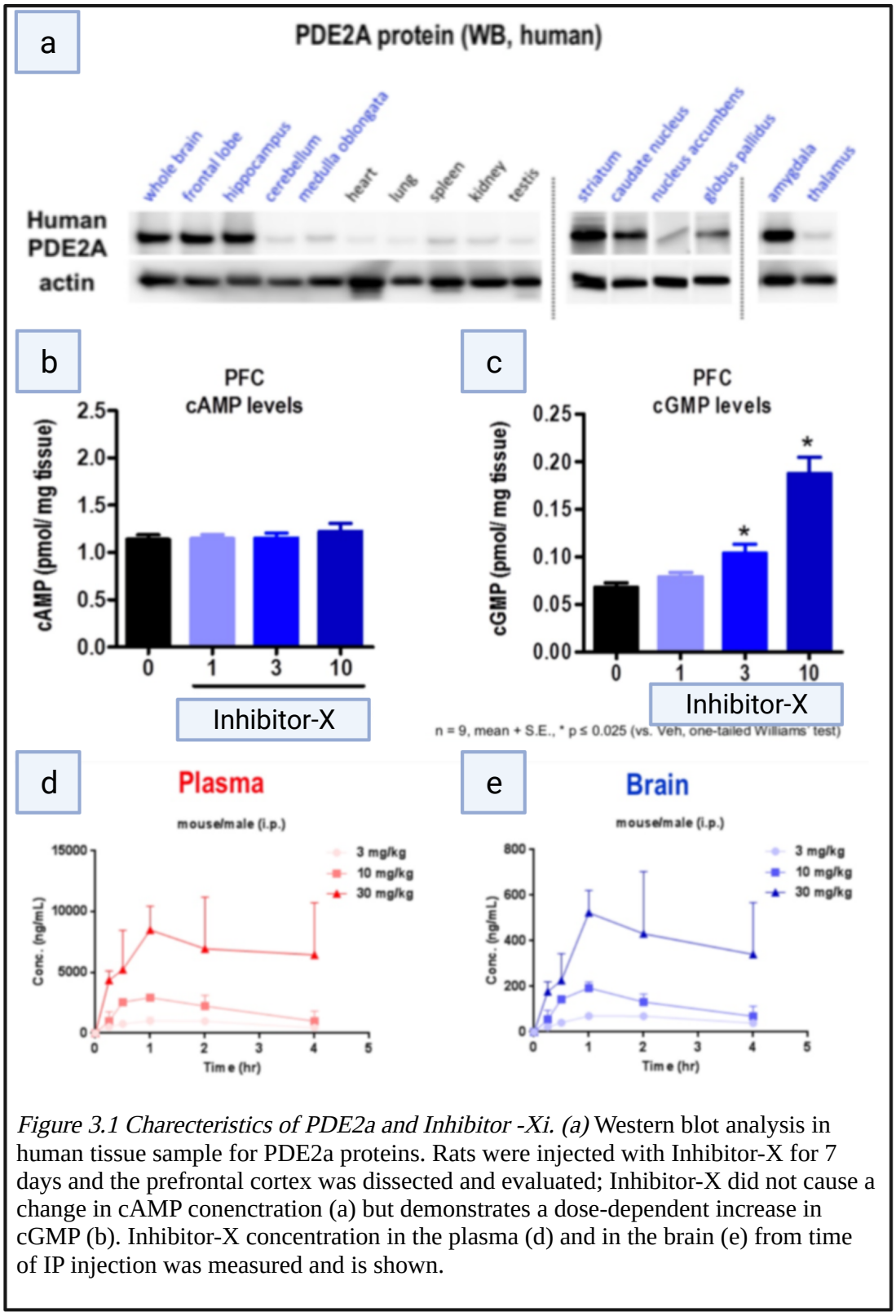

Figure 3.1 Charecteristics of PDE2a and Inhibitor -Xi. (a) Western blot analysis in human tissue sample for PDE2a proteins. Rats were injected with Inhibitor-X for 7 days and the prefrontal cortex was dissected and evaluated; Inhibitor-X did not cause a change in cAMP conenctration (a) but demonstrates a dose-dependent increase in cGMP (b). Inhibitor-X concentration in the plasma (d) and in the brain (e) from time of IP injection was measured and is shown.

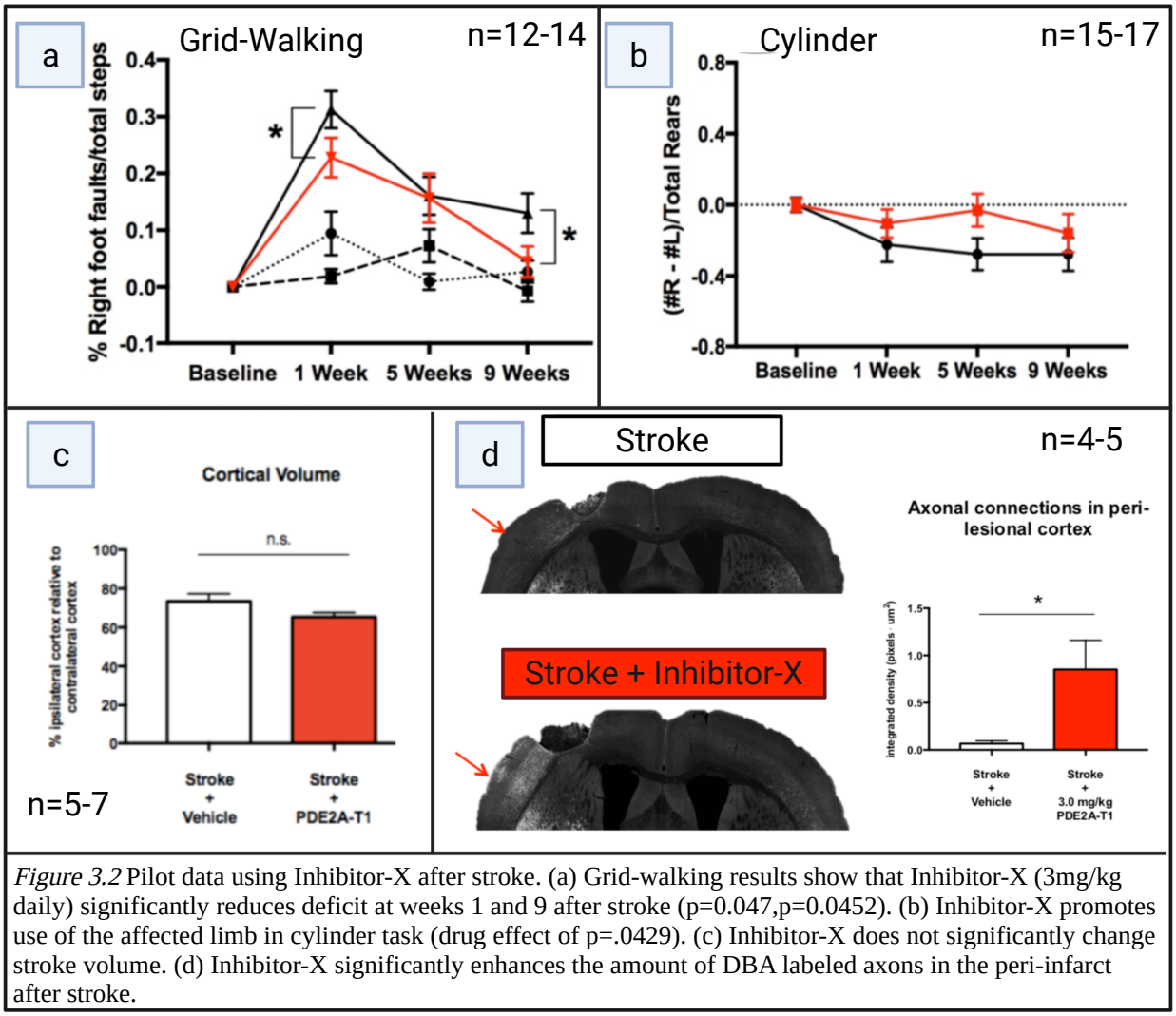

Figure 3.2 Pilot data using Inhibitor-X after stroke. (a) Grid-walking results show that Inhibitor-X (3mg/kg daily) significantly reduces deficit at weeks 1 and 9 after stroke (p=0.047,p=0.0452). (b) Inhibitor-X promotes use of the affected limb in cylinder task (drug effect of p=.0429). (c) Inhibitor-X does not significantly change stroke volume. (d) Inhibitor-X significantly enhances the amount of DBA labeled axons in the peri-infarct after stroke.

Section 3.6 References

1. Lepski, G., Jannes, C. E., Nikkhah, G. & Bischofberger, J. cAMP promotes the differentiation of neural progenitor cells in vitro via modulation of voltage-gated calcium channels. *Front. Cell. Neurosci.* (2013) doi:10.3389/fncel.2013.00155.
2. Knott, E. P., Assi, M., Rao, S. N. R., Ghosh, M. & Pearse, D. D. Phosphodiesterase inhibitors as a therapeutic approach to neuroprotection and repair. *Int. J. Mol. Sci.* **18**, 1–38 (2017).
3. Pifferi, S., Boccaccio, A. & Menini, A. Cyclic nucleotide-gated ion channels in sensory transduction. *FEBS Lett.* **580**, 2853–2859 (2006).
4. Muñoz-Llancao, P. *et al.* Exchange protein directly activated by cAMP (EPAC) regulates neuronal polarization through Rap1B. *J. Neurosci.* **35**, 11315–11329 (2015).
5. Kiermayer, S. *et al.* Epac activation converts cAMP from a proliferative into a differentiation signal in PC12 cells. *Mol. Biol. Cell* **16**, 5639–5648 (2005).
6. Lakics, V., Karran, E. H. & Boess, F. G. Quantitative comparison of phosphodiesterase mRNA distribution in human brain and peripheral tissues. *Neuropharmacology* **59**, 367–374 (2010).
7. Boess, F. G. *et al.* Inhibition of phosphodiesterase 2 increases neuronal cGMP, synaptic plasticity and memory performance. *Neuropharmacology* **47**, 1081–1092 (2004).
8. I., H., H.H., F. & H., E. Efficacy and tolerance of vinpocetine in ambulant patients suffering from mild to moderate organic psychosyndromes. *International clinical psychopharmacology* vol. 6 31–43 (1991).
9. Rutten, K. *et al.* Phosphodiesterase inhibitors enhance object memory independent of cerebral blood flow and glucose utilization in rats. *Neuropsychopharmacology* **34**, 1914–

1925 (2009).

10. Trifilieff, P. *et al.* Foreground contextual fear memory consolidation requires two independent phases of hippocampal ERK/CREB activation. *Learn. Mem.* **13**, 349–358 (2006).

11. Ramos, B. P. *et al.* Dysregulation of Protein Kinase A Signaling in the Aged Prefrontal Cortex: New Strategy for Treating Age-Related Cognitive Decline functions dependent on the amygdala and posterior cor-tices (Barros et al PKA activity can also be increased through the sys. *Neuron* **40**, 835–845 (2003).

12. Prickaerts, J., Steinbusch, H. W. M., Smits, J. F. M. & De Vente, J. Possible role of nitric oxide-cyclic GMP pathway in object recognition memory: Effects of 7-nitroindazole and zaprinast. *Eur. J. Pharmacol.* **337**, 125–136 (1997).

13. Grass, H. *et al.* Sildenafil (Viagra®): Is there an influence on psychological performance? *Int. Urol. Nephrol.* **32**, 409–412 (2001).

14. Schultheiss, D. Central effects of sildenafil (Viagra) on auditory selective attention and verbal recognition memory in humans: A study with event-related brain potentials. *World J. Urol.* **19**, 46–50 (2001).

15. Van Der Staay, F. J. *et al.* The novel selective PDE9 inhibitor BAY 73-6691 improves learning and memory in rodents q. doi:10.1016/j.neuropharm.2008.07.005.

16. Rodefer, J. S., Murphy, E. R. & Baxter, M. G. PDE10A inhibition reverses subchronic PCP-induced deficits in attentional set-shifting in rats. *Eur. J. Neurosci.* **21**, 1070–1076 (2005).

17. Reneerkens, O. A. H., Rutten, K., Steinbusch, H. W. M., Blokland, A. & Prickaerts, J. Selective phosphodiesterase inhibitors: A promising target for cognition enhancement.

Psychopharmacology vol. 202 419–443 (2009).

18. Ghosh, M. *et al.* The interplay between cyclic AMP, MAPK, and NF- B pathways in response to proinflammatory signals in microglia. *Biomed Res. Int.* **2015**, (2015).
19. Ghosh, M., Xu, Y. & Pearse, D. D. Cyclic AMP is a key regulator of M1 to M2a phenotypic conversion of microglia in the presence of Th2 cytokines. *J. Neuroinflammation* **13**, (2016).
20. Walsh, J. G. *et al.* Executioner caspase-3 and caspase-7 are functionally distinct proteases. *PNAS* (2008).
21. Lu, P., Yang, H., Jones, L. L., Filbin, M. T. & Tuszynski, M. H. Development/Plasticity/Repair Combinatorial Therapy with Neurotrophins and cAMP Promotes Axonal Regeneration beyond Sites of Spinal Cord Injury. (2004) doi:10.1523/JNEUROSCI.1492-04.2004.
22. Sasaki, T. *et al.* The phosphodiesterase inhibitor rolipram promotes survival of newborn hippocampal neurons after ischemia. *Stroke* **38**, 1597–1605 (2007).
23. García-Osta, A., Cuadrado-Tejedor, M., García-Barroso, C., Oyarzábal, J. & Franco, R. Phosphodiesterases as therapeutic targets for Alzheimer's disease. *ACS Chem. Neurosci.* **3**, 832–844 (2012).
24. Puzzo, D., Sapienza, S., Arancio, O. & Palmeri, A. Role of phosphodiesterase 5 in synaptic plasticity and memory. *Neuropsychiatr. Dis. Treat.* **4**, 371–387 (2008).
25. Martinez, S. E. *et al. Crystal structure of the tandem GAF domains from a cyanobacterial adenylyl cyclase: Modes of ligand binding and dimerization*. *PNAS February* vol. 22 www.pnas.orgcgidoi10.1073pnas.0409913102 (2005).
26. Ding, L. *et al.* Protective effects of phosphodiesterase 2 inhibitor on depression-and

anxiety-like behaviors: Involvement of antioxidant and anti-apoptotic mechanisms. *Behav. Brain Res.* **268**, 150–158 (2014).

27. Menniti, F. S., Faraci, W. S. & Schmidt, C. J. Phosphodiesterases in the CNS: Targets for drug development. *Nat. Rev. Drug Discov.* **5**, 660–670 (2006).

28. Rivet-Bastide, M. *et al.* cGMP-stimulated cyclic nucleotide phosphodiesterase regulates the basal calcium current in human atrial myocytes. *J. Clin. Invest.* **99**, 2710–2718 (1997).

29. Loughney, K. *et al.* Isolation and characterization of cDNAs encoding PDE5A, a human cGMP-binding, cGMP-specific 3',5'-cyclic nucleotide phosphodiesterase. *Gene* **216**, 139–147 (1998).

30. Chambers, R. J. *et al.* A new chemical tool for exploring the physiological function of the PDE2 isozyme. *Bioorganic Med. Chem. Lett.* **16**, 307–310 (2006).

31. Marshall, J. D. *et al.* Cell-Type-Specific Optical Recording of Membrane Voltage Dynamics in Freely Moving Mice. *Cell* **167**, 1650-1662.e15 (2016).

32. Brown, C. E., Aminoltejari, K., Erb, H., Winship, I. R. & Murphy, T. H. In vivo voltage-sensitive dye imaging in adult mice reveals that somatosensory maps lost to stroke are replaced over weeks by new structural and functional circuits with prolonged modes of activation within both the peri-infarct zone and distant sites. *J. Neurosci.* **29**, 1719–1734 (2009).

33. Lin, M. Z. & Schnitzer, M. J. Genetically encoded indicators of neuronal activity. *Nat. Neurosci.* **19**, 1142–1153 (2016).

34. Abdelfattah, A. S. *et al.* A bright and fast red fluorescent protein voltage indicator that reports neuronal activity in organotypic brain slices. *J. Neurosci.* **36**, 2458–2472 (2016).

35. Han, Z., Platisa, J. L., Cohen, J. B. & Baker, L. B. Fluorescent Protein Voltage Probes

Derived from ArcLight that Respond to Membrane Voltage Changes with Fast Kinetics. *PLoS One* **8**, 81295 (2013).

36. Bacaj, T. *et al.* Asynchronous Phases of Neurotransmitter Release. *Neuron* **80**, 947–959 (2014).

37. Grienberger, C. & Konnerth, A. Imaging Calcium in Neurons. *Neuron* **73**, 862–885 (2012).

38. Markram, H., Lübke, J., Frotscher, M. & Sakmann, B. Regulation of synaptic efficacy by coincidence of postsynaptic APs and EPSPs. *Science (80-.).* **275**, 213–215 (1997).

39. Spruston, N., Schiller, Y., Stuart, G. & Sakmann, B. Activity-dependent action potential invasion and calcium influx into hippocampal CA1 dendrites. *Science (80-.).* **268**, 297–300 (1995).

40. Ali, F. & Kwan, A. C. Interpreting in vivo calcium signals from neuronal cell bodies, axons, and dendrites: a review. *Neurophotonics* **7**, 1 (2019).

41. Nakai, J., Ohkura, M. & Imoto, K. A high signal-to-noise ca2+ probe composed of a single green fluorescent protein. *Nat. Biotechnol.* **19**, 137–141 (2001).

42. Chen, T. W. *et al.* Ultrasensitive fluorescent proteins for imaging neuronal activity. *Nature* **499**, 295–300 (2013).

43. Wang, D., Tai, P. W. L. & Gao, G. Adeno-associated virus vector as a platform for gene therapy delivery. *Nat. Rev. Drug Discov.* **18**, 358–378 (2019).

44. Hioki, H. *et al.* Efficient gene transduction of neurons by lentivirus with enhanced neuron-specific promoters. *Gene Ther.* **14**, 872–882 (2007).

45. Costa, L. D. F. & Sporns, O. Hierarchical features of large-scale cortical Connectivity. *Eur. Phys. J. B* **48**, 567–573 (2005).

46. Grefkes, C. *et al.* Cortical Connectivity after subcortical stroke assessed with functional magnetic resonance imaging. *Ann. Neurol.* **63**, 236–246 (2008).

47. Rehme, A. K., Fink, G. R., Yves Von Cramon, D. & Grefkes, C. The Role of the Contralesional Motor Cortex for Motor Recovery in the Early Days after Stroke Assessed with Longitudinal fMRI. *Cereb. Cortex* **21**, 756–768 (2011).

48. Pineiro, R., Pendlebury, ; S, Johansen-Berg, ; H & Matthews, ; P M. *Altered Hemodynamic Responses in Patients After Subcortical Stroke Measured by Functional MRI*. www.frmib.ox.ac.uk/fsl/ (2002).

49. Nachev, P., Kennard, C. & Husain, M. Functional role of the supplementary and pre-supplementary motor areas. *Nat. Rev. Neurosci.* **9**, 856–869 (2008).

50. Ward, N. S. *et al.* Motor system activation after subcortical stroke depends on corticospinal system integrity. *Brain* **129**, 809–819 (2006).

51. Stinear, C. M. *et al.* Functional potential in chronic stroke patients depends on corticospinal tract integrity. *Brain* **130**, 170–180 (2007).

52. Grefkes, C. & Fink, G. R. Reorganization of cerebral networks after stroke: New insights from neuroimaging with connectivity approaches. *Brain* **134**, 1264–1276 (2011).

53. Bullmore, E. & Sporns, O. Complex brain networks: Graph theoretical analysis of structural and functional systems. *Nat. Rev. Neurosci.* **10**, 186–198 (2009).

54. Zalesky, A., Fornito, A. & Bullmore, E. T. Network-based statistic: Identifying differences in brain networks. (2010) doi:10.1016/j.neuroimage.2010.06.041.

55. Achard, S. & Bullmore, E. Efficiency and Cost of Economical Brain Functional Networks. doi:10.1371/journal.pcbi.0030017.

56. Honey, C. J. *et al. Predicting human resting-state functional connectivity from structural*

connectivity. www.pnas.orgcgidoi10.1073pnas.0811168106 (2009).

57. Alstott, J., Breakspear, M., Hagmann, P., Cammoun, L. & Sporns, O. Modeling the Impact of Lesions in the Human Brain. *PLoS Comput Biol* **5**, 1000408 (2009).

58. Tuladhar, A. M. *et al.* Default Mode Network Connectivity in Stroke Patients. *PLoS One* **8**, (2013).

59. Carter, A. R. *et al.* Resting state inter-hemispheric fMRI connectivity predicts performance after stroke. *Ann. Neurol.* NA-NA (2009) doi:10.1002/ana.21905.

60. Vincent, J. L. *et al.* Intrinsic functional architecture in the anaesthetized monkey brain. *Nature* **447**, 83–86 (2007).

61. Warren, J. E., Crinion, J. T., Ralph, M. A. L., Wise, R. J. S. & Warren, J. Anterior temporal lobe connectivity correlates with functional outcome after aphasic stroke. *A J. Neurol.* doi:10.1093/brain/awp270.

62. James, G. A. *et al.* Changes in resting state effective connectivity in the motor network following rehabilitation of upper extremity poststroke paresis. *Top. Stroke Rehabil.* **16**, 270–281 (2009).

63. Urbin, M. A., Hong, X., Lang, C. E. & Carter, A. R. Resting-state functional connectivity and its association with multiple domains of upper-extremity function in chronic stroke. *Neurorehabil. Neural Repair* **28**, 761–769 (2014).

64. Silasi, G. & Murphy, T. H. Stroke and the connectome: How Connectivity guides therapeutic intervention. *Neuron* **83**, 1354–1368 (2014).

65. Latifi, S. *et al.* Neuronal network topology indicates distinct recovery processes after stroke. *Cereb. Cortex* **30**, 6363–6375 (2020).

Chapter IV: Methods and Pipeline

Section 4.1 Achieving the Mouse Model

The mouse model for the proposed imaging studies has a few necessary characteristics:

1) a transparent window to the cortex and a method of accessing that window chronically and with as little mechanical disturbance as possible;

2) a reporter of neural function, which may be visualized;

3) a consistent and reproducible method of producing an ischemic infarct at a targeted location above the cortical window.

Our model fulfills these criteria: wild-type C57 mice receive a craniotomy procedure, with stereotaxic AAV-GCaMP6s viral delivery during the procedure. The procedure is finalized by fixing a head-bar to the mouse's skull, which allows for stable head-fixation during recordings. The craniotomy procedure was pioneered in 1997 while scientists were observing recordings of calcium dynamics during whisker stimulation in rats[1]; it has since provided the foundation for hundreds of in vivo imaging studies to follow. In the following two decades, many refinements to the technique have been published and proposed[2-4]. One such advancement was the advent of genetically encoded indicators, which allow for chronic imaging, The simplest form of the craniotomy procedure was used to allow chronic longitudinal imaging as described above. The video protocol published by the Portera lab at UCLA is a practical, visual tool similar to the craniotomy protocol which was followed here[2]. A comprehensive protocol published by several note-worthy scientists in the field was used as a general guide when first learning the craniotomy procedure[3]. The protocol discusses timing, critical steps which could ruin the procedure, and a helpful troubleshooting table for common issues. This guide is highly recommended reading to any researcher pursuing chronic in-vivo imaging.

As discussed in Section 3.3, GCaMP6 is a valuable tool for studying calcium transients in-vivo. Adeno-Associated Virus 9 (AAV9) with GCaMP6s under the CaMKII promoter was purchased from AddGene (Catalog #107790-AAV9, previously AV-9-PV4365 from Penn Vector Core). These AAV9 particles drive expression GCaMP6s in CaMKII-expressing cells, primarily pyramidal neurons. Each viral order was delivered as a volume of 100uL of at least $1x10^{13}$ vg/mL titer. This volume was aliquoted to 5uL volumes, which could be individually thawed on the day of use. Steps 1-3 under *Stereotaxic Viral Injections* may be initiated during any waiting stages of the craniotomy procedures, while the remaining steps must occur after the cortex is exposed. For the present studies, three injections were delivered: one 500nL injection to the primary motor cortex (M1) and two to the secondary motor areas (M2). Coordinates for these areas were based on the Allen Adult Mouse Atlas (http://atlas.brain-map.org/) defined MOp (primary motor area) and MOs (secondary motor area) and an approximation of the center of these areas.

After craniotomy and viral injection, mice were allowed to recover while the GCaMP expression ramps up. GCaMP6s expression was typically observed to begin 21 days after surgery but may take up to 6 weeks. Photothrombotic stroke was applied 6-8 weeks after surgery and at least three baseline imaging and behavioral sessions (not including habituation). The photothrombotic model is based on Rose Bengal, a compound that causes endothelial damage, platelet activation, and thrombosis when activated by light. Initially proposed in 1985, the photothrombotic stroke allows the researcher to generate a reproducible infarct at a specific location by injecting Rose Bengal and using a light source to target a particular region of the brain[4]. Specific protocol steps will be provided below.

Animal procurement

All procedures were performed per the National Institutes of Health Animal Protection Guidelines and reviewed by the UCLA Animal Research Committee (ARC). 12 week old C57BL/6 were procured through UCLA's Division of Laboratory Animal Medicine (DLAM) for all studies. Animals were housed in a light-controlled environment with a reverse light cycle and free access to irradiated pellets (LabDiet PicoLab, Rodent Diet 20) and sterilized water. Housing temperatures were maintained between 20-21 C, and standard humidity was held between 30-70%. Mice were administered seven days of antibiotics (Sulfamethazaxole) in the drinking water after craniotomy procedures.

Craniotomy Procedure

1) Anesthetize the mouse with 4% isoflurane and 100% O2 in an induction box until the mouse is unconscious and irresponsive to tail pinch.

2) Move the mouse to the stereotaxic frame (Model 900, Kopf) with direct 1.4-2% isoflurane for surgery duration. Apply eye ointment to avoid dehydration and insert a rectal temperature probe to maintain the body at 37.0 °C +/-0.5°C via a homeothermic heating pad.

3) Administer 2ug/g dexamethasone (0.04 mL of 2mg/mL solution) as an intramuscular injection to reduce inflammation and cerebral edema (HenrySchein DexaJect Veterinary Solution).

4) Shave the hair off the top of the scalp with an electric razor. Optionally, a depilatory cream (Nair) may be used to remove hair after shaving with a razor, leading to a cleaner scalp and decreased likelihood of hair contaminating the craniotomy.

5) Wash the scalp with three serial washes of 70% ethanol, followed by betadine solution. A pentagonal piece of skin is removed using surgical scissors, going as posterior as the edge of the

temporalis and as far anteriorly as possible without disturbing the orbit. Optional: a lidocaine and epinephrine mixture may be applied to any bleeding, but this is not usually a problem.

6) Using a razor blade, gently scrape the periosteum away from the skull to allow for better adherence later. Hydrate the skull with normal saline.

7) Use a permanent marker to mark Bregma, which will be used as a landmark for imaging.

8) Outline the area of the cranial window. 4mm #0 cranial windows (Warner Instruments) were used. A 4mm outline was etched with the aid of a reused window, after which it was returned for reuse. A pristine window is used for implant.

9) Drill slowly using a 1/4" drill bit, applying saline every several seconds to avoid overheating, damaging the underlying tissue. As the outlined groove thins, the cortical vasculature is visualized and allows the researcher to avoid any vessels while drilling. Once the bone island within the outline is easily moved with a gentle tap of the forceps, it is left to sit in cortex buffer for 7-10 minutes to facilitate removal further.

10) Insert the sharp tip of a fine forceps (FineScienceTools, 5HDC) into the spongy bone and carefully lift the central flap of bone with as minor damage as possible to the underlying dura. Optional: The viral injection protocol may or may not be needed, as in the case of transgenic GCaMP mice.

Stereotaxic Viral Injections

1) Grab 5uL aliquot and let it thaw on ice. Microcentrifuge the tube to drag particles down. Dilute the particles 1:4, such that a 500 nL injection is 100 nL viral solution and 400 nL saline.

2) Prepare pre-pulled glass pipettes by breaking their tip and filling them with mineral oil before attaching to nanoliter injector (Drummond Nanoject III). Once the pipette is secured in an air-tight

manner, set the injector to inject 1-2 uL of oil to make room for the viral solution. Attach the pipette to the stereotaxic frame to tightly control the tip's movement in three spatial directions.

3) Using a microscope, place the tip of pulled pipette a few mm above a piece of parafilm. Using a 2uL pipette, pipette 1-2uL of diluted viral solution and place it as a bolus directly under the tip of the glass pipette. Stereotaxically, move the pipette into the center of the bolus and set the injector to withdraw at a steady rate. Once the investigator notices the bolus is almost entirely withdrawn, the withdrawal may be stopped.

4) Cortex should always be kept hydrated with saline or cortex buffer once the cranial bone flap is removed. Before injections can be initiated, calibration of the stereotaxic grid is necessary. Locate Bregma on the mouse skull (should be at the medial edge of the cranial window) and bring a glass pipette directly above Bregma, taking care not to let the tip hit any object as it is very fragile. Once at Bregma, the X and Y axes are set to zero on the stereotaxic instrument.

5) The pipette is moved to designated injection sites. The primary motor cortex site (i.e., caudal forelimb area) was centered 1.5 mm lateral to Bregma without any movement in the A/P direction. The secondary motor cortex (i.e., rostral forelimb area) was centered 1.6-1.7 mm anterior to Bregma and 1.5 mm lateral. These coordinates were selected based on resources supplied by Allen Brain Institute.

6) Pipette is lowered 500um from the top of the cortex manually at a rate of 200um per minute. The nanoinjector is set to inject 500nL at a rate of 1nL per second. Once the injection is complete, the pipette is left in the cortex for an additional few minutes to further the diffusion of the virus in the tissue. Pipette is then slowly pulled up out of the brain at a rate of 200um per minute. Step 6 is repeated for each injection.

Craniotomy Procedure Continued

11) Remove any bony filaments on the craniotomy border and use GelFoam to absorb any cortical bleeds. Keep cortex well hydrated and cleaned before placing and adhering cover glass, which is permanent.

12) Wash new 4mm cover glass with ethanol followed by saline, then place cover glass flush above the buffered, exposed cortex. GelFoam may be used to absorb any extra fluid and allow the cover glass to remain flush with the tissue.

13) Allow a drop of tissue-safe adhesive (3M Vetbond) to slightly harden by leaving it in the open air, then use a wooden applicator to carefully apply it to the edge of the cover glass and the skull. Since the adhesive is opaque once it hardens, any adhesive above the tissue will not allow imaging through it. Optional: a wooden applicator may be fitted onto the stereotaxic frame and placed to push down on the cover glass, allowing more accessible application of adhesive.

14) Apply a thin layer of gel cyanoacrylate (Loctite Gel Control Super Glue) on any exposed skull. Place custom-made titanium head-bar parallel with the head, and allow a glue drop to bind the two. More surface area between the metal bar and the skull allows for strong adhesion and a lower probability that the head-bar is displaced.

15) Mix dental acrylic (Jet Acrylic, Lang Dental) with catalyst liquid in an appropriate ratio. The cement is forming, mold it into a skull cap that covers any exposed tissue and encapsulates the center of the head-bar. Take special care to create an acrylic wall around the window to facilitate holding a drop of water during imaging. Allow cement to harden.

16) Stop gas flow to mouse and remove the head from ear-bar. Allow the mouse to recover consciousness while the temperature probe is still inserted. Once the mouse starts to move, place

the mouse into a warmed recovery chamber with access to food pellets and water. Clean workspace wholly or prepare it for the following procedure.

Motor Cortex Photothrombotic (MC-PT) Stroke

1) Induce mouse to anesthesia in a 4% isoflurane and 100% O2 box and place in a stereotaxic frame (Model 900, Kopf) under 2% maintenance anesthesia for the duration the procedure.

2) Set up laser light source to 520 nm and turn it on at a low power level. Move beam to Bregma and set stereotaxic axes to 0. Move light 1.5 mm lateral from Bregma to reach the final infarct location, the primary motor cortex above the coverglass. Turn off laser (CLD1010LP, ThorLabs; laser diode LP520-MF100, ThorLabs).

3) Inject Rose Bengal (10mg/mL in sterile PBS) intraperitoneally at 100mg/kg. Allow 5 minutes for the compound to spread through the circulatory system.

4) Change laser power to 11 mW and turn the laser on for 10 minutes to induce a focal infarct centered at the selected coordinate. Safety glasses must always be on when a high-intensity laser is turned on.

5) Allow the mouse to recover.

Section 4.2 Two-Photon Microscopy for Longitudinal Studies

The theory behind two-photon microscopy was conceptualized in 1931 and elaborated on epifluorescent technology. Epifluorescent microscopy sends light through an excitation filter and then through an objective and onto a specimen, typically on a slide, for imaging. Two-photon absorption was a novel concept that employed two photons half as energetic, typically in the near-infrared (NIR) wavelength spectrum, to excite a fluorescent molecule. Because a single photon does not excite the molecule, this lends favorable properties for imaging using this light.

Two-photon microscopy was pioneered in 1990 and, when combined with excitation microscopy, has established itself as the foremost imaging modality for high spatial resolution in vivo imaging. As photon density decreases exponentially from the light source, an intense laser beam is required to excite a specimen volume as small as ~0.1 um3[5]. Fast scanning mirrors are then added to coordinate the laser onto the specimen and map out its fluorescent image. Applying near-infrared (NIR) light significantly reduces excitation events, which carry a risk of photobleaching (i.e., phototoxicity), and is thus much less toxic to the tissue. These wavelengths also have higher tissue penetration due to reduced scattering and absorption by endogenous tissue[6]. They have since allowed thousands of peer-reviewed articles studying live brain tissue.

Components used

In the present study, a resonant scanning two-photon microscope (Neurolabware) was used. The light source used was a Chameleon III laser (Coherent Inc.) at a fixed wavelength of 920 nm. The 8kHz resonant raster scanner equates to 512 lines at 30 Hz bidirectionally, which results in image capture at 15.5 Hz. A dichroic mirror (Semrock) is used to filter the captured light and allow for green and red channel imaging. The objective used was a 16x water-based lens (Nikon, 0.8NA).

Image capture was relayed to Scanbox, an acquisition software that runs through Matlab (https://scanbox.org/), and a screenshot of which can be seen in Figure 4.2. This software allows control of the shutter, the laser power, and the wavelength of light produced. It also allows convenient tools for quick analyses, such as manual registration for quickly assessing fluorescent variation over time in a region of interest (ROI). These tools were handy at the early stages of GCaMP6s expression when the researcher could more clearly establish certain features as neurons.

The typical imaging session

A typical experimental day of imaging session(s) in the present studies closely followed several steps so that the videos acquired during different days relative to a stroke may be compared. The imaging day is initiated by powering the laser on and setting the wavelength to 920nm through *Scanbox*. Nex, the first mouse for imaging is removed from its home cage and placed on the treadmill (Section 4.4). The mouse's head-bar is screwed into place in the metal clamp (Figure 4.2b) to fix its head. The objective is lowered above the cover glass, and a drop of distilled water is placed between the two. The microscope's internal camera is activated, and Bregma (identified by permanent marker during surgery) is located. The stereotaxic coordinates are set to zero at this defined location. Stereotaxic controls are then used to move the objective over the cover glass, and any previously identified vasculature may be reidentified.

The user enters into *Scanbox* the mouse identification, data, and area to be imaged. The user turns off the camera and activates the PMT to be used: the green, the red, or both channels simultaneously. All external lights must be completely turned off when any PMT is in use. A live imaging session may be initiated through *Scanbox* without saving the images to a video file. This mode is used to find the population of neurons to be imaged initially. For example, the primary motor cortex is immediately lateral of Bregma. So when identifying this region, the researcher will move to that general area relative to Bregma and use the live mode to find the exact location of fluorescent neurons. In the early stages of GCaMP expression, a projected average or maximum projection may be required to visualize neurons. Live manual registration of ROIs can also help the user determine if the observed objects resemble neurons in their fluorescent activity.

Once the proper population to be imaged is identified, the exact coordinates relative to Bregma are noted in *Scanbox*. In subsequent imaging sessions, these coordinates are used in conjunction with visual inspection to record as much of the same population of neurons as possible.

When the researcher is satisfied with the imaging location, the gain of each PMT may be adjusted to achieve ideal imaging. All adjustments are noted in the metadata of the saved file, and these notes may be accessed at later imaging dates to coordinate as similar of an imaging population as possible. When the user is ready to record and save the imaging file, the live mode may be turned off, and the record mode is engaged.

Spontaneous sessions were recorded for 3000 frames (approximately 195 seconds), and Forced sessions were recorded for 2000 frames (approximately 135 seconds). Behavioral cameras (Section 4.4) may also be turned on or off to record behavior concurrently. After imaging is completed, the objective is moved, and the mouse is set free and back to its home cage. The treadmill is cleaned and readied for the next mouse.

Section 4.3 From Raw Files to Population Dynamics

Scanbox, the software used for 2-photon image acquisition, exports raw ".mat" files for the calcium and behavioral recordings. A schematic of the steps involved in the processing pipeline for calcium imaging is provided in Figure 4.5 and discussed in this section. All steps outlined here apply to a single video file, and these steps were repeated or completed in batch for all video recordings. The same scripts used here for calcium imaging have been used in peer-reviewed studies recently published, one from the Carmichael lab investigating calcium imaging in stroke[7] and another from the Levine lab investigating Huntington's disease models[8]. These studies used the same steps for pre-processing, segmenting the recordings and extracting calcium transients from their traces. Scripts used in these steps can be found as supplementary files to this thesis.

<u>Pre-processing</u>

The first step is to convert the raw imaging files to the more usable tiff video format, accomplished through a Matlab script (sbx2tif). All calcium files were assessed for any motion and the EZcalcium tool was used for motion correction of the files when necessary[9]. Any videos with excessive motion artifact which could not be fixed by motion correction were excluded from the dataset. The tiff file is then imported to ImageJ for further processing, including the generation of an "average projection" and a "maximum projection" of all images in the recording. The segmentation algorithm will use the maximum projection image to help determine outlines of ROIs. The average projection is used to calculate the average background fluorescence by measuring and noting the median fluorescence of a 30x30 pixel box of the darkest area of the average projection image.

Segmentation and ROI Selection

The cal_dff script automatically identifies regions of interest (ROIs) which correspond to islands of correlated pixels with an average intensity >130% of background fluorescence. These ROIs are also size constrained from 140μm2 to 400 μm2. The tiff file, maximum projection image, and the average background fluorescence are input to the cal_dff Matlab script. The output is a map with all potential ROIs and their fluorescent traces.

The all_cells_analysis script is applied, and each ROI is manually inspected for its morphology and fluorescent traces. Any ROIs which were suspicious of being somata or over-expressing GCaMP6s were excluded from the data analysis (Figure 4.5b). Fluorescent intensity is converted ΔF/F values calculated by subtracting average fluorescence of the ROI by current fluorescence at a particular frame, then divided by the average fluorescence. This commonly used metric allows easier visualization of changes in fluorescence and helps to decrease noise in the signal. MATLAB smoothing and peak detection functions are applied to these traces and identified

as Ca2+ transients. Amplitudes of each transient were calculated as the peak of the transient from baseline ΔF/F over the prior 49 frames from the detected transient to account for any drift in the fluorescence. Peaks which were less than the root-mean square of the ΔF/F were not considered Ca2+ transients. Frequency was calculated by dividing the number of identified Ca2+ transient peaks and dividing by seconds being imaged, resulting in the number of transients per time (Hz).

Correlation within a neuronal recording session

The final code of the all_cells_analysis file applies a temporal deconvolution to all ΔF/F traces to remove the slow chemical decay of the GCaMP6s signal, thus increasing the signal-to-noise ratio of the Ca2+ transients. The Pearson product-moment Correlation Coefficient (PCC) for each deconvolved trace was calculated about all other deconvolved paths, which correspond to all different ROIs. Thus, PCC is a measure of the correlation between one neuron and another neuron in the population. A table of PCC values may be generated, n columns by n rows, where n represents the number of neurons in the analyzed file.

Next, the script runs a Monte-Carlo simulation which randomly shifts each deconvolved ΔF/F trace in time by 0.032 seconds up to 259.32 seconds. The back end of the trace is relocated to the beginning of the trace. The PCC value for each time-shifted trace is recalculated to all non-shifted deconvolved traces. Time-shifted simulations are repeated 100 times for each trace, and the distribution of all observed PCC values is generated. The 99th percentile of this distribution is used as a threshold to define a "significant PCC value" for each trace. The original PCC values are compared to this threshold, and only values exceeding this threshold are defined as significant. A table of all significant connections, and the two ROIs which are "functionally connected" to each other, is generated. The average PCC value of these significant connections is calculated and is referred to as the *average PCC* for the particular recording.

For each mouse subject, there are at least three *baseline* imaging sessions before the experimental variable is applied-- in this case, a stroke to the underlying cortex. The average PCC value for each baseline video is noted, and an aggregate average is calculated, referred to as the *threshold* for a particular mouse.

Generating %FC and FC Maps

Once the *threshold* for a particular mouse is determined, the "netExt" script is applied which uses the threshold as a cutoff for all videos for a particular mouse. All significant PCC values (defined above) above the *threshold* were defined as FCs (Functional Connections) of the recordings. Simply put, these are the values which are above the average of the baseline PCC values, signifying them as "functional connections" of this network over the timeseries.

The FCs can then be represented as edges and the neurons participating in the connection can be filled in as nodes. This allows the generation of FC maps, and an example may be viewed in Figure 4.5d. The number of nodes may also be compared across time to determine if neurons were entering or leaving the network of highly connected neurons.

The FCs of a particular recording can also be normalized for the total number of neurons imaged in that recording. This can be done by dividing by the total number of possible connections, which may be calculated by squaring the number of neurons. The square of the number of connecting units represents the maximum number of connections that could occur in that network. Functional Connections (FCs) divided by the square of the ROIs, gives %FC: the ratio of connections which were functional (compared to the animal's baseline) to the total possible connections. The normalization of FC by the total possible connections makes it possible to compare the number of FCs across animals, which have variable number of neurons in the recorded population.

All statistics were run through *Graphpad Prism* and graphs were generated within the program as well. Data was always plotted ±SEM. Figures were created with BioRender.com.

Section 4.4 Head-fixed Evaluation of Forelimb Function

The motor system, as discussed in Chapter 1, is the system most often affected by stroke. Infarct to any of several parts of the nervous system can disturb the neuromuscular wiring of the organism and may lead to a variety of behavioral deficits. Quantitatively measuring these deficits is an integral part of studying animal models of stroke. As discussed previously, the photothrombotic (PT) stroke model functions by occluding small vessels and causing a cortical infarct by shining a specific wavelength light onto the respective region. Advantages of this method include that it is minimally invasive, reproducible, and induces a minor diameter stroke which mimics most human strokes[10]. Further, the cortex lends itself to neuroimaging as it is the most superficial region, and there are physical limits on the depths of imaging with current optical techniques. For the present experiments, a behavioral assay was needed, which was compatible with PT strokes and *in-vivo* imaging.

A handful of behavioral assays have been used to assess behavioral deficits after stroke, including the rotarod test, cylinder test, adhesive removal test, and the foot fault test[11]. However, the studies that have used each assay can be pretty distinct as there are multiple stroke models and animal models used. One study reported that the foot fault test, water-maze, and beam walk were sensitive to assess functional deficits after cortical trauma[12]. The foot fault test is a simple assay in which mice are placed on an elevated grid composed of 2.5cm2 squares. The mouse must grip the metal bars to walk across the grid while a camera records all of its steps. The experimenter then counts the number of foot faults and the total number of steps for each paw. The Carmichael lab

has employed the foot fault test extensively in peer-reviewed studies as a way to quantify PT-stroke deficits and recovery involving EphrinA5 inhibition[13], GDF10 activation[14], and CREB overexpression[15]. In all of these studies of PT strokes, the foot fault test demonstrated the most significant deficits one week post-stroke and which plateaus at ~50-70% recovery by six weeks. Similarly, enhancement of behavioral recovery on this task was typically observed as a slightly smaller maximum deficit at week one and a higher recovery rate in the following weeks, ending with a plateau slightly above foot fault percentage of sham animals. In these studies, the ipsilesional paw remained unaffected with a foot fault percentage similar to the animal's baseline.

The foot fault assay is an excellent fit for our experimental model, but it was not designed for head-fixed experiments. *In vivo* imaging requires a stable field of view throughout the imaging session. Minimization of head motion is accomplished by a craniotomy surgery and adhering a metal head-bar to the posterior skull of the mouse. During an imaging session, the head-bar is clamped into place, and the objective is lowered onto the cranial window while the head remains motionless. Often, *in vivo* imaging experiments do not require a behavioral assay, and the mouse is anesthetized during these experiments. In experiments where anesthesia would confound results, mice have been placed on an airlifted Styrofoam ball where they can rest or move in any direction without moving their head. More complex learning experiments have designed tasks requiring paw movement without any head movement to correlate time-locked behavioral events, such as pulling a lever, with specific neuronal firing patterns.

The present experiments require longitudinal head-fixed imaging for approximately three months and a functional readout of behavior throughout that time. An adapted version of the foot fault assay was created for this requirement (Figure 4.6). The same grid which is used in the non-head-fixed foot fault task was cut into ~7 inch wide sections and were fit into the backs of a 9"

hamster running wheel. This "gridded treadmill" moved freely, and mice were able to move forward, backward or rest while head-fixed on this apparatus. A further adaptation was added to facilitate accurate analysis of behavioral function: a small DC motor was connected to the axle of the wheel such that the grid could be driven forward at an adjustable rate. Different grid speeds were piloted, and a voltage was found to operate the treadmill at a safe pace for the mice. This adaptation forces the mouse to move forward. This adaptation was necessary to properly assess deficits after stroke, as mice will tend to rest after stroke, thus not giving researchers the ability to properly gauge deficits between groups, especially in the first couple of weeks after stroke. A disadvantage of the forced version of the task is that mice will become tired over time, adding confounding factors if imaging for long periods. Thus, a *Spontaneous* and a *Forced-use* version of the gridded treadmill were generated. The Spontaneous task is less taxing on the mice, and the researcher can image multiple brain areas in a single session.

In contrast, the *forced-use* task was used for a single recording per session to serve as a behavioral readout at that time. IR lights and IR sensitive cameras were placed facing the mouse and from the side of the mouse to record locomotion while all lights are turned off for 2-photon imaging. These cameras captured video at a 30Hz, and the multiple angles may prove helpful for future automated behavioral analysis, which will be further commented on in Chapter 6.

Section 4.5 Timeline for PDE2a-inhibition Stroke Imaging Studies

The experiments reported in this thesis come primarily from four cohorts of mice imaged longitudinally for the length of the study. Three cohorts of mice were ran, each beginning with four mice per group (16 mice total). Mice were eliminated due to a) a problem with the cranial window’s clarity over time or b) a lack of at least three viable baseline imaging recordings which

did not show any aberration of data. Final counts of mice per group were between 8 and 11 (compared to a possible 12 mice per group).

An experimental timeline is provided in Figure 4.1b as a companion to this section and was applied to each cohort of mice. Each mouse received a craniotomy and viral injections as described in Section 4.1. After approximately three weeks, initial imaging was begun so that researchers may gauge GCaMP6s expression levels. At this time, the mice were also habituated to the behavioral platform and the imaging conditions. Baseline imaging and behavioral sessions may commence when the researcher is satisfied that the neurons are adequately filled with GCaMP and the quality of the recording is acceptable. Live imaging tools in *Scanbox* which assess ROI fluorescence over time can significantly assist with this. Between 3-5 baseline sessions for each version of the task and each brain region were recorded per animal.

After baseline imaging, mice were randomly divided into four groups: stroke + PDE inhibition, stroke + vehicle, sham + PDE inhibition, and sham + vehicle. These groups were meant to assess the effects of stroke and PDE inhibition on neuronal activity. PT strokes were induced in the appropriate mice by injecting Rose Bengal and shining a laser at the motor cortex for 10 minutes. Only the saline was injected in sham mice, but the rest of the procedure was conducted identically. Mice were injected daily with PDE2A-T1 beginning one day after the stroke or sham. The PDE inhibitor was prepared as described in Section 4.1 or with the vehicle for the solution without the PDE-inhibitor. Mice were injected daily in the evening for 40 days after stroke. On days of imaging, mice were injected after the imaging sessions were complete for the day. Each mouse was imaged for two sessions per week after stroke, one session for the spontaneous treadmill and one for the forced treadmill. Each spontaneous recording was 3000 frames, equating

to approximately three minutes and 15 seconds at the 2-photon recording rate; forced-use recordings were 2000 frames.

During a spontaneous session, both the motor cortex and premotor cortex were recorded for multiple sessions per animal. However, during a forced session, the mice were typically only imaged for one recording. The forced sessions in the present experiments are meant to gauge each group's performance, as further explained in Section 4.3, but they were minimized as much as possible. Twenty days after discontinuing the drug, one more forced-use session was recorded as the final recording. Raw files were transferred from the original computer of recording to a personal hard drive, and processing was initiated as described in Section 4.3.

Section 4.6 Figures

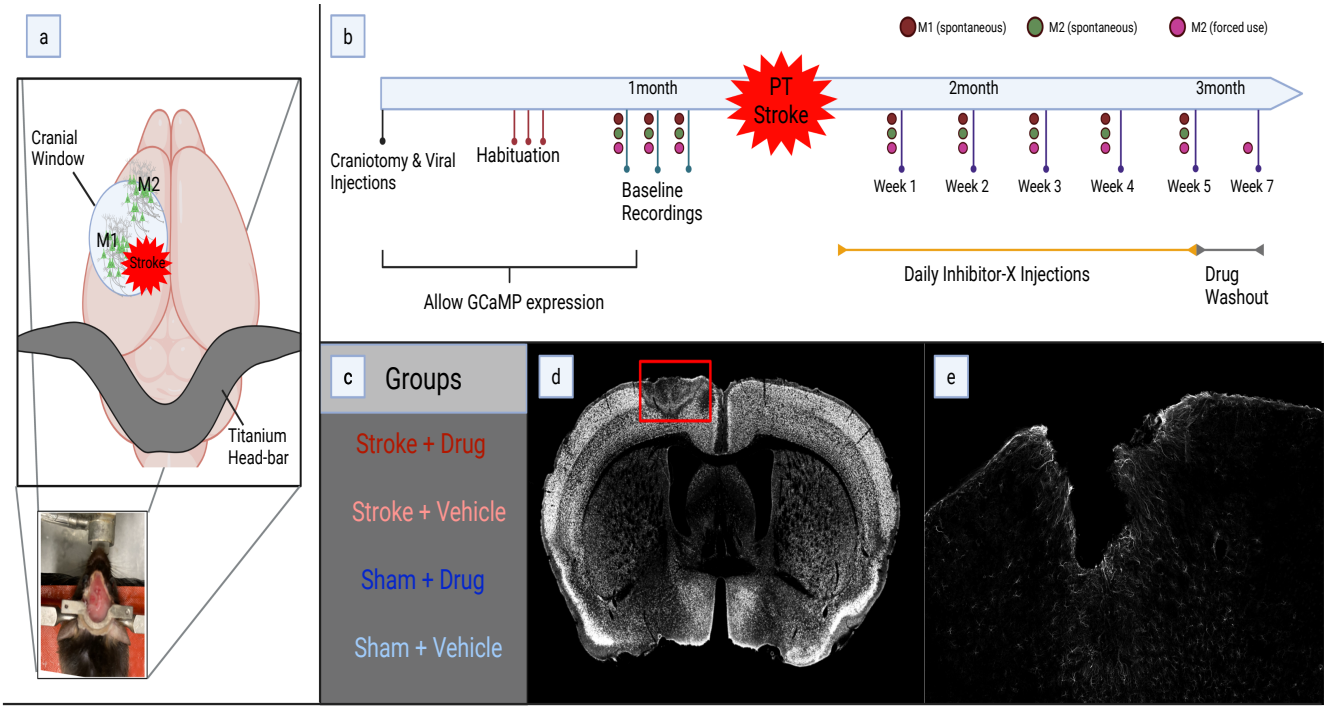

Figure 4.1 Aspects of the animal model for live imaging of PT stroke. (a) Schematic of AAV viral injections at M1 and M2 during craniotomy and application of a 4mm coverglass over region; approximate location of stroke is designated. (b) Timeline for the imaging studies, starting with craniotomy/injections, through imaging, stroke and drug injection; time since craniotomy is indicated on the timeline; colored circles represent imaging sessions for 3 contexts (Spontaneous M1, Spontaneous M2 and Forced M2).(c) List of the four experimental groups in the study: Group 1 (Stroke+Drug), Group 2 (Stroke+Vehicle), Group 3(Sham+Drug) and Group4 (Sham+Vehicle). (d) 4x coronal NeuN stain 14 days after a 12 minute PT stroke to the motor cortex; red rectangle indicates stroke core and loss of live neurons in the region. (e) 10x magnification of the stroke core with GFAP staining, indicating recruitment of GFAP+ astrocytes around the core.

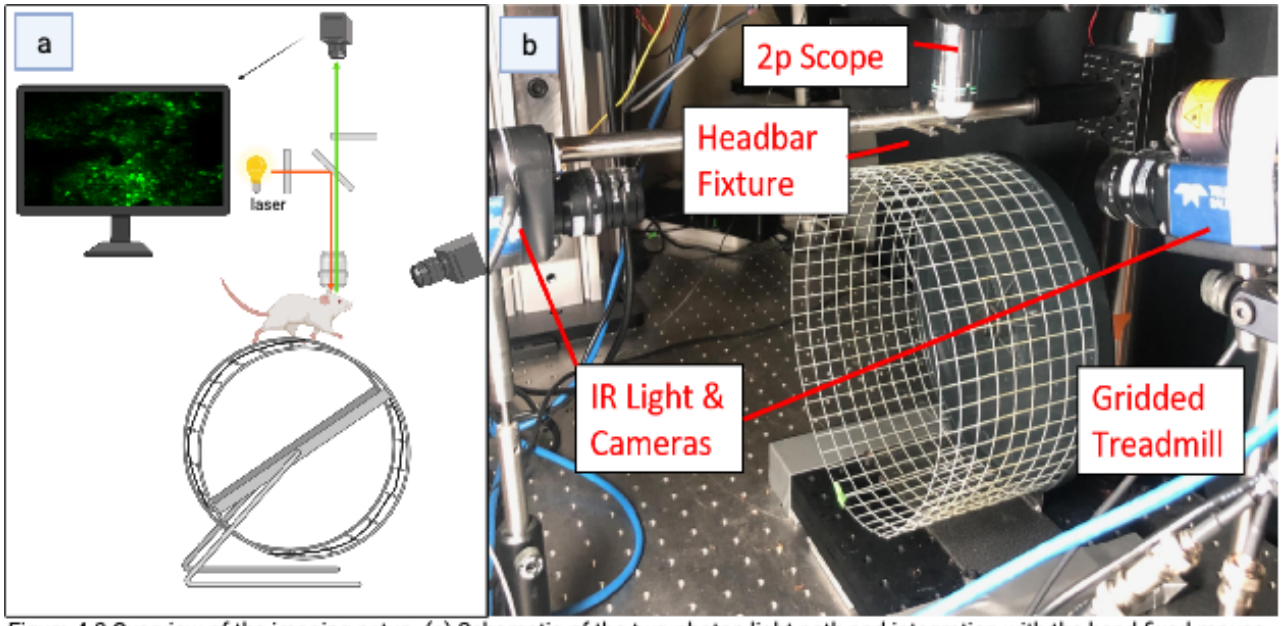

Figure 4.2 Overview of the imaging setup. (a) Schematic of the two-photon light path and integration with the head-fixed mouse for calcium imaging. (b) Photograph of the setup including the headbar fixture (where the mouse is head-fixed), the gridded treadmill and the IR-sensitive cameras capturing behavior.

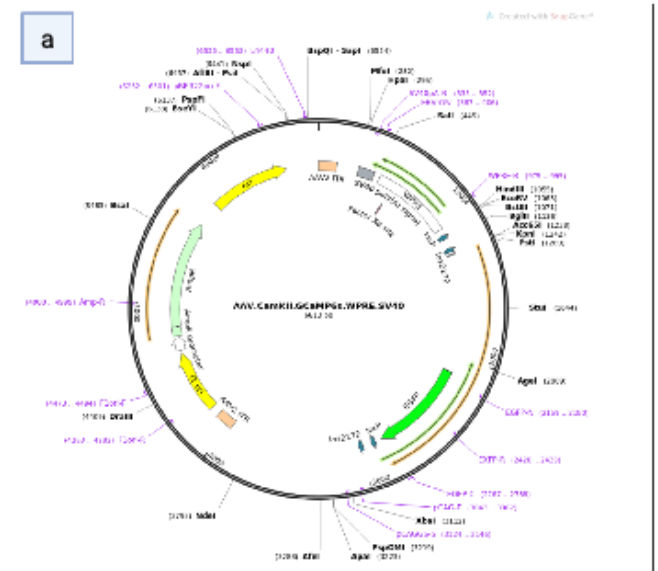

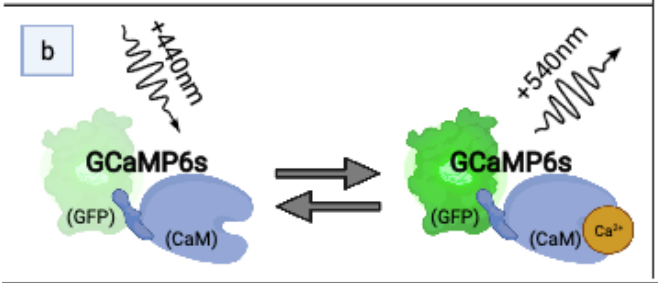

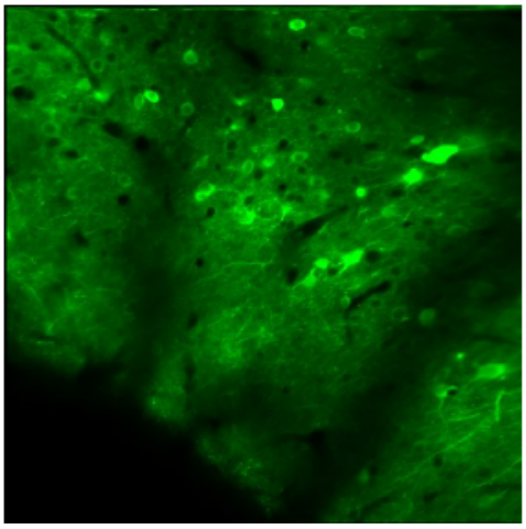

Viral Injections		
	Volume injected	Stereotaxic Coordinates
M1	1*500nL	(1.6,0.3)
M2	2*500nL	(1.5,1.5)

Figure 4.3 GCaMP6s use as a Calcium Indicator. *(a)* Schematic of the AAV vector which was injected, containing GCaMP6s under control of a CaMKII promoter. (b) When calcium and light stimulation is added to GCaMP6s (left), it is excited and fluoresces different-wavelength photons which are captured by the sensor. (c) Coronal 10x section after GCaMP injection, validating neuronal expression.

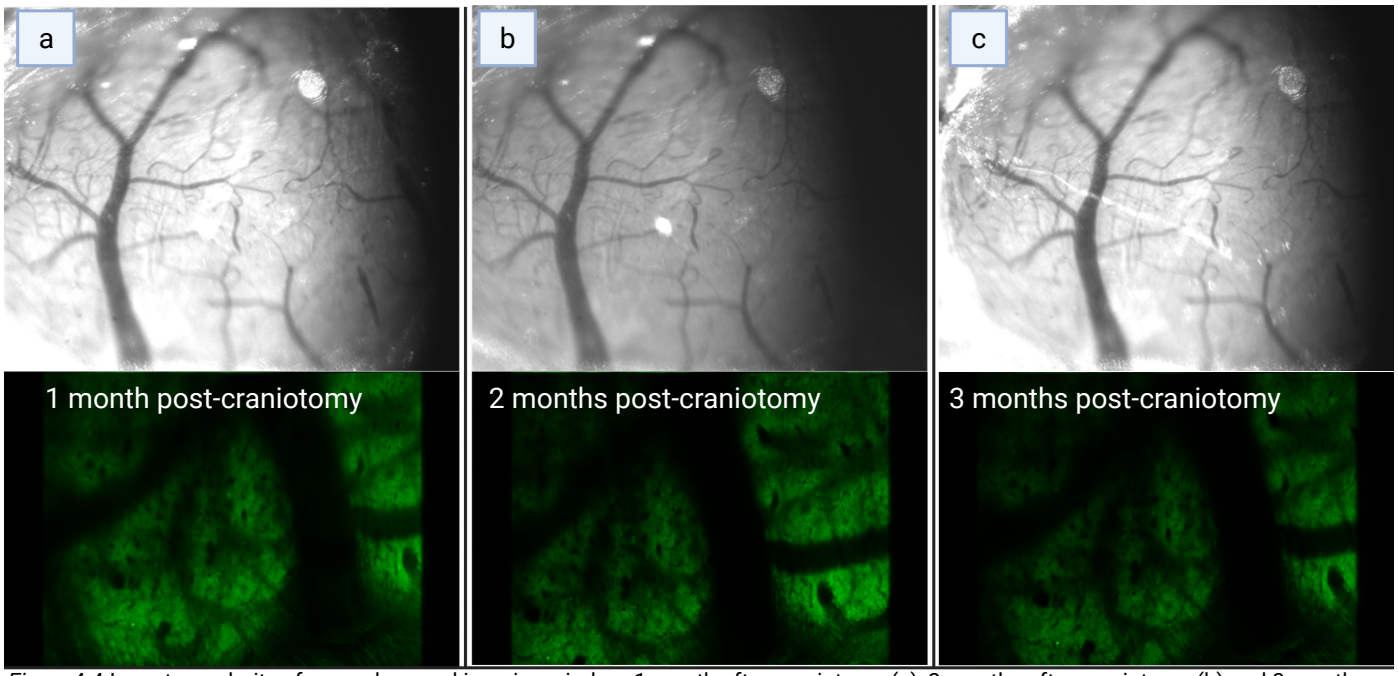

Figure 4.4 Long term clarity of coverglass and imaging window, 1 month after craniotomy (a), 2 months after craniotomy (b) and 3 months after craniotomy (c).

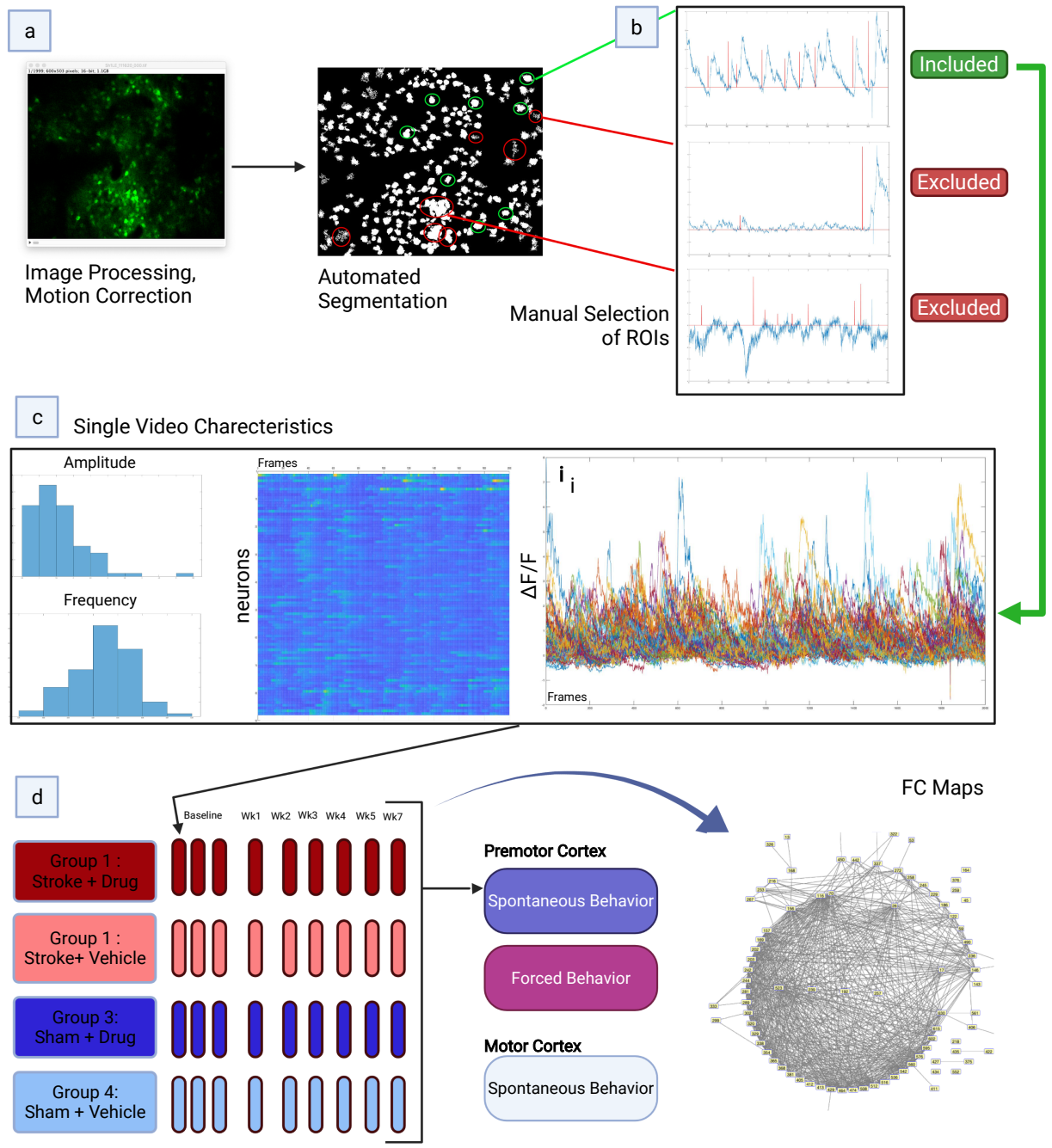

Figure 4.5 Schematic for calcium recording processing. (a) Each recording is first assessed for image stability and videos are motion corrected if motion artifact is present. Regions of interest (ROIs) were automatically generated (segmentation) and (b) then each trace is manually evaluated for inclusion or exclusion into the dataset. (c) Each recording generates a ΔF/F trace per neuron, and this can also be visualized as a heat-map (with warmer colors referring to increased ΔF/F). Amplitude and Frequency of calcium transients can be visualized as histograms for each recording. (d) Depiction of the number of recording files for one animal, across the four experimental groups; additionally, these files are representative of one of three behavioral contexts (Spontaneous M1, Spontaneous M2, Forced M2).Comparisons of correlation changes across time for a mouse generates the number of functional connections (FC) between neurons, visualized as edges and nodes in FC maps.

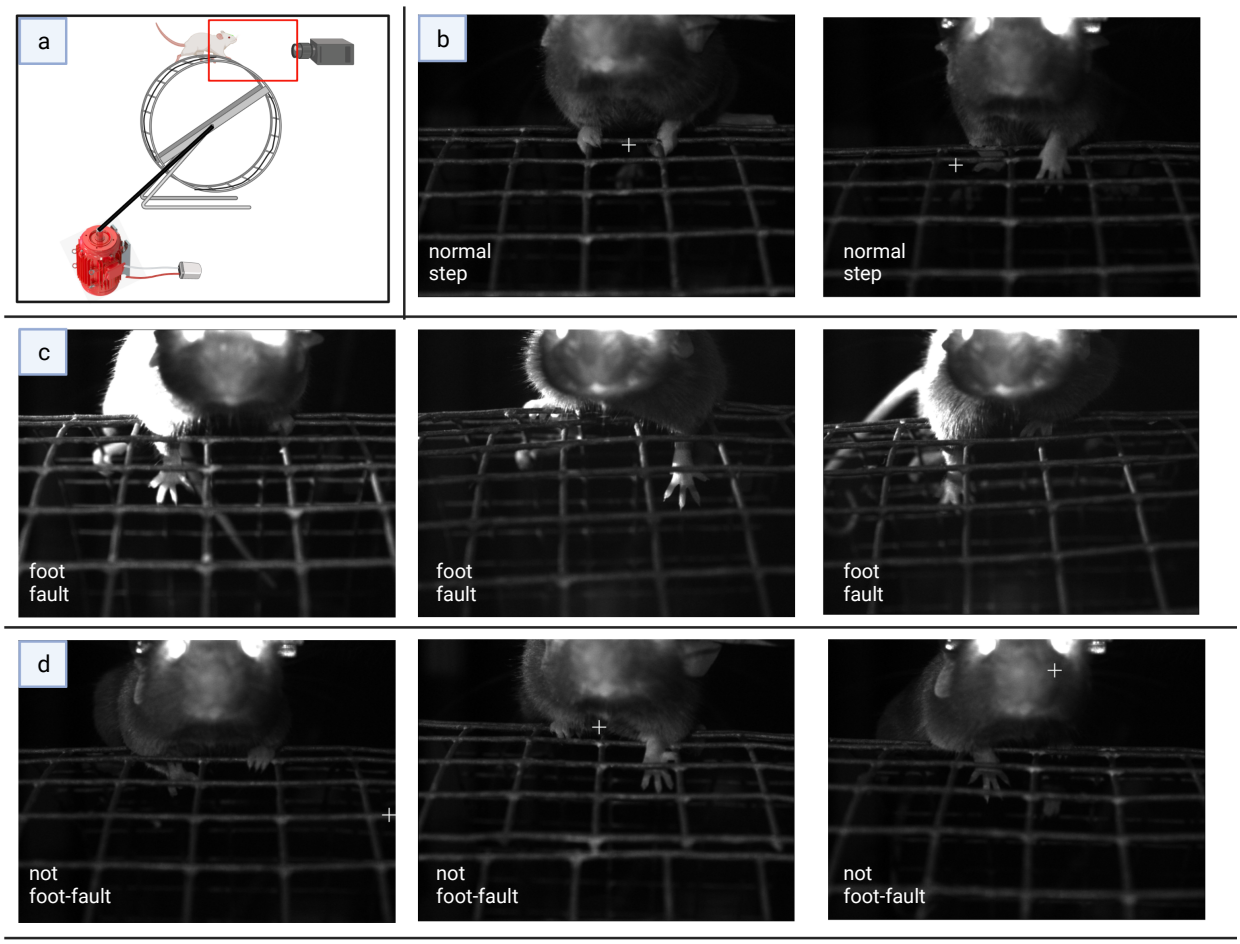

Figure 4.6 Scoring of Head-fixed performance on the gridded treadmill. (a) Schematic of the gridded treadmill, hooked up to a small DC motor which moved the grid at a slow constant rate. (b) Examples of normal steps during manual scoring ot behavior videos. (c) Examples of left and right foot faults, at the point where the forearms are fully extended. (d) Examples of variations of normal steps which were not counted as foot-faults.

Section 4.7 References

1. Svoboda, K., Denk, W., Kleinfeld, D. & Tank, D. W. In vivo dendritic calcium dynamics in neocortical pyramidal neurons. *Nature* **385**, 161–165 (1997).
2. Mostany, R. & Portera-Cailliau, C. A craniotomy surgery procedure for chronic brain imaging. *J. Vis. Exp.* **1**, 161–166 (2008).
3. Holtmaat, A. *et al.* Long-term, high-resolution imaging in the mouse neocortex through a chronic cranial window. *Nat. Protoc.* **4**, 1128–1144 (2009).
4. Watson, B. D., Dietrich, W. D., Busto, R., Wachtel, M. S. & Ginsberg, M. D. Induction of reproducible brain infarction by photochemically initiated thrombosis. *Ann. Neurol.* **17**, 497–504 (1985).
5. Zipfel, W. R. *et al. Live tissue intrinsic emission microscopy using multiphoton-excited native fluorescence and second harmonic generation*. *PNAS June* vol. 10 www.pnas.orgcgidoi10.1073pnas.0832308100 (2003).
6. Svoboda, K. & Yasuda, R. Principles of Two-Photon Excitation Microscopy and Its Applications to Neuroscience. *Neuron* **50**, 823–839 (2006).
7. Latifi, S. *et al.* Neuronal network topology indicates distinct recovery processes after stroke. *Cereb. Cortex* **30**, 6363–6375 (2020).
8. Donzis, E. J. *et al.* Cortical Network Dynamics Is Altered in Mouse Models of Huntington's Disease. *Cereb. Cortex* **30**, 2372–2388 (2020).
9. Cantu, D. A. *et al.* EZcalcium: Open-Source Toolbox for Analysis of Calcium Imaging Data. *Front. Neural Circuits* **14**, (2020).
10. Carmichael, S. T. Rodent models of focal stroke: Size, mechanism, and purpose. *NeuroRx* **2**, 396–409 (2005).
11. Balkaya, M., Kröber, J. M., Rex, A. & Endres, M. Assessing post-stroke behavior in

mouse models of focal ischemia. *J. Cereb. Blood Flow Metab.* **33**, 330–338 (2013).

12. Shelton, S. B. *et al.* A simple, efficient tool for assessment of mice after unilateral cortex injury. *J Neurosci Methods* **168**, 431–442 (2008).

13. Overman, J. J. *et al.* A role for ephrin-A5 in axonal sprouting, recovery, and activity-dependent plasticity after stroke. *Proc. Natl. Acad. Sci. U. S. A.* **109**, E2230-9 (2012).

14. Li, S. *et al.* GDF10 is a signal for axonal sprouting and functional recovery after stroke. *Nat. Neurosci.* **18**, 1737–1745 (2015).

15. Caracciolo, L. *et al.* CREB controls cortical circuit plasticity and functional recovery after stroke. *Nat. Commun.* **9**, (2018).

Chapter V: Results

The data which was collected and analyzed during the time of this dissertation included the generation of a head-fixed behavioral platform and the concurrent recording of primary and secondary motor areas after stroke. PDE2a-inhibition was also evaluated via daily injection after stroke and controlled for with daily vehicle-injection groups. Analysis of these groups demonstrate significant effects of stroke and PDE2a-inhibition on the Functional Connectivity (FC) of the networks, identifying FC as a reliable measure of network function in these studies. The negative effect of stroke in these studies matches prior results Latifi et al. obtained in the Carmichael lab, further validating the use of FC as a measure of neuronal networks. Specific results will be presented in the sections below and a deeper discussion of these studies will follow in Chapter 6.

Section 5.1 Results of Head-Fixed Behavior after Stroke

The traditional grid-walking task described in Chapter 4 is a robust measure of forelimb dexterity and has been repeatedly used to demonstrate behavioral deficits. The grid-walk test has been used in various stroke models, including the PT strokes employed in this study. The 1”x1” grid used for this task was morphed onto a treadmill to form a head-fixed version of the task (Figure 4.2). This novel application allows for simultaneous forelimb assessment and head-fixed two-photon imagin. A small DC motor was connected to the axel of the treadmill, applying a constant voltage to the motor and moving the treadmill forward at a slow rate. In this forced-use task, the subject was forced to locomote and use both of its forelimbs. Videos captured from IR-sensitive cameras were later manually scored and the results obtained are described in this section.

<u>Scoring forced-use video files and calculating foot-fault %</u>

Raw behavioral videos were converted to .tiff files, and the time point for each video was blinded from the scorer. Each video was manually scored frame-by-frame in ImageJ. Data was organized in Excel, noting the total number of steps for each paw and the frame number for any foot-faults. Each paw was scored separately to achieve a more accurate number of total steps. The researcher found the most accurate scoring by defining a "foot-fault" as a fully extended forelimb (Figure 4.6c); if the center of mass for the forelimb remains near the grid (Figure 4.6d), it indicates that the paw or wrist are still on the grid and the mouse did not commit a foot-fault. Foot-Fault % (FF%) was calculated by dividing the foot-faults by the total number of steps for each paw. The FF% for each time-point, including the average baseline FF%, were input to Graphpad Prism for graphing and statistical testing. Average FF% of the left paw and the right paw (Figure 5.1a-b) are graphed for each group and timeline; these values were normalized by dividing by baseline to obtain fold change of FF% (Figure 5.1c-d).

The gridded-treadmill is a robust measure of head-fixed forelimb function

After habituation, baseline FF% for all groups was between 2-6% and remained within this range throughout all behavioral recordings, indicating a high proficiency at this task without any training. The unaffected forelimb, the left paw, remained at this high proficiency independent of any group, indicating that neither stroke nor drug affects the ipsilesional paw on this task (Figure 5.1a,c). The right paw of the sham groups (Group 3, Group 4) remained at 3-6 FF% throughout the recordings (Figure 5.1b,d). Mixed-effects analysis (MEA) revealed no significant differences at any of these time-points in the left paw or the sham groups' right paw. These results confirm that this behavioral task can report consistent forelimb performance in naïve mice and the unaffected limb after stroke. Furthermore, the consistency of the low FF% in the later imaging

sessions also suggests that the intensity and dose of this forced task do not induce enough stress to decrease performance in the animal (further discussed in Section 6.1).

Stroke causes increased Foot-Fault % in the affected limb, followed by recovery

As expected, motor forelimb strokes cause a significant increase in the FF% of the contralesional paw on the gridded treadmill task (Figure 5.1b). Group 2 (Stroke+Vehicle) has significantly increased FF% every week after stroke when compared with Group 3 (Sham+Drug) and Group 4 (Sham+Vehicle). Group 1 (Stroke+Drug) had a lower average FF% than Group 2 at every time-point after stroke. A three-way mixed model analysis of FF% indicated a statistically significant fixed effect of stroke ($p<.001$) but not for drug ($p=.5638$). As the gridded treadmill is a test of behavioral deficit, administering the drug by itself was not expected to enhance performance on the highly proficient naïve mice.

Relative to its own baseline, stroke alone (Group 2) had significantly increased behavioral deficit at every time point. In contrast, Stroke+Drug was significantly increased only in Weeks 1 and 2, relative to its baseline (Figure 5.1b). Groups 3 and 4 were never significantly different from their baseline. Thus, stroke alone causes a statistically significant increase in FF%, and the addition of Inhibitor-X returns the performance to non-significantly different levels by Week 3. This data matches the non-head-fixed data presented in Figure 3.2, demonstrating significant effects of Inhibitor-X enhancing recovery after stroke.

Inhibitor-X was injected for 40 days after stroke and discontinued after the Week 5 imaging. Mice were recorded for a final Week 7 session, serving as a trial after two weeks of drug washout. Behaviorally there were no significant differences, but the trend for recovery continued for Groups 1 and 2 (Stroke groups). Further discussion of the effects of washout may be found in Section 6.3.

Section 5.2 Spontaneous Recovery in the Primary Motor Cortex (M1)

The primary motor cortex (M1) was highlighted in Chapter 2 as having the most direct connections over different muscle groups; stroke to this region disrupts those connections. Here, the calcium imaging data from nearby neurons are assessed after a stroke to M1. Careful deliberation was taken when picking the field of view (FOV) for M1 imaging, attempting to not overlap with the region which will later become the stroke core. This is favorable as these experiments try to capture the same population of neurons over time. While we cannot remove the possibility that some neurons in this region died due to stroke, a relatively consistent number of active neurons across time points suggests that similar populations of neurons were being recorded. Data from single recording sessions: number of neurons, amplitude, and frequency will be presented first, then functional connections (FC) and FC maps will be assessed.

Number of imaged M1 neurons does not change after stroke

Single GCaMP recordings were processed according to the steps in Figure 4.5a-c. After ROI segmentation, fluorescent traces for each neuron is extracted, and the ΔF/F is calculated (F(t)-F0/F0). The average number of ROIs ±SEM of the M1 recordings for each group is plotted in Figure 5.2, and no trends were found across any of the groups. It is important to note that populations of virally transfected neurons will naturally vary, and averages across groups will diverge randomly. However, within a group, the average number of neurons should remain relatively constant since they are the same animals and the same regions imaged. All values passed the Shapiro-Wilk and Kolmogorov-Smirnov tests for normally distributed data (Table 5.2).

Amplitude and frequency of calcium transients does not change in M1

Calcium transients are detected by Matlab peak detection functions, and the amplitude and frequency of these transients were then calculated (Figure 4.3b).

The average amplitude and frequency ±SEM of the neurons from M1 are plotted in Figure 5.4a and Figure 5.5a, respectively. No significant differences in either of these measures were found across the groups and across the time-points. Average amplitude for each time-point ranged from 1-2.5 ΔF/F, and average frequencies ranged from .6-.8 Hz. MEA determined no significant effect of stroke or drug on amplitude or frequency in the primary motor cortex.

Functional Connectivity (FC) of M1 after stroke

The connectivity methods used here rely on the Pearson correlation coefficient (PCC) values between each ROI pair in a particular recording, based on the normalized covariance between neurons (Section 4.3 and Figure 4.5d). Functional Connections (FC) were defined as any PCC connection above the threshold PCC, the calculated average from all baseline recordings of an animal. The square of the ROIs involved and is the total possible connections that could be made. Dividing functional connections (FC) by total possible connections gives %Functional Connection (%FC), which is determined for every recording. The average %FC ±SEM in M1 (Figure 5.5a) and the fold change over baseline (Figure 5.5b) are plotted.

ROIs which participate in FC were defined as 'nodes'; changes in the number of nodes for a video would indicate a change in the number of neurons contributing to highly functional connections. The average number of nodes ±SEM is plotted (Figure 5.7a). No significant effects on the number of nodes were appreciated, and MEA determined no significant differences.

Functional Connectivity (FC) maps may also be generated from nodes, and FCs discussed above. Nodes in the graph represent neurons participating inactive connections, and edges can be drawn to represent those active connections. A representative subject was selected for each group, and a map was created for each of its imaging files. Figure 5.8 shows these representative FC maps in the primary motor cortex.

Inhibitor-X increases %FC

Inhibitor-X alone (Group 3) demonstrates a significant enhancement of %FC at all weeks, while the control (Group 4, Sham+Vehicle) remained constant (Figure 5.5). Mixed-effects analysis of the %FC data determined a significant effect of the drug ($p=0.0241$). This data was then normalized by dividing each value by the average baseline for that mouse, reporting the output as Fold change (Figure 5.5b). Group 3 is the group with the highest average every week after stroke, indicating that these animals had a higher percent increase from their baseline than any other group. Mixed-effects analysis of the normalized data also determines a significant effect of the drug ($p=0.0455$).

Stroke decreases %FC in the peri-infarct (M1)

Stroke alone (Group 2) shows a significant decrease in %FC in M1 after a stroke to a nearby region of the primary motor cortex (M1). Stroke (Group 2) demonstrates an adverse effect of FC% (Figure 5.5a) and maintains this deficit for three weeks post-stroke. Stroke + Inhibitor-X (Group 1) also offers a similar deficit at Week 1, nearly halving its %FC; however, Week 2 and Week 3 show increasing %FC in Group 1. There was a high degree of variation in Week 4, while Week 5 indicates that only Group 3 maintained an increase in %FC. Mixed-effects analysis of %FC determined a highly significant stroke effect on the network data ($p<0.0001$). Fold change analysis (Figure 5.5b) demonstrates a significant decrease in Group 2 versus Group 1, indicating the positive effect of Inhibitor-X described above.

Section 5.3 Recovery in the Secondary Motor Areas (M2)

The secondary motor areas (M2) compose connected frontal cortex regions uniquely situated to recover lost motor pathways after stroke. These areas are analogous to the premotor

(PMC) of the human brain, and these terms may be used here interchangeably. GCaMP was injected anteromedial to the stroke site to target the M2 areas in the current experiments, and this section will detail the results of those recordings. Like the primary motor cortex studies, the same M2 location was imaged 3-5 times before stroke and then weekly for five weeks during spontaneous recovery. Additionally, this is the location that was imaged concurrently during the forced-use behavior, and both contexts will be considered here.

Recording the same neuronal populations

Similar to the studies of M1, single M2 recordings were acquired and processed in identical ways (Figure 4.1,4.5). Stereotaxic coordinates were tracked and used to image M2 neurons at the same area throughout all recording sessions during spontaneous and forced-use behavior. Still, slight changes in the z-axis will change the field of view (FOV) on different neurons, imaging a somewhat different neuronal population. Forced-use after stroke is a unique context that induces activity that may only be detected during forced movement; similarly, there may be only active neurons in the spontaneous M2 recordings. The average number of neurons ±SEM for each group and for each time-point during spontaneous and forced-use behavior are plotted (Figure 5.2b-c). There may be random differences across groups for the number of imaged neurons, but this number should remain stable over time within a group since they represent the same populations of neurons being imaged. The number of neurons per imaging session did not significantly change before or after stroke for any of the groups (Figure 5.2); the distributions for the numbers of neurons imaged all passed the Shapiro-Wilk and Kolmogorov-Smirnov tests of normality (Table 5.2).

<u>Amplitude and frequency of calcium transients does not change in M2 after stroke</u>

Each acquired GCaMP recording is processed and analyzed according to the steps in Figure 4.5. A neuronal trace is generated by using ΔF/F and is then assessed for calcium transients, calculating the amplitude and frequency of these transients. Average amplitude (Figure 5.3b-c) and frequency (Figure 5.4b-c) ±SEM are plotted per group. No significant differences were statistically noted (Tables 5.4-5.5) across any group. Stroke and drug were not found to have significant effects on amplitude or frequency.

Stroke decreases functional connectivity in M2 populations

Pearson correlation coefficients (PCC) values between each pair of neurons are calculated; %FC is calculated as the ratio of above threshold PCC values over the total possible connections. FC maps can also be generated, connecting participating neurons (nodes) by their FCs (edges).

Average %FC ±SEM in M2 neurons are plotted during spontaneous recovery (Figure 5.6a) and forced-use (Figure 5.6b). These values were further normalized by dividing by baseline, outputting fold change (Figure 5.6c-d). Stroke had a negative effect on %FC of the premotor cortex during forced-use in all weeks after baseline, but this effect was not observed in the spontaneous imaging. Stroke was determined to significantly affect %FC only in forced-use imaging (Figure 5.6c, $p=0.0164$) but not in spontaneous imaging (Figure 5.6a, $p=.6838$). Spontaneous behavior is a combination of rest, motion, and grooming epochs that the investigator does not affect, while forced-use employs the motor-driven treadmill; the implications of the differential effect of stroke on these contexts will be discussed in Section 6.1.

Nodes were defined in Section 4.3 as the neurons participating in functional connections of the network. The average number of nodes ±SEM was evaluated for M2 studies in the spontaneous and forced-use behavior (Figure 5.7b-c). Differences between groups are be due to random fluctuations in the number of transfected neurons in the field-of-view (FOV). Within

groups, fluctuations in nodes would indicate neurons joining or leaving the network based on FCs. MEA did not find any significant differences across any group suggesting no neurons were entering or leaving the networks (Table 5.7b-c). Representative mice were selected from each group to generate an FC map from the nodes and edges from the spontaneous context (Figure 5.9) and the forced-use context (Figure 5.10).

Inhibitor-X enhances functional connectivity in M2 populations

PDE2a-inhibition was found to enhance functional connectivity in the M2 recordings, indicating higher levels of correlated connections in the network ($p=0.0055$ for spontaneous recovery and $p<.0001$for forced-use). Weeks 1 and 2 showed significantly increased levels %FC, as noted in Figure 5.7c by dark blue asterisks. FC maps also demonstrate this effect in Group 3 (Sham + drug) of spontaneous recovery (Figure 5.10) and of forced-use recovery (Figure 5.11). In the generation of these FC maps, the %FC was increasing relative to baseline such that applying baseline threshold was generating maps with very high numbers of nodes and edges. In some cases, these files could not be rendered, and in other cases, the images looked saturated, and no trend was visually observable. A threshold of 1.25, the baseline threshold was applied for the generation of Group 3 in Figures 5.10 and 5.11 (indicated by a gold star on the figures). The threshold was applied to all videos for both particular subjects, allowing comparison of the groups. Drug washout in Figure 5.7c also indicates a decrease in %FC after washout of the drug in Group 1 and Group 3, and this decrease may also be visualized in the corresponding FC map in Figure 5.11

Section 5.4 Figures

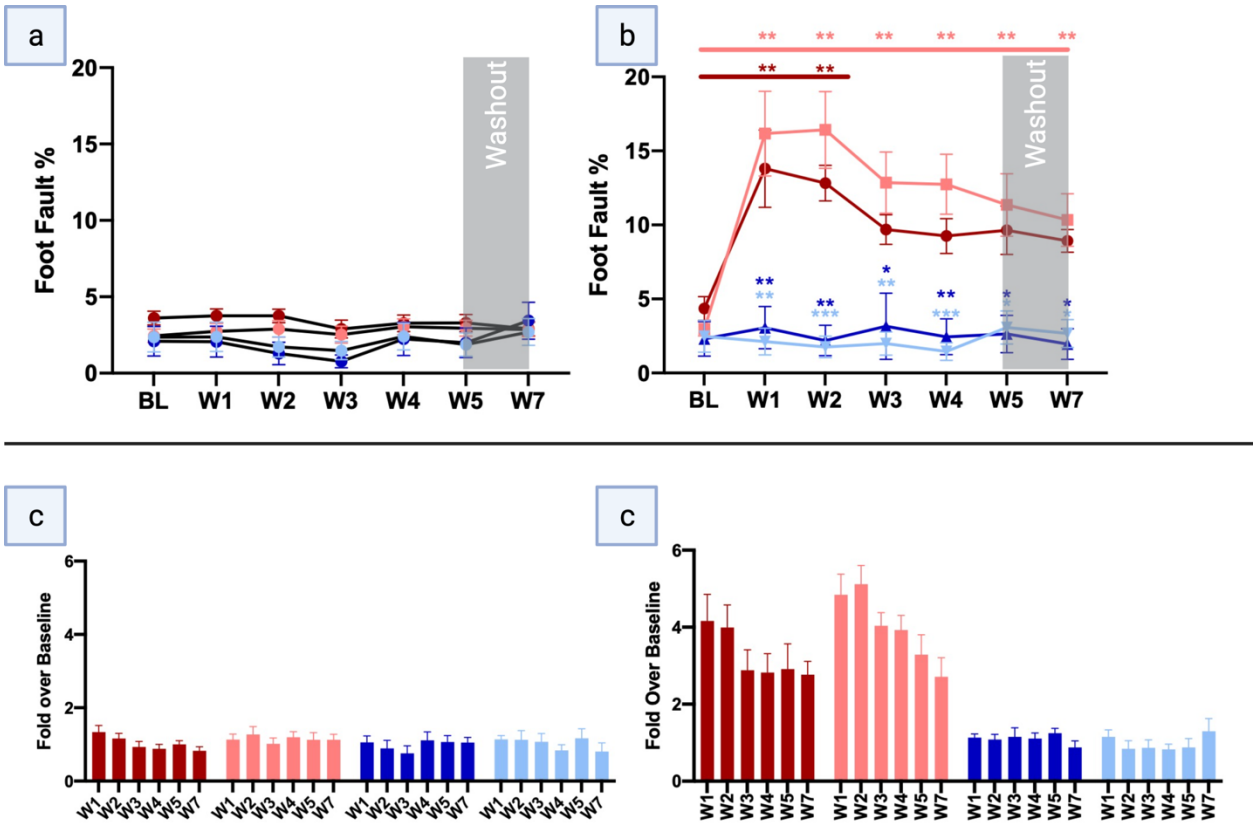

Figure 5.1. Foot fault % (number foot faults / total number steps) measured at different time-points for the left paw (a) and the right paw (b). Fold change over baseline is calculated for each respective paw (c-d). Washout of Inhibitor-X is indicated by grey bar. Mean FF% and fold change are plotted ±SEM. Stroke has a negative effect on performance ($p<0.0001$) in the affected paw. Asterisk on Groups 3 and 4 indicate significant difference from Stroke. Asterisks across a bar indicate significant increase from that respective group's baseline. Inhibitor-X significantly enhances recovery back to baseline by Week 3. n=8-11 mice per group.

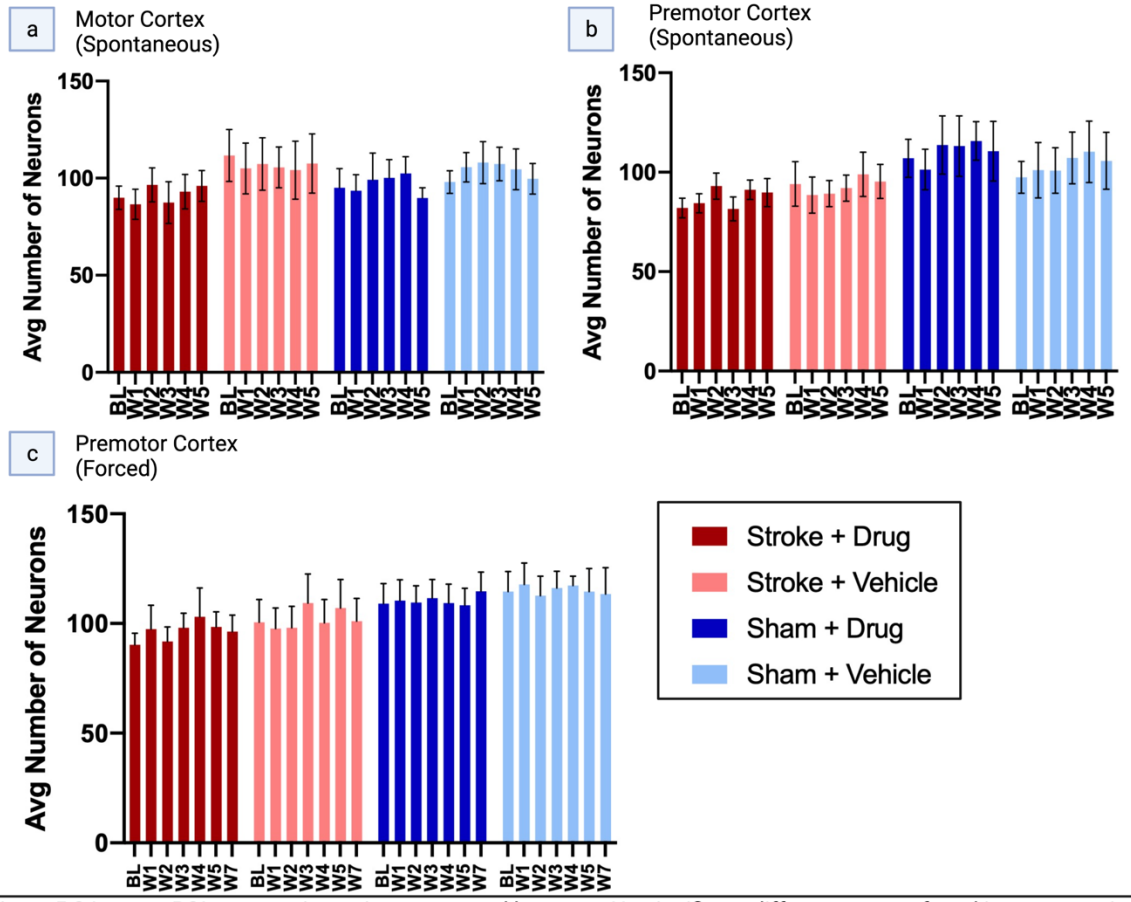

Figure 5.2 Average ROIs across timepoints, separated by group. No significant differences were found in any group in either MC or PMC. All groups passed the Shapiro-Wilk test and Kolmogorov-Smirnov tests for normality.

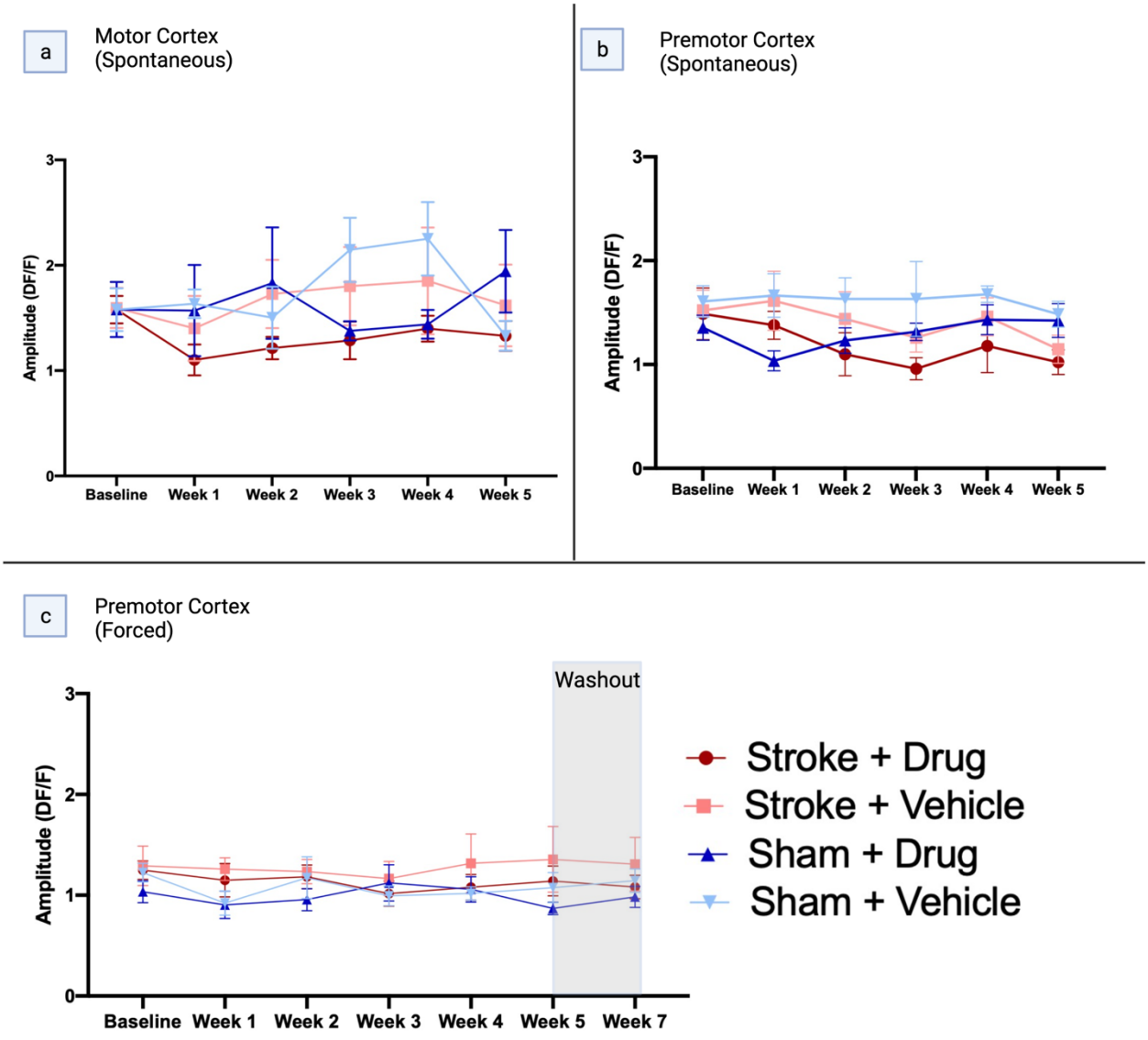

Figure 5.3 Average amplitude of each calcum transient across all time points across the four experimental groups. This is shown for spontaneously behaving mice in the (a) motor cortex and (b) premotor cortex, as well as forced-use mice imaged in the premotor cortex (c). n=7-11

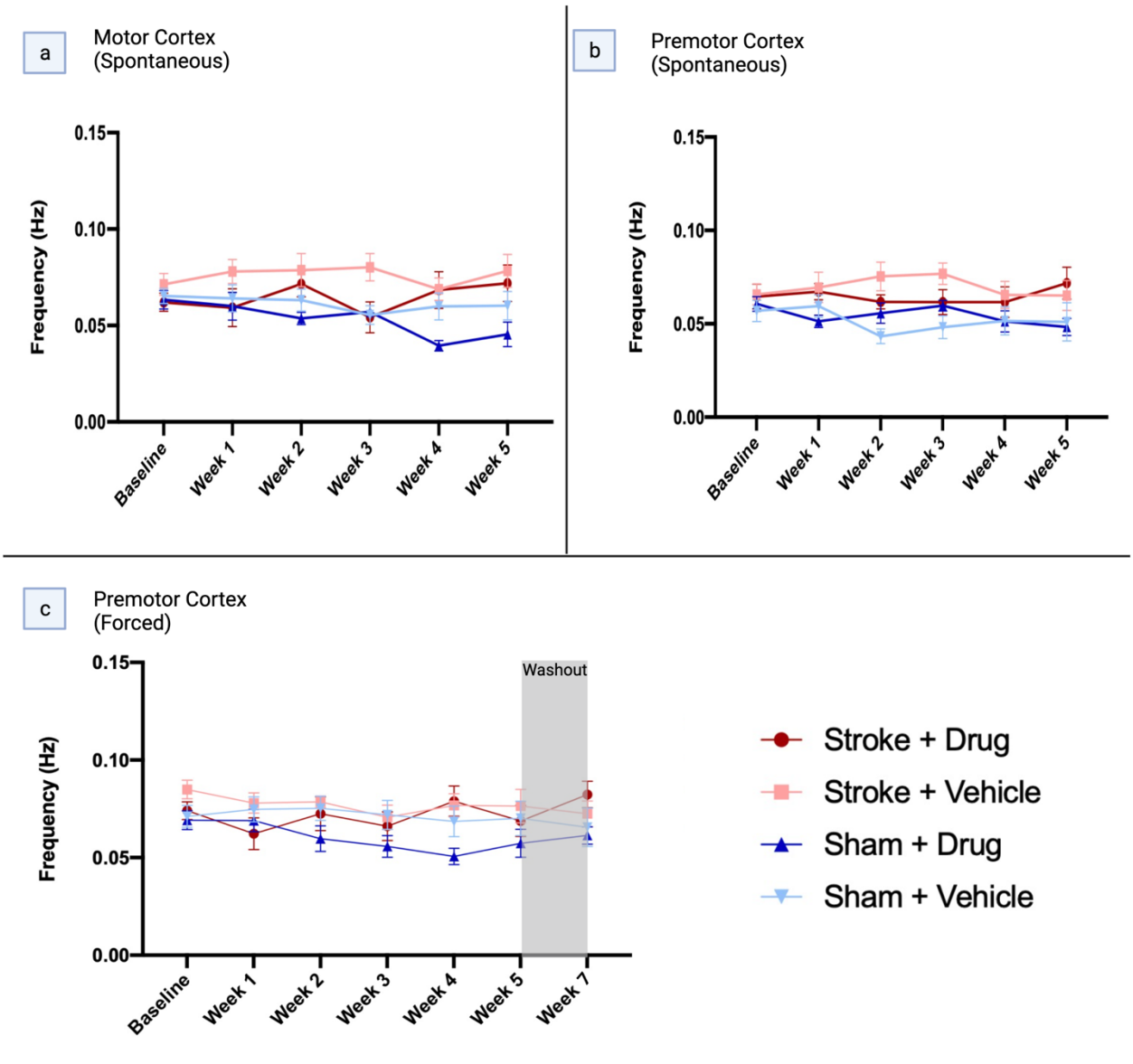

*Figure 5.*4 Frequency of calcium transients in calcium imaging from the spontaneous recovery of M1 (a), the spontaneous recovery of M2 (b) and forced-use recovery of M2 (c). n=8-11

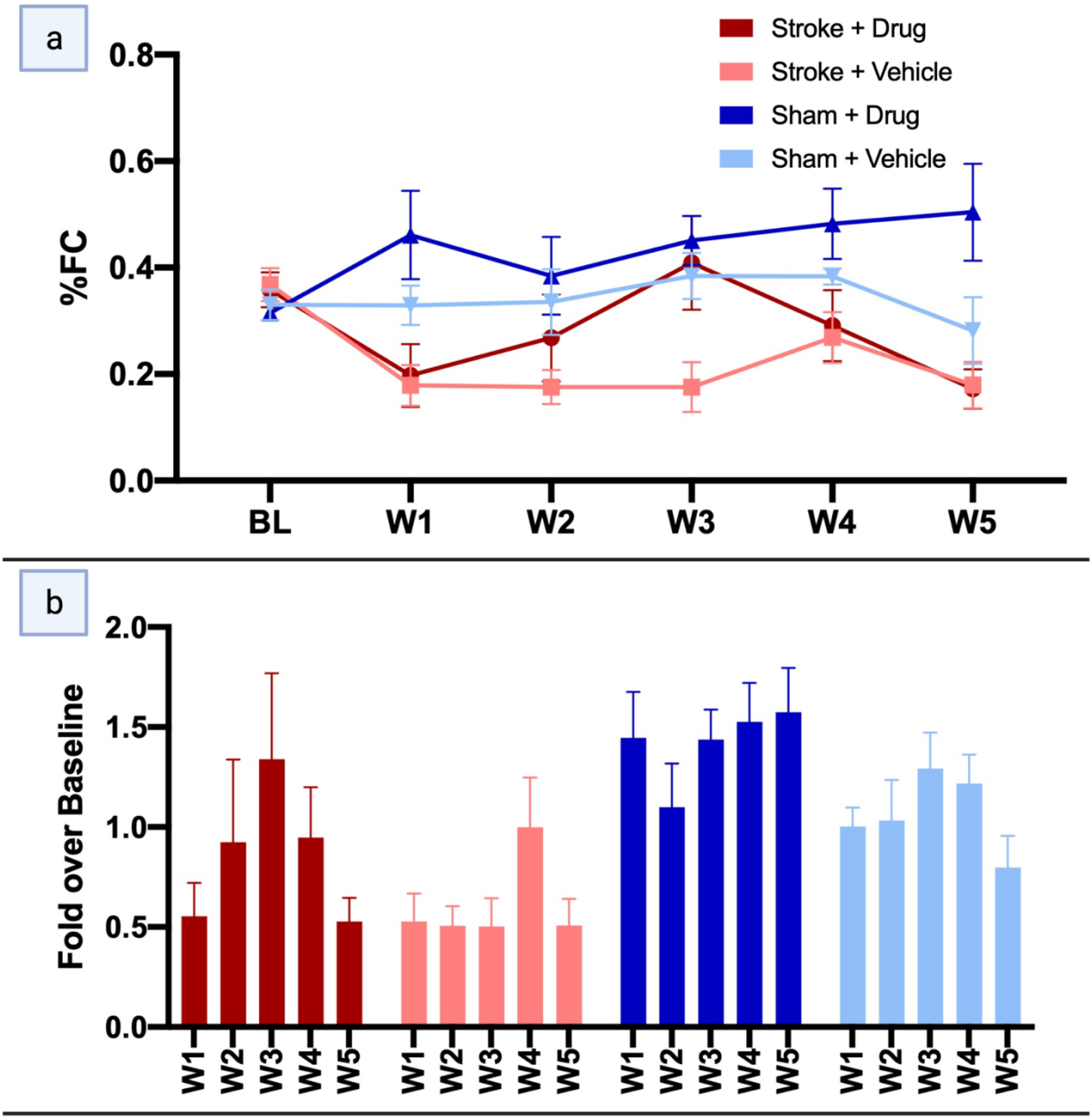

F*igure 5.5* Functional connections (FCs) of the motor cortex. (a) %FC (FC over ROI^2) is plotted for each group with SEM error bars. Mixed Effects Analysis (MFE) determined a significant effect of stroke (p=.0001) and of drug (p=0.0241). (b) Fold change of %FC over baseline for each group. Asterisks indicate significant timepoints compared to Group 4 (Sham + Vehicle). n=7-11

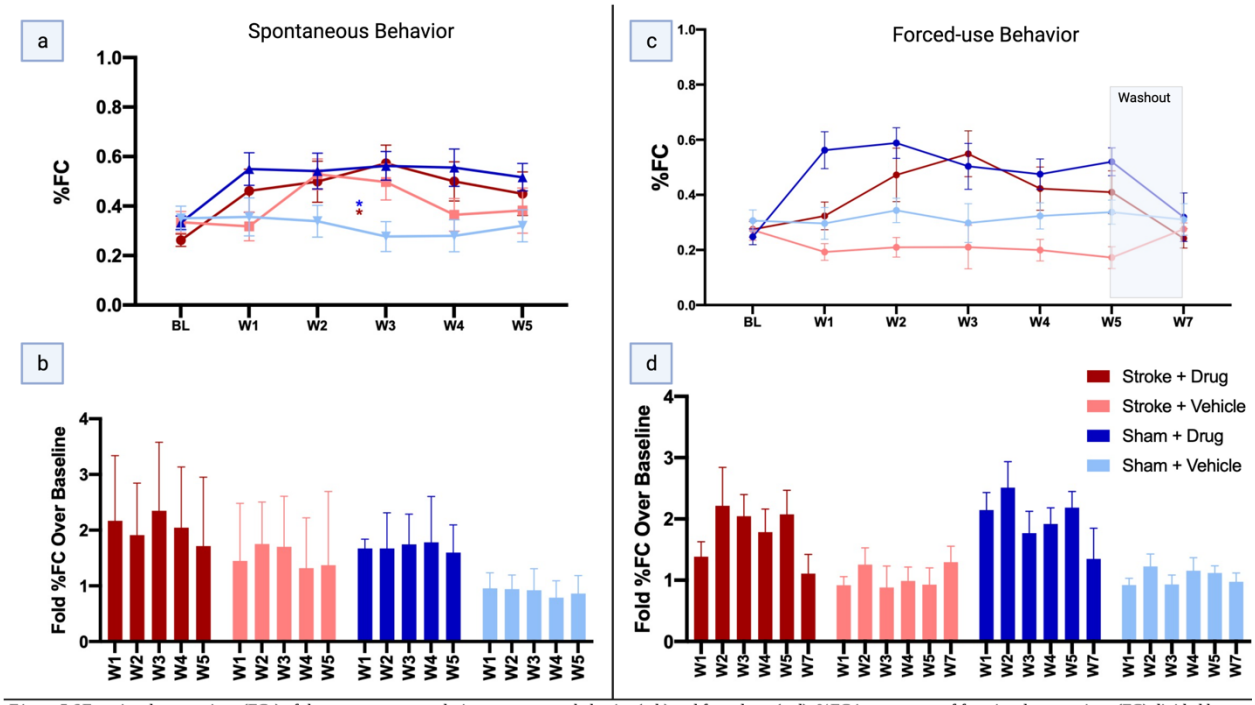

Figure 5.6 Functional connections (FCs) of the premotor cortex during spontaneous behavior (a-b) and forced use (c-d). %FC is a measure of functional connections (FC) divided by total possible connections (ROI^2); Fold %FC over baseline divides FC by baseline for each animal. In the spontaneous condition (a), drug has a positive effect on %FC ($p=0.0055$) but stroke did not ($p=.6838$). In forced-use (c), drug has a positive effect on %FC ($p<0.0001$) and stroke has a negative effect on %FC ($p=0164$). n=7-11

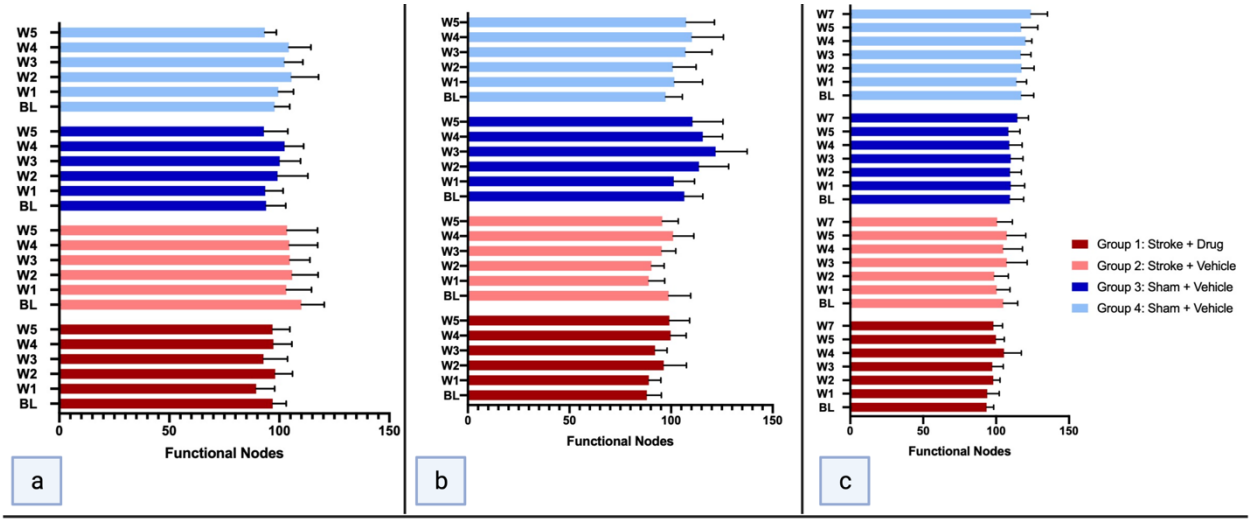

Figure 5.7 Functional Nodes from the primary motor cortex (a) and secondary motor cortex (b, c) participating in functional connections (FC). Mixed effects analysis indicates no significant differences across any group or any timepoint. Average nodes are plotted ±SEM error bars. n=7-11

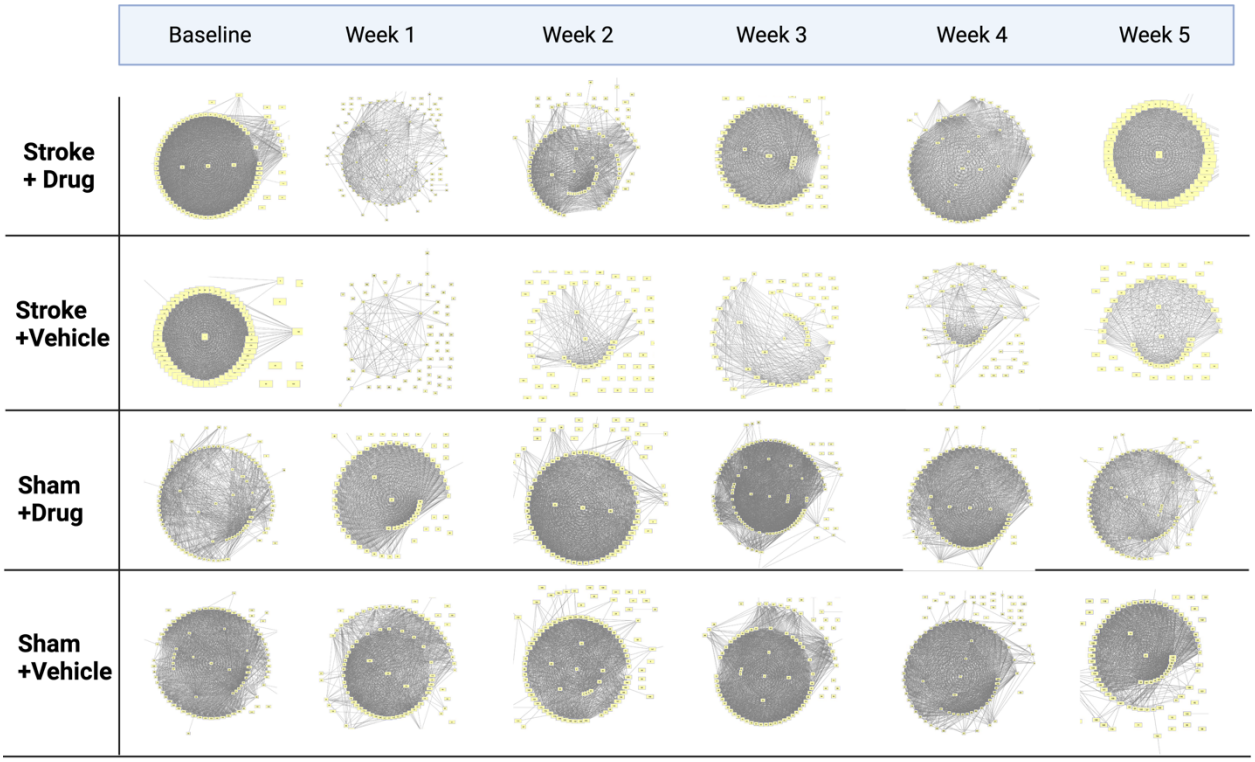

Figure 5.8 Functional Connectivity (FC) Maps of the motor cortex during spontaneous recovery after stroke. FC Maps were generated by identifying and counting all PCC values above the defined baseline threshold, and plotting these values to nodes which represent neurons.

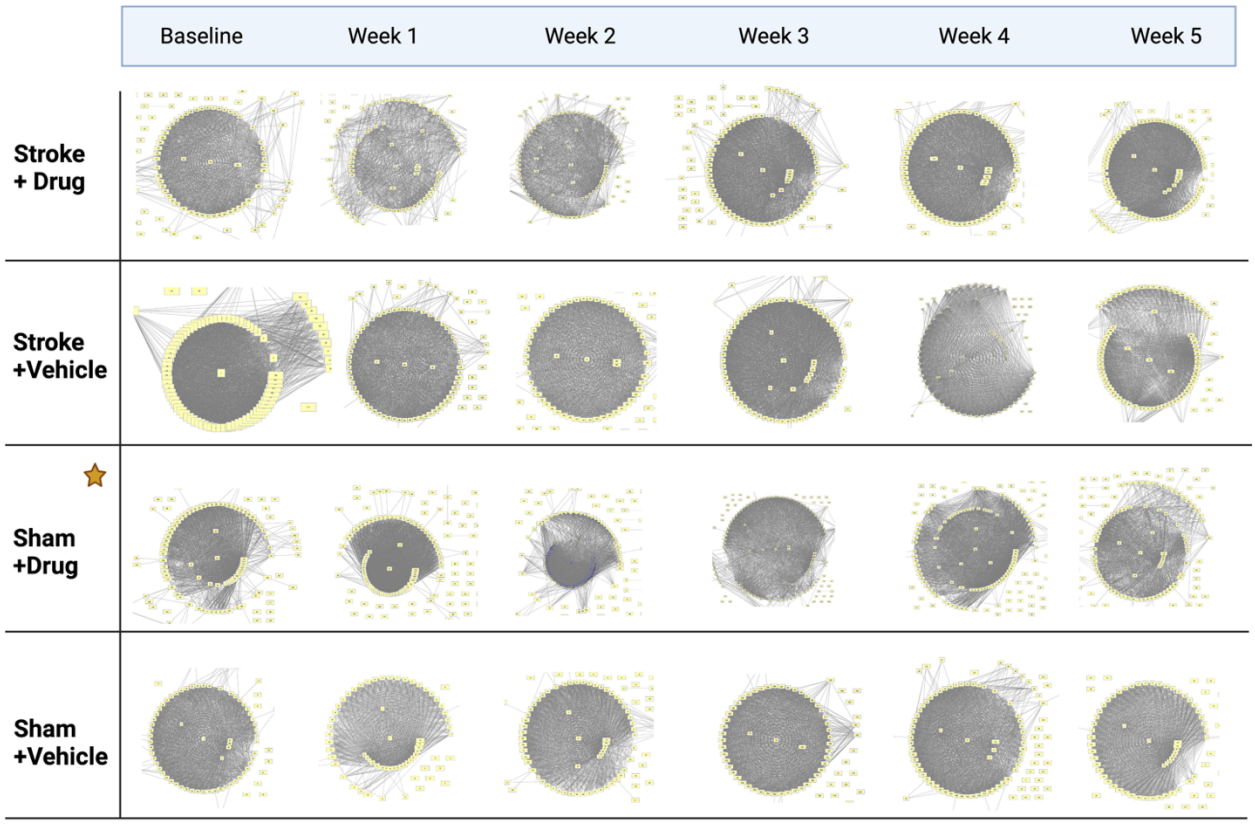

Figure 5.9 Functional Connectivity (FC) Maps of the Premotor Cortex during Spontaneous behavior. One subject from each group was selected as a representative datapoint for each timepoint. FC Maps were generated by identifying and counting all PCC values above the defined baseline threshold, and plotting these values to nodes which represent neurons; thresholds are applied across all videos in a series equally. Gold star (Sham+Drug Group) indicates a 1.25x threshold was applied due to over-saturation of edges and an inability to display the image.

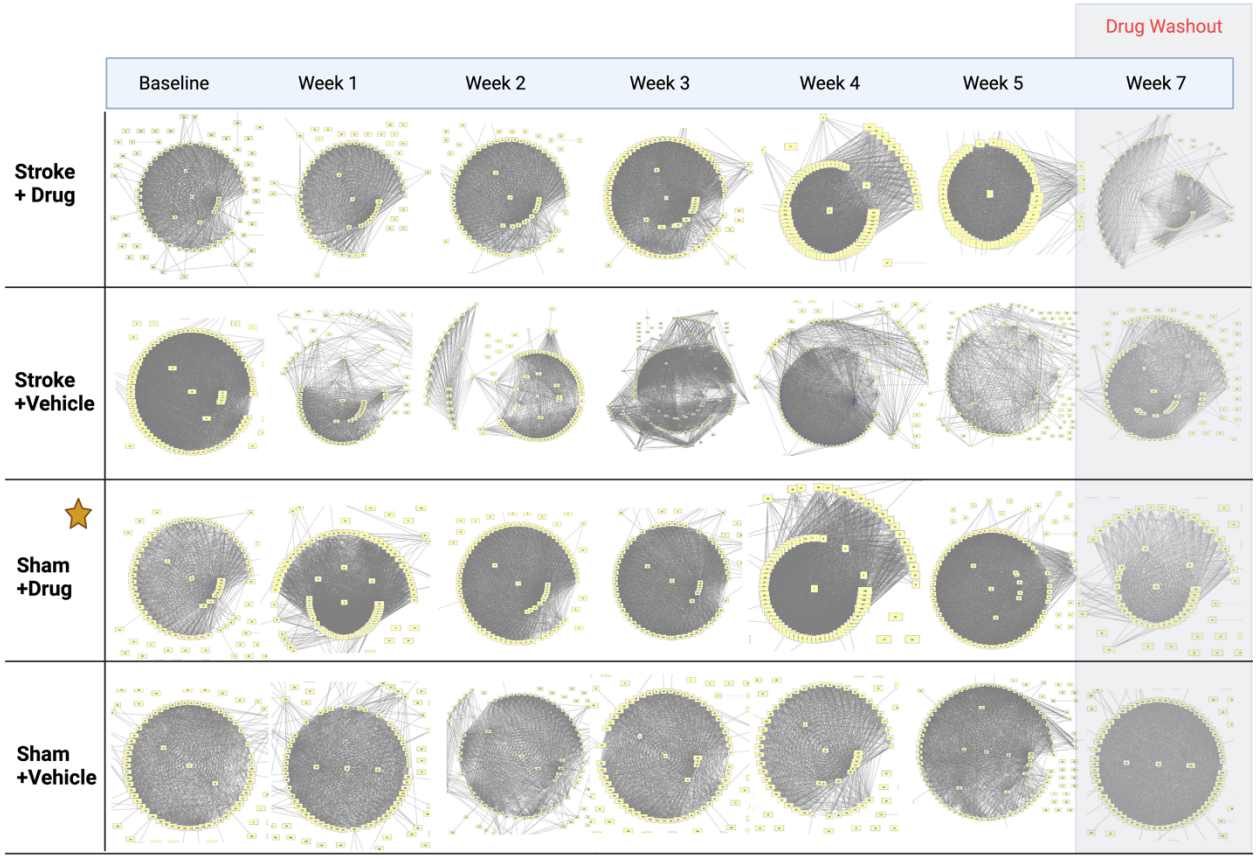

Figure 5.10 Functional Connectivity (FC) Maps of the Premotor Cortex during Forced Use. One subject from each group was selected as a representative for each timepoint. FC Maps were generated by identifying and counting all PCC values above the defined baseline threshold, and plotting these values to nodes which represent neurons. Gold star (Sham+Drug Group) indicates a 1.25x threshold was applied due to over-saturation of edges and an inability to display the image.

Section 5.5 Data Tables

Table 5.1 Behavior Data

Left Paw

Table Analyzed	LP Foot Faults				
Mixed-effects model (REML)	Matching by factor: Row factor				
Assume sphericity?	No				
Alpha	0.05				
Fixed effects (type III)	P value	P value summary	Statistically significant	F (DFn, DFd)	Geisser-Greenhou
Row factor	0.0474	*	Yes	F (3.874, 11	0.6456
Stroke	0.0503	ns	No	F (1, 32) = 4.137	
Drug	0.7859	ns	No	F (1, 32) = 0.07503	
Row factor x Stroke	0.2043	ns	No	F (6, 180) = 1.433	
Row factor x Drug	0.9002	ns	No	F (6, 180) = 0.3652	
Stroke x Drug	0.5078	ns	No	F (1, 32) = 0.4486	
Row factor x Stroke x Drug	0.4043	ns	No	F (6, 180) = 1.035	
Random effects	SD	Variance			
Subject	1.659	2.751			
Residual	0.9707	0.9423			
Was the matching effective?					
Chi-square, df	192.2, 1				
P value	<0.0001				
P value summary	****				
Is there significant matching (P <	Yes				

Right Paw

Table Analyzed	RP Foot Faults				
Mixed-effects model (REML)	Matching by factor: Mouse				
Assume sphericity?	Yes				
Alpha	0.05				
Fixed effects (type III)	P value	P value summary	Statistically significant	F (DFn, DFd)	
Mouse	<0.0001	****	Yes	F (6, 191) = 12.37	
Stroke	<0.0001	****	Yes	F (1, 33) = 37.67	
Drug	0.5638	ns	No	F (1, 33) = 0.3401	
Mouse x Stroke	<0.0001	****	Yes	F (6, 191) = 13.00	
Mouse x Drug	0.8536	ns	No	F (6, 191) = 0.4369	
Stroke x Drug	0.434	ns	No	F (1, 33) = 0.6272	
Mouse x Stroke x Drug	0.2673	ns	No	F (6, 191) = 1.282	
Random effects	SD	Variance			
Subject	3.917	15.34			
Residual	3.162	9.998			
Was the matching effective?					
Chi-square, df	126.0, 1				
P value	<0.0001				
P value summary	****				
Is there significant matching (P <	Yes				

Table 5.2 Normality of ROI Data

Spontaneous M1 Neurons

Shapiro-Wilk test				
W	0.9048	0.8969	0.9595	0.8901
P value	0.4028	0.356	0.816	0.3188
Passed normality test (alpha=0.0	Yes	Yes	Yes	Yes
P value summary	ns	ns	ns	ns
Kolmogorov-Smirnov test				
KS distance	0.1814	0.2328	0.2021	0.235
P value	>0.1000	>0.1000	>0.1000	>0.1000
Passed normality test (alpha=0.0	Yes	Yes	Yes	Yes
P value summary	ns	ns	ns	ns

Spontaneous M2 Neurons

Shapiro-Wilk test				
W	0.9048	0.8969	0.9595	0.8901
P value	0.4028	0.356	0.816	0.3188
Passed normality test (alpha=0.0	Yes	Yes	Yes	Yes
P value summary	ns	ns	ns	ns
Kolmogorov-Smirnov test				
KS distance	0.1814	0.2328	0.2021	0.235
P value	>0.1000	>0.1000	>0.1000	>0.1000
Passed normality test (alpha=0.0	Yes	Yes	Yes	Yes
P value summary	ns	ns	ns	ns

Forced-Use M2 Neurons

Shapiro-Wilk test				
W	0.9411	0.8568	0.8593	0.94
P value	0.6483	0.1416	0.1492	0.6385
Passed normality test (alpha=0.0	Yes	Yes	Yes	Yes
P value summary	ns	ns	ns	ns
Kolmogorov-Smirnov test				
KS distance	0.197	0.2927	0.2277	0.1987
P value	>0.1000	0.0709	>0.1000	>0.1000
Passed normality test (alpha=0.0	Yes	Yes	Yes	Yes
P value summary	ns	ns	ns	ns

Table 5.3 Amplitude and Frequency for M1

Amplitude

Table Analy	Spontaneous MC (Amp)				
Mixed-effec	Matching: Stacked				
Assume spl	No				
Alpha	0.05				
Fixed effect	P value	P value sun	Statistically	F (DFn, DFc	Geisser-Gre
Row Factor	0.4391	ns	No	F (3.946, 96	0.7891
Column Fac	0.3636	ns	No	F (3, 25) = 1.110	
Row Factor	0.1466	ns	No	F (15, 122) = 1.424	
Random efl	SD	Variance			
Subject	0.4515	0.2039			
Residual	0.5421	0.2939			
Was the matching effective?					
Chi-square	37.47, 1				
P value	<0.0001				
P value sun	****				
Is there sigr	Yes				
Data summary					
Number of (	4				
Number of r	6				
Number of s	29				
Number of r	3				

Frequency

Table Analy	Spontaneous MC (Freq)				
Mixed-effec	Matching: Stacked				
Assume spl	No				
Alpha	0.05				
Fixed effect	P value	P value sun	Statistically	F (DFn, DFc	Geisser-Gre
Row Factor	0.4095	ns	No	F (2.956, 72	0.5912
Column Fac	0.0541	ns	No	F (3, 25) = 2.913	
Row Factor	0.2046	ns	No	F (15, 122) = 1.313	
Random efl	SD	Variance			
Subject	0.01215	0.000148			
Residual	0.01518	0.000231			
Was the matching effective?					
Chi-square	33.14, 1				
P value	<0.0001				
P value sun	****				
Is there sigr	Yes				
Data summary					
Number of (	4				
Number of r	6				
Number of s	29				
Number of r	3				

Table 5.4 Amplitude and Frequency for Spontaneous Activity in M2

Amplitude

Table Analy	Spontaneous PMC (Amp)				
Mixed-effec	Matching: Stacked				
Assume spl	No				
Alpha	0.05				
Fixed effect	P value	P value sun	Statistically	F (DFn, DFd	Geisser-Gre
Time	0.2767	ns	No	F (4.093, 11	0.8185
Column Fac	0.159	ns	No	F (3, 29) = 1.857	
Time x Colu	0.3636	ns	No	F (15, 139) = 1.098	
Random eff	SD	Variance			
Subject	0.3543	0.1255			
Residual	0.3932	0.1546			
Was the matching effective?					
Chi-square	49.45, 1				
P value	<0.0001				
P value sun	****				
Is there sign	Yes				
Data summary					
Number of (	4				
Number of r	6				
Number of s	33				
Number of r	6				

Frequency

Table Analy	Spontaneous PMC (Freq)				
Mixed-effec	Matching: Stacked				
Assume spl	No				
Alpha	0.05				
Fixed effect	P value	P value sun	Statistically	F (DFn, DFd	Geisser-Gre
Row Factor	0.5977	ns	No	F (3.928, 11	0.7857
Column Fac	0.0459	*	Yes	F (3, 29) = 3.015	
Row Factor	0.2916	ns	No	F (15, 141) = 1.183	
Random eff	SD	Variance			
Subject	0.0128	0.000164			
Residual	0.0136	0.000185			
Was the matching effective?					
Chi-square	54.56, 1				
P value	<0.0001				
P value sun	****				
Is there sign	Yes				
Data summary					
Number of (	4				
Number of r	6				
Number of s	33				
Number of r	4				

Table 5.5 Amplitude and Frequency for Forced-use in M2

Amplitude

Table Analy	Forced PMC (Amp)				
Mixed-effec	Matching: Stacked				
Assume spl	No				
Alpha	0.05				
Fixed effect	P value	P value sun	Statistically	F (DFn, DFd	Geisser-Gre
Time	0.6458	ns	No	F (4.179, 11	0.6964
Column Fac	0.2108	ns	No	F (3, 29) = 1.600	
Time x Colu	0.97	ns	No	F (18, 158) = 0.4621	
Random eff	SD	Variance			
Subject	0.2607	0.06796			
Residual	0.3474	0.1207			
Was the matching effective?					
Chi-square	35.08, 1				
P value	<0.0001				
P value sun	****				
Is there sign	Yes				
Data summary					
Number of c	4				
Number of r	7				
Number of s	33				
Number of r	16				

Frequency

Table Analy	Forced PMC (Freq)				
Mixed-effec	Matching: Across row				
Assume spl	No				
Alpha	0.05				
Fixed effect	P value	P value sun	Statistically	F (DFn, DFd	Geisser-Gre
Row Factor	0.7644	ns	No	F (6, 198) = 0.5567	
Column Fac	0.0053	**	Yes	F (2.097, 13	0.6988
Row Factor	0.8139	ns	No	F (18, 198) = 0.6950	
Random eff	SD	Variance			
Subject	0	0			
Residual	0.02009	0.000404			
Was the matching effective?					
Chi-square, df					
P value					
P value summary					
Is there sign	No				
Data summary					
Number of c	4				
Number of re	7				
Number of su	69				
Number of m	50				

Table 5.6 Functional Connectivity in M1

%FC (FC/ROI^2)

Table Analyzed	Spontaneous MC (%FC)				
Mixed-effects model (REML)	Matching by factor: Row factor				
Assume sphericity?	No				
Alpha	0.05				
Fixed effects (type III)	P value	P value summary	Statistically significant	F (DFn, DFd)	Geisser-Greenhou
Row factor	0.1465	ns	No	F (3.196, 77	0.6392
Stroke	<0.0001	****	Yes	F (1, 25) = 21.86	
Drug	0.0177	*	Yes	F (1, 25) = 6.453	
Row factor x Stroke	0.0299	*	Yes	F (5, 121) = 2.574	
Row factor x Drug	0.4271	ns	No	F (5, 121) = 0.9895	
Stroke x Drug	0.4043	ns	No	F (1, 25) = 0.7196	
Row factor x Stroke x Drug	0.165	ns	No	F (5, 121) = 1.601	
Random effects	SD	Variance			
Subject	0.03377	0.001141			
Residual	0.1509	0.02278			
Was the matching effective?					
Chi-square, df	0.6728, 1				
P value	0.4121				
P value summary	ns				
Is there significant matching (P <	No				

Fold Change %FC Over Baseline

Table Analyzed	Spontaneous MC (FoldFC)				
Mixed-effects model (REML)	Matching by factor: Row factor				
Assume sphericity?	No				
Alpha	0.05				
Fixed effects (type III)	P value	P value summary	Statistically significant	F (DFn, DFd)	Geisser-Greenhou
Row factor	0.1398	ns	No	F (2.267, 54	0.5667
Stroke	0.0017	**	Yes	F (1, 25) = 12.30	
Drug	0.0455	*	Yes	F (1, 25) = 4.431	
Row factor x Stroke	0.7253	ns	No	F (4, 97) = 0.5144	
Row factor x Drug	0.7838	ns	No	F (4, 97) = 0.4339	
Stroke x Drug	0.7142	ns	No	F (1, 25) = 0.1372	
Row factor x Stroke x Drug	0.1193	ns	No	F (4, 97) = 1.885	
Random effects	SD	Variance			
Subject	0.278	0.07729			
Residual	0.5684	0.323			
Was the matching effective?					
Chi-square, df	7.043, 1				
P value	0.008				
P value summary	**				
Is there significant matching (P <	Yes				

Table 5.7 Functional Connectivity in Spontaneous Activity of M2

%FC (FC/ROI^2)

Table Analyzed	Forced PMC (%FC)				
Mixed-effects model (REML)	Matching by factor: Row factor				
Assume sphericity?	No				
Alpha	0.05				
Fixed effects (type III)	P value	P value summary	Statistically significant	F (DFn, DFd)	Geisser-Greenhou
Row factor	0.0097	**	Yes	F (4.480, 12	0.7467
Stroke	0.0164	*	Yes	F (1, 29) = 6.497	
Drug	<0.0001	****	Yes	F (1, 29) = 22.59	
Row factor x Stroke	0.2354	ns	No	F (6, 164) = 1.356	
Row factor x Drug	<0.0001	****	Yes	F (6, 164) = 5.349	
Stroke x Drug	0.6896	ns	No	F (1, 29) = 0.1628	
Row factor x Stroke x Drug	0.7153	ns	No	F (6, 164) = 0.6185	
Random effects	SD	Variance			
Subject	0.07151	0.005114			
Residual	0.1499	0.02248			
Was the matching effective?					
Chi-square, df	13.22, 1				
P value	0.0003				
P value summary	***				
Is there significant matching (P <	Yes				

Fold Change %FC Over Baseline

Table Analyzed	Spontaneous PMC (FoldFC)				
Mixed-effects model (REML)	Matching by factor: Row factor				
Assume sphericity?	No				
Alpha	0.05				
Fixed effects (type III)	P value	P value summary	Statistically significant	F (DFn, DFd)	Geisser-Greenhou
Row factor	0.5329	ns	No	F (3.511, 10	0.8776
Stroke	0.0221	*	Yes	F (1, 30) = 5.827	
Drug	0.0031	**	Yes	F (1, 30) = 10.39	
Row factor x Stroke	0.8658	ns	No	F (4, 117) = 0.3175	
Row factor x Drug	0.7881	ns	No	F (4, 117) = 0.4281	
Stroke x Drug	0.4888	ns	No	F (1, 30) = 0.4911	
Row factor x Stroke x Drug	0.9513	ns	No	F (4, 117) = 0.1742	
Random effects	SD	Variance			
Subject	0.4862	0.2364			
Residual	0.7167	0.5137			
Was the matching effective?					
Chi-square, df	20.66, 1				
P value	<0.0001				
P value summary	****				
Is there significant matching (P <	Yes				

Table 5.8 Functional Connectivity in Forced-use of M2

%FC (FC/ROI^2)

Table Analyzed	Forced PMC (%FC)				
Mixed-effects model (REML)	Matching by factor: Row factor				
Assume sphericity?	No				
Alpha	0.05				
Fixed effects (type III)	P value	P value summary	Statistically significant	F (DFn, DFd)	Geisser-Greenhou
Row factor	0.0097	**	Yes	F (4.480, 12	0.7467
Stroke	0.0164	*	Yes	F (1, 29) = 6.497	
Drug	<0.0001	****	Yes	F (1, 29) = 22.59	
Row factor x Stroke	0.2354	ns	No	F (6, 164) = 1.356	
Row factor x Drug	<0.0001	****	Yes	F (6, 164) = 5.349	
Stroke x Drug	0.6896	ns	No	F (1, 29) = 0.1628	
Row factor x Stroke x Drug	0.7153	ns	No	F (6, 164) = 0.6185	
Random effects	SD	Variance			
Subject	0.07151	0.005114			
Residual	0.1499	0.02248			
Was the matching effective?					
Chi-square, df	13.22, 1				
P value	0.0003				
P value summary	***				
Is there significant matching (P <	Yes				

Fold Change %FC Over Baseline

Table Analyzed	Forced PMC (FoldFC)				
Mixed-effects model (REML)	Matching by factor: Row factor				
Assume sphericity?	No				
Alpha	0.05				
Fixed effects (type III)	P value	P value summary	Statistically significant	F (DFn, DFd)	Geisser-Greenhou
Row factor	0.0078	**	Yes	F (3.776, 11	0.7552
Stroke	0.6763	ns	No	F (1, 32) = 0.1775	
Drug	0.0014	**	Yes	F (1, 32) = 12.19	
Row factor x Stroke	0.6311	ns	No	F (5, 153) = 0.6909	
Row factor x Drug	0.0098	**	Yes	F (5, 153) = 3.151	
Stroke x Drug	0.6235	ns	No	F (1, 32) = 0.2458	
Row factor x Stroke x Drug	0.6811	ns	No	F (5, 153) = 0.6248	
Random effects	SD	Variance			
Subject	0.6518	0.4249			
Residual	0.6635	0.4402			
Was the matching effective?					
Chi-square, df	63.16, 1				
P value	<0.0001				
P value summary	****				
Is there significant matching (P <	Yes				

Table 5.9 Active Nodes in FC Maps

M1:Spontaneous Activity

Table Analyzed	MC: Nodes				
Mixed-effects model (REML)	Matching by factor: Row factor				
Assume sphericity?	No				
Alpha	0.05				
Fixed effects (type III)	P value	P value summary	Statistically significant	F (DFn, DFd)	Geisser-Greenhou
Row factor	0.5032	ns	No	F (3.738, 91	0.7475
Stroke	0.8811	ns	No	F (1, 25) = 0.02283	
Drug	0.4639	ns	No	F (1, 25) = 0.5532	
Row factor x Stroke	0.7372	ns	No	F (5, 123) = 0.5512	
Row factor x Drug	0.9725	ns	No	F (5, 123) = 0.1722	
Stroke x Drug	0.732	ns	No	F (1, 25) = 0.1200	
Row factor x Stroke x Drug	0.9262	ns	No	F (5, 123) = 0.2747	
Random effects	SD	Variance			
Subject	23.6	557.1			
Residual	13	169.1			
Was the matching effective?					
Chi-square, df	138.2, 1				
P value	<0.0001				
P value summary	****				
Is there significant matching (P <	Yes				

M2: Spontaneous Activity

Table Analyzed	Spon PMC: Nodes				
Mixed-effects model (REML)	Matching by factor: Row factor				
Assume sphericity?	No				
Alpha	0.05				
Fixed effects (type III)	P value	P value summary	Statistically significant	F (DFn, DFd)	Geisser-Greenhou
Row factor	0.0292	*	Yes	F (3.981, 99	0.7962
Stroke	0.1815	ns	No	F (1, 26) = 1.885	
Drug	0.6714	ns	No	F (1, 26) = 0.1841	
Row factor x Stroke	0.5045	ns	No	F (5, 125) = 0.8684	
Row factor x Drug	0.6053	ns	No	F (5, 125) = 0.7259	
Stroke x Drug	0.637	ns	No	F (1, 26) = 0.2279	
Row factor x Stroke x Drug	0.3751	ns	No	F (5, 125) = 1.079	
Random effects	SD	Variance			
Subject	26.43	698.5			
Residual	11.82	139.7			
Was the matching effective?					
Chi-square, df	182.5, 1				
P value	<0.0001				
P value summary	****				
Is there significant matching (P <	Yes				

M2: Forced-use Activity

Table Analyzed	Forced PMC: Nodes				
Mixed-effects model (REML)	Matching by factor: Row factor				
Assume sphericity?	No				
Alpha	0.05				
Fixed effects (type III)	P value	P value summary	Statistically significant	F (DFn, DFd)	Geisser-Greenhou
Row factor	0.6356	ns	No	F (4.304, 13	0.7173
Stroke	0.1154	ns	No	F (1, 32) = 2.619	
Drug	0.4661	ns	No	F (1, 32) = 0.5440	
Row factor x Stroke	0.3733	ns	No	F (6, 183) = 1.084	
Row factor x Drug	0.4863	ns	No	F (6, 183) = 0.9136	
Stroke x Drug	0.861	ns	No	F (1, 32) = 0.03117	
Row factor x Stroke x Drug	0.8378	ns	No	F (6, 183) = 0.4591	
Random effects	SD	Variance			
Subject	23.93	572.8			
Residual	11.44	131			
Was the matching effective?					
Chi-square, df	251.2, 1				
P value	<0.0001				
P value summary	****				
Is there significant matching (P <	Yes				

Chapter VI: Discussion

Stroke initiates pathological cascades resulting in the necrotic stroke core and a unique area primed for recovery—the peri-infarct. In the motor system, stroke of the primary motor cortex causes behavioral deficits and the nearby motor areas are known to contribute to recovery. Specifically, PDE2a inhibition was found to enhance axonal sprouting from the secondary motor areas (M2) to the stroke core (Figure 3.2c). After the initial phases of stroke damage, excitability of the peri-infarct has been linked to enhanced recovery by a variety of means, including drug-delivery, non-invasive and optogenetic stimulation. The excitatory effects of cAMP/cGMP in neurons indicate PDE enzymes as an inhibitory mechanism, and suggest PDE2a-inhibition as a means of enhancing excitability and recovery. The results of PDE2a-inhibition and of stroke described in Chapter 5 are further evaluated here, with specific discussion of the usefulness of the data and its application.

Section 6.1 Gridded Treadmill is a Novel Tool for *in vivo* Imaging of Stroke

The primary experimental variable was the induction of stroke to M1, which had apparent effects on the mice's behavior and calcium imaging. As expected, stroke induces a similar deficit to the grid-walking of head-fixed animals as it does in non-head-fixed. This deficit was highest at weeks one and two post-stroke, but animals show spontaneous behavioral recovery by week 5.

Correlating forced-use behavior to calcium imaging

The head-fixed forced-use task (Section 4.4, Figure 4.6) was a robust test of stroke deficit and recovery. MEA determined a highly significant effect of stroke on foot fault percentage ($p=0.001$). Sham mice and the unaffected paw had consistently low foot fault percentages, ranging from 2-6%, across all time points. In the stroke group, the affected paw (right paw) increases its

foot fault percentage from <4% to about 15% after week 1 (Figure 5.1b), an average change of 4-5 fold (Figure 5.2b). This increased foot fault % persisted but decreased over time, indicating recovery. The advantage of acquiring this data concurrently with calcium imaging is that we definitively know the amount of deficit or recovery each group has at each time point and can correlate this information to changes in the calcium activity of M1 and M2.

The imaging of forced behavior vs spontaneous behavior

The forced-use condition was initially introduced to measure behavioral deficits in the same mice that were being imaged. Mice spent most of their time resting during the spontaneous recording of their behavior after stroke and thus did not move enough steps for researchers to capture their deficits consistently. By forcing locomotion, the forced-use context elicited enough steps to allow the researcher accurate scoring of the behavior. However, forcing movement is a unique behavioral and neural state which has effects that should be considered. One comprehensive study evaluated the effects of voluntary vs. involuntary vs. forced exercise in groups of rats and found that the forced-exercise group decreased BDNF and recovery compared to the other rehabilitative conditions[1]. Researchers also noted an increase in agitation and restlessness of the mice during prolonged imaging of forced-use condition of these experiments; furthermore, sequential recordings of forced-use were found to have increasing %FF. This indicated that the mice become exhausted with the task over time. For these reasons, imaging during forced-use was only limited to one session (M2). The effect of forced behavior on M1 connectivity is an interesting follow-up experiment to consider; however, if the same adverse effects of forced-use observed in M2 were applied to M1, a floor effect may already be observed as stroke already induces significantly decreased connectivity even during spontaneous behavior.

Section 6.2 Functional Connectivity is a Robust Marker of Post-Stroke Connectivity

Viral injection of GCaMP6s, under the control of the CaMKII promoter, led to robust and long-lasting expression in excitatory neurons of the rodent cortex (Figure 4.3c). The craniotomy procedure implants a cover-glass that can remain clear and allows for *in vivo* expression longitudinally after stroke (Figure 4.4). GCaMP6s is an efficient intracellular reporter of calcium[9], which is a critical second messenger in neuronal excitability[10].

Inducing the stroke in a nearby region of M1 designates the M1 imaging as the *peri-infarct*, the radial region surrounding stroke known for its unique activity and expression patterns after stroke[2–5]. M2 has demonstrated special features during stroke recovery as well[6–8]. While M2 may also be referred to as peri-infarct, stroke is known to have radial effects which emanate from the ischemic core[3]. This dictates that M1 should demonstrate the impact of stroke more so than M2 due to its closer location. The present section will 1) investigate the efficacy of *in vivo* calcium imaging as a way of evaluating brain networks after stroke and 2) discuss any differential effects observed between M1 and M2, which may give insight into the radial effects of stroke on Functional Connectivity (FC).

Measuring Functional Connectivity (FC) is a robust measure of network correlation

FCS were defined in Section 4.3 as pairwise connections between two neurons above the mouse's threshold, which is based on the average pairwise correlations across all baseline recordings. The total number of connections can be calculated as the square of the ROIs, and dividing by this value normalizes any minor deviations in the number of neurons from different recordings in a single animal. Figure 5.5 and 5.6 graphs the %FC (FCs/Total connections) in M1 and M2 populations. Group 4 (Sham+Vehicle) is the true control of the experiment, as neither stroke nor drug was applied. There were no observable changes to %FC in Group 4 in M1 or M2,

and no statistically significant differences were found between any time-points. Observing no differences in this control group indicates that %FC is a robust measure of network connectivity and may be used to measure a change to the network.

Calcium transients are not a reliable indicator of network state due to stroke or drug

Imaging files are segmented into ROIs, representing neurons (Figure 4.5), and the fluorescent traces from these ROIs are evaluated for calcium transients. These calcium transients can then be assessed for amplitude (the difference of peak fluorescence) and frequency. Figure 5.2 plots the average number of neurons (ROIs) across each group and each time-point. Mixed-effects analysis (MEA) found no significant effect of drug or stroke across any time-point in each group (Table 5.12). Similarly, the amplitude and frequency of calcium transients were also found to remain relatively constant in each group across all time points (Figure 5.3-5.4). MEA did not determine a significant effect of drug or stroke in these measures as well. Thus, while %FC found substantial changes due to stroke and drug, this was not reflected in the amplitude or frequency of calcium transients. This indicates that the correlated-ness of a region will change positively or negatively without affecting the essential characteristics of intracellular calcium transients.

Stroke decreases Functional Connectivity (FC) in M1

The most considerable stroke effect was found in the M1 region, the closest region to the infarct. A found a highly significant stroke effect ($p=0.0001$), and it remained decreased in Group 2 (Stroke +Vehicle) until Week 4. Similarly, Group 1 (Stroke + Drug) has a reduced %FC relative to Group 3 (Sham + drug) at every time-point. This data is consistent with the known molecular mechanisms and electrical dysfunctions which occur in the peri-infarct[11–13]. More directly, it is compatible with two recent comprehensive studies of functional connectivity using calcium imaging after stroke[14,15] which both presented decreased correlatedness in the peri-infarct.

Additionally, Latifi et al. also showed that these changes were independent of the amplitude and frequency of calcium transients. These studies corroborate the present findings, indicating %FC in the peri-infarct is a promising biomarker for stroke. However, while behavioral recovery is observed as a decrease of %FF during Weeks 2-5, there is no parallel increase in M1 %FC at that time. Behavioral recovery occurs while the measures of FC in M1 did not recover. One possibility is that the radiating damage for the ischemic core causes permanent network damage to its nearest neighbors (M1) but that further motor regions (M2) correlate more with recovery.

Forced-use induces adverse effects to %FC in M2 after stroke

M2 is further away from the ischemic core and displays a more complex relationship with its %FC. MEA analysis found a significant negative effect of stroke when the mice were in the forced-use condition, forcing them to use their affected limbs. This may correlate to studies of CIMT[16–18], although a significant difference is the constraint of the unaffected limb. In these studies, the affected limb was forced weekly for approximately 5 minutes (from time on the platform to time off the platform). While this very sparse training regimen may not induce adverse effects on behavior, it may negatively affect the FC of M2. Stroke was found to significantly negatively affect %FC in M2 only in the forced-use condition ($p=0.0164$) but not in the spontaneous state ($p=0.6838$). During the spontaneous behavior, the stroke did not affect M2 at Week 1 and showed an increased average %FC at Weeks 2 and 3. However, these differences were not significant, and the drug did not affect the network %FC. This data indicates that forced-use reduces %FC and causes the network to be less correlated with itself. One possibility is that forced use induces decreased correlated activity of a network and that, over time, this limits behavioral recovery after stroke. In our study, a single weekly session may not induce behavioral inhibition of recovery, but it does decrease %FC.

Section 6.3 PDE2a-Inhibition is a Promising Target for Enhancing Post-Stroke Excitability

Phosphodiesterase (PDEs) were discussed as a ubiquitous superfamily of enzymes which play inhibitory roles in neuronal excitability (Figure 2.1). By catalyzing the breakdown of the stimulatory cyclic nucleotides (cAMP, cGMP), PDEs inhibit the mechanisms associated with recovery[10,19,20]. Much like increased GABA currents[21,22] after stroke, PDEs carry out inhibitory roles, and their inhibition has enhanced axonal sprouting and recovery outcomes after neural injury[23–26]. Although PDE inhibition is widely successful as a drug target for erectile dysfunction, congestive heart failure, and inflammatory lung disease- it has yet to be approved for any neurological disease. One of the primary considerations for a drug target in the brain is non-specific targeting. This can cause side effects such as significant nausea and vomiting. In collaboration with a pharmaceutical company, we evaluated a novel PDE2a inhibitor that they generated; the PDE2a subfamily of enzymes possesses highly favorable expression patterns that pose a strong candidate for drug targeting. In the current section, PDE2a-inhibition and Inhibitor-X specifically will be evaluated as targets for stroke therapy.

<u>PDE2a inhibition enhances behavioral recovery after Stroke</u>

Inhibitor-X is a potent inhibitor of PDE2a, and it was administered as a drug therapy daily after stroke in the present experiments. Before these experiments, pilot studies with this drug significantly enhanced behavioral recovery after stroke in grid-walking and spontaneous forelimb use tasks (Figure 3.2a-b). Injected daily at 3mg/kg, Inhibitor-X was also shown to significantly enhance axonal connections in the peri-infarct (Figure 3.2d).

The present studies generated a new head-fixed behavioral paradigm and established a similar role of PDE2a inhibition in this context. FF%, which demonstrates forelimb deficits, increase dramatically after stroke (Group 2). When the drug is administered daily, the average

FF% is decreased at every time-point after stroke (Group 1), but the drug's effect was not determined to be significant. As this task is a test of forelimb dexterity, the drug was not expected to have an independent effect. Instead, comparing each group's deficit to baseline shows that the drug allows a significantly faster return to normalcy or faster recovery. Furthermore, these data points corroborate the findings reported in Figure 3.2a, which mirror the same trends across all four groups.

PDE2a-inhibition increases Functional Connectivity (FC) in all networks measured

A significant finding of the present experiments is that Inhibitor-X positively affected network connectivity across all conditions. Inhibitor-X was found to significantly positively affect %FC in M1 ($p=0.001$ Figure 5.6a), a measure of highly-correlated pairs of neurons in the network. This was independent of any effects of amplitude or frequency. The number of neurons in the FC network, also called nodes, did not change about the drug either (Figure 5.2a). This may suggest no movement of neurons in or out of this network, but rather that the positive correlation is due to increasing pairwise correlations between existing pairs. This hypothesis would fit the current framework of increasing neuronal excitability during PDE inhibition (Section 2.5, 3.1) which would be expected to enhance the correlation of the affected neurons. Further studies interrogating the mechanism of PDE inhibition on %FC enhancements would be required to probe whether this effect is purely by enhancing neuronal excitability.

As in M1, Inhibitor-X was found to have a significant effect in M2 neurons during spontaneous recovery ($p=0.0055$) and during forced use ($p<0.0001$). The positive impact of the drug in these conditions mimics the effects during M1 spontaneous imaging noted above, solidifying a role for PDE inhibition as a positive enhancer of %FC. As a systemically acting drug, we would expect the effects of the drug to be independent of location and possibly independent of

behavior. This seems to be the case, as Inhibitor-X has a positive impact independent of sites (M1 or M2) and behavior (spontaneous and forced-use).

PDE2a is an ideal molecular target for Stroke recovery

The ultimate goal of these studies is to contribute to finding and applying novel therapies for stroke recovery. Here, a novel PDE2a inhibitor, Inhibitor-X, was assessed as a pharmaceutical enhancer of stroke recovery. The PDE2a enzyme was highly expressed in the human forebrain, and its inhibition was shown to have dose-dependent enhancement of cGMP in the prefrontal cortex of rat tissue (Figure 3.1a-c). Furthermore, the drug is bioavailable in the plasma and the CSF of the brain (Figure 3.1d-e). As described above, PDE2a inhibition alters the connectivity of the cortex without changing fundamental neuronal calcium transient dynamics. This has the potential for safer neurological drugs, which may impact the network state without the risks that accompany directly enhancing neuronal firing. Finally, this drug shows the capacity for enhancing behavioral recovery through well-documented neuroplasticity mechanisms. These experiments indicate PDE2a as a novel and exciting target for further research as a pharmaceutical therapy after stroke.

Section 6.4 Advances of the Field and Future Considerations

The data presented in Chapter 5 and the discussion points in the current chapter are novel data for concurrent imaging of neuronal activity and forelimb function. It is also the only live-imaging study evaluating chronic drug administration for stroke recovery. Still, the rapid pace of advancements in this field promises innovative and time-saving methods for future studies similar to those presented here. Some of the applicable advances will be discussed here and some of the future studies implicated by the present studies.

Automating behavioral analysis and optimizing segmentation

Manual behavioral scoring is an old-fashioned but straightforward approach to assessing behavioral function in the rodent[27]. The major disadvantages of manual behavioral scoring constitute a significant time requirement from the scorer, a necessity for blinding the data, and an inherent confounding factor in the subjectivity of scoring the behavior. Automating behavioral scoring would allow the analysis to be based on algorithmic rules that confer the opposite advantages: potentially much faster scoring, a decrease in the researcher's workload, and an unbiased approach to scoring the files. Furthermore, it allows for controlling things that would be much more difficult with human scoring. For example, it is impossible to blind the researcher for left vs. right paw during behavioral scoring of videos (Figure 4.6), which was not done in these experiments. The computerized analysis would allow for this, further enhancing the controls for the model.

Machine learning and neural networks have been increasingly maturing tools in the last two decades. By its nature, machine learning is highly versatile and may be applied to any repeatable task which needs to be categorized by its data outputs. This can be used for image categorization ("computer vision") to allow for advancements like self-driving cars. These same concepts have been applied to images acquired from behavioral recordings. A leading and open-source implementation of this idea is DeepLabCut, a software package designed by the Mathis lab at Harvard, which promises 3D markerless pose estimation[28,29]. This software has developed a neural network that may be trained to tag behavioral videos with labels. This network learns the rules of labeling, allowing it to label other images without human intervention. This project has been implemented in several human and animal behavior models and is a promising tool for automated behavioral scoring of head-fixed behavior.

Segmentation of behavioral epochs during spontaneous recovery

The spontaneous imaging of M1 and M2 was behaviorally recorded and initially analyzed. It was discovered that spontaneous recordings were difficult to obtain forelimb behavior results after stroke. Unsurprisingly, this is because mice will rest for the vast majority of the time after a stroke rather than use their affected limbs. Without any movement, behavioral recordings could not be assessed for forelimb function after stroke. A major addressable weakness of the present data is that all spontaneous imaging acquired is composed of at least three behavioral states: rest, motion, and grooming. More specifically, to interrogate the network, the behavioral state may split calcium analysis (rest, movement, grooming) to achieve more specific results. For example, the %FC may change in the active network during rest but not during motion. The forced-use condition may be more correlated to the movement epoch and less correlated with the resting epochs- or forced-use may be uncorrelated with any spontaneous epoch.

Analyzing the networks for normal steps vs foot faults

Another interesting point of complexity is to segment the forced-use data further. As mentioned in Section 4.4 and Figure 4.6, behavioral forced-use data was scored by counting the number of total steps and categorizing each of them as a "good step" or a "foot fault." This begs the question- how are brain states different during a good step vs. a foot fault, and can this difference be observed by calcium imaging? One advantage is that this data is already collected but needs further analysis. This would be applied by writing Matlab code which cuts a recording up into small collections of frames, each corresponding to a single step. The characteristics discussed in this dissertation (amplitude, frequency, %FC, nodes) may all be calculated for step, and the averages between good and dysfunctional steps may be compared.

Furthermore, differences between good and bad steps may be assessed during baseline vs. after stroke and with vehicle vs. drug administration. Two major questions are the efficacy of calculating PCC in a series only a few frames long and whether the frames evaluated should be time-shifted a certain number of frames before the foot fault occurs. In any case, separating the normal steps versus faulty steps is an addressable and highly pertinent next step.

Section 6.5 References

1. Ke Z, Yip SP, Li L, Zheng X-X, Tong K-Y. The Effects of Voluntary, Involuntary, and Forced Exercises on Brain-Derived Neurotrophic Factor and Motor Function Recovery: A Rat Brain Ischemia Model. doi:10.1371/journal.pone.0016643
2. Sigler A, Murphy TH. In vivo 2-photon imaging of fine structure in the rodent brain: Before, during, and after stroke. *Stroke*. 2010;41(10 SUPPL. 1):S117-S123. doi:10.1161/STROKEAHA.110.594648
3. Carmichael ST. The 3 Rs of Stroke Biology: Radial, Relayed, and Regenerative. *Neurotherapeutics*. 2016;13(2):348-359. doi:10.1007/s13311-015-0408-0
4. Carmichael ST, Archibeque I, Luke L, Nolan T, Momiy J, Li S. Growth-associated gene expression after stroke: Evidence for a growth-promoting region in peri-infarct cortex. *Exp Neurol*. 2005;193(2):291-311. doi:10.1016/j.expneurol.2005.01.004
5. Li S, Nie EH, Yin Y, et al. GDF10 is a signal for axonal sprouting and functional recovery after stroke. *Nat Neurosci*. 2015;18(12):1737-1745. doi:10.1038/nn.4146
6. Dancause N, Barbay S, Frost SB, et al. Extensive cortical rewiring after brain injury. *J Neurosci*. 2005;25(44):10167-10179. doi:10.1523/JNEUROSCI.3256-05.2005
7. Willett FR, Deo DR, Avansino DT, et al. Hand Knob Area of Premotor Cortex Represents the Whole Body in a Compositional Way. *Cell*. 2020;181(2):396-409.e26. doi:10.1016/j.cell.2020.02.043
8. Tennant KA, Kerr AL, Adkins DL, et al. Age-dependent reorganization of peri-infarct "premotor" cortex with task-specific rehabilitative training in mice. *Neurorehabil Neural Repair*. 2015;29(2):193-202. doi:10.1177/1545968314541329
9. Chen TW, Wardill TJ, Sun Y, et al. Ultrasensitive fluorescent proteins for imaging

neuronal activity. *Nature*. 2013;499(7458):295-300. doi:10.1038/nature12354

10. Kandel ER. The molecular biology of memory: cAMP, PKA, CRE, CREB-1, CREB-1, CPEB. *Mol Brain*. 2012;5(1):1-12. http://molecularbrain.biomedcentral.com/articles/10.1186/1756-6606-5-14.

11. Carmichael ST, Chesselet MF. Synchronous neuronal activity is a signal for axonal sprouting after cortical lesions in the adult. *J Neurosci*. 2002;22(14):6062-6070. doi:10.1523/jneurosci.22-14-06062.2002

12. Brown CE, Aminoltejari K, Erb H, Winship IR, Murphy TH. In vivo voltage-sensitive dye imaging in adult mice reveals that somatosensory maps lost to stroke are replaced over weeks by new structural and functional circuits with prolonged modes of activation within both the peri-infarct zone and distant sites. *J Neurosci*. 2009;29(6):1719-1734. doi:10.1523/JNEUROSCI.4249-08.2009

13. Carmichael ST. Brain excitability in stroke: The yin and yang of stroke progression. *Arch Neurol*. 2012;69(2):161-167. doi:10.1001/archneurol.2011.1175

14. Latifi S, Mitchell S, Habibey R, et al. Neuronal network topology indicates distinct recovery processes after stroke. *Cereb Cortex*. 2020;30(12):6363-6375. doi:10.1093/cercor/bhaa191

15. Cramer J V., Gesierich B, Roth S, Dichgans M, Düring M, Liesz A. In vivo widefield calcium imaging of the mouse cortex for analysis of network connectivity in health and brain disease. *Neuroimage*. 2019;199(November 2018):570-584. doi:10.1016/j.neuroimage.2019.06.014

16. Kitago T, Liang J, Huang VS, et al. Improvement after constraint-induced movement therapy: Recovery of normal motor control or task-specific compensation? *Neurorehabil*

Neural Repair. 2013;27(2):99-109. doi:10.1177/1545968312452631

17. Dromerick AW, Lang CE, Birkenmeier RL, et al. Very early constraint-induced movement during stroke rehabilitation (VECTORS): A single-center RCT. *Neurology*. 2009;73(3):195-201. doi:10.1212/WNL.0b013e3181ab2b27

18. Wolf SL, Winstein CJ, Miller JP, Morris D. Effect of Constraint-Induced Movement. *Jama*. 2006;296(17):2095-2104.

19. Maurice DH, Ke H, Ahmad F, Wang Y, Chung J, Manganiello VC. Advances in targeting cyclic nucleotide phosphodiesterases. *Nat Rev Drug Discov*. 2014;13(4):290-314. doi:10.1038/nrd4228

20. Menniti FS, Faraci WS, Schmidt CJ. Phosphodiesterases in the CNS: Targets for drug development. *Nat Rev Drug Discov*. 2006;5(8):660-670. doi:10.1038/nrd2058

21. Clarkson AN, Huang BS, MacIsaac SE, Mody I, Carmichael ST. Reducing excessive GABA-mediated tonic inhibition promotes functional recovery after stroke. *Nature*. 2010;468(7321):305-309. doi:10.1038/nature09511

22. Redecker C, Wang W, Fritschy JM, Witte OW. Widespread and long-lasting alterations in GABAA-receptor subtypes after focal cortical infarcts in rats: Mediation by NMDA-dependent processes. *J Cereb Blood Flow Metab*. 2002;22(12):1463-1475. doi:10.1097/01.WCB.0000034149.72481.BD

23. Rodefer JS, Saland SK, Eckrich SJ. Selective phosphodiesterase inhibitors improve performance on the ED/ID cognitive task in rats. *Neuropharmacology*. 2012;62(3):1182-1190. doi:10.1016/j.neuropharm.2011.08.008

24. Reneerkens OAH, Rutten K, Steinbusch HWM, Blokland A, Prickaerts J. Selective phosphodiesterase inhibitors: A promising target for cognition enhancement.

Psychopharmacology (Berl). 2009;202(1-3):419-443. doi:10.1007/s00213-008-1273-x

25. Domek-Łopacińska KU, Strosznajder JB. Cyclic GMP and nitric oxide synthase in aging and alzheimer's disease. *Mol Neurobiol*. 2010;41(2-3):129-137. doi:10.1007/s12035-010-8104-x

26. Sasaki T, Kitagawa K, Omura-Matsuoka E, et al. The phosphodiesterase inhibitor rolipram promotes survival of newborn hippocampal neurons after ischemia. *Stroke*. 2007;38(5):1597-1605. doi:10.1161/STROKEAHA.106.476754

27. Ölveczky BP. Motoring ahead with rodents. *Curr Opin Neurobiol*. 2011;21(4):571-578. doi:10.1016/j.conb.2011.05.002

28. Nath T, Mathis A, Chen AC, Patel A, Bethge M, Mathis MW. Using DeepLabCut for 3D markerless pose estimation across species and behaviors. *Nat Protoc*. doi:10.1038/s41596-019-0176-0

29. Weygandt Mathis M, Bethge M. DeepLabCut: markerless pose estimation of user-defined body parts with deep learning. doi:10.1038/s41593-018-0209-y